CARDIFF UNIVERSITY

School of Psychology

DOCTORAL THESIS

# The development and application of advanced methods for MEG and EEG data analysis

Author:

Megan GODFREY

Supervisors:

Prof. Krish SINGH

Prof. Khalid HAMANDI

*A thesis submitted to Cardiff University*

*for the degree of Doctor of Philosophy*


May 27, 2021

# *Summary*


**The development and application of advanced methods for MEG and EEG data analysis**

Magnetoencephalography (MEG), in combination with complex analysis techniques, has made large contributions to our understanding of the brain. However, MEG research often considers only oscillatory activity within the brain, whereas most brain activity appears to be more disorderly. During this thesis, rank-vector entropy (RVE), a time-resolved measure of neuronal irregularity, was found to be useful as a complement to oscillatory measures in the analysis of MEG data. The parameters of the RVE measure were first optimised to maximise temporal resolution and, separately, the temporal correlation between the RVE and oscillatory amplitude envelopes of virtual sensor timecourses. The RVE of MEG was then found to exhibit temporal correlation with the BOLD signal; this was positive in task-activated areas but negative in regions comprising the default mode network.

An important development put forward in this thesis was the extension to multi-scale RVE, which measures dynamic neuronal entropy over a range of temporal scales. MRVE correlation was shown to provide insight into functional connectivity across temporal scales in health and disease and gave complementary information to that given by measures based on oscillatory synchronisation. It was also found that functional connectivity measurements, as calculated using MRVE correlation and the more conventional method of oscillatory amplitude envelope correlation (AEC), depended on the data cleaning method used. The removal of eye movement artefacts using ICA was found to increase sensitivity to connectivity alterations in a cohort at genetic neurodevelopmental risk.

The final chapter of this thesis attempts to address the inferior sensitivity of MEG to deeper sources by performing source localisation using simultaneous MEG and EEG (MEEG). MEEG was not shown to improve source localisation in the deep brain over MEG alone. However, MEG alone was found to be able to detect activity within the medial temporal lobe during a spatial memory task.

# Statements and Declaration

**Statement 1** This thesis is being submitted in partial fulfilment of the requirements for the degree of PhD.

*Signed:* *Date:* 16/12/20

**Statement 2** This work has not been submitted in substance for any other degree or award at this or any other university or place of learning, nor is it being submitted concurrently for any other degree or award (outside of any formal collaboration agreement between the University and a partner organisation).

*Signed:* *Date:* 16/12/20

**Statement 3** I hereby give consent for my thesis, if accepted, to be available in the University's Open Access repository (or, where approved, to be available in the University's library and for inter-library loan), and for the title and summary to be made available to outside organisations, subject to the expiry of a University-approved bar on access if applicable.

*Signed:* *Date:* 16/12/20

**Declaration** This thesis is the result of my own independent work, except where otherwise stated, and the views expressed are my own. Other sources are acknowledged by explicit references. The thesis has not been edited by a third party beyond what is permitted by Cardiff University's Use of Third Party Editors by Research Degree Students Procedure.

*Signed:* *Date:* 16/12/20

# Data Collection

All analyses presented in this thesis were performed by me. The simultaneous MEG and EEG data presented for in chapter 6 were collected by me.

The MEG Partnership data presented in chapters 2 and 4 were collected by Dr Bethany Routley and Dr Lorenzo Magazzini.

The MEG data presented in chapter 5 were collected by Dr Gavin Perry, Dr Beth Routley, Dr Lorenzo Magazzini, Dr Sonya Foley, Dr Mark Drakesmith and Dr Joanne Doherty.

The MEG and fMRI data presented in chapter 3 was collected by Dr Bethany Routley and Dr Phoebe Asquith. They are currently unpublished.

# Impact of this Thesis

The work contained in chapter 4 has been published (Godfrey and Singh, 2021).

# *Acknowledgements*

I'd like to take a moment to thank all the people who have helped me through the past four years.

I am grateful to the EPSRC Doctoral Training Partnership and the Cardiff University School of Psychology for provision of financial support throughout my PhD.

I'd next like to thank my supervisors, Krish and Khalid. Your support and guidance over the years have helped me so much, and I am so grateful. Krish, thank you for being the most laid-back supervisor ever! Thank you for all the advice you've given me in countless emails and visits to your office, and for always having confidence in me. I admit, at first your confidence confused me, but over the years, it has helped me to believe in my own abilities. And Khalid, thank you for teaching me everything I know about epilepsy! Including taking me to a surgical planning meeting at the Heath – that was a great and memorable experience. I'm sorry that no epilepsy work made it into the thesis, but you've given me an interest that will stay with me after the PhD is done.

I'd also like to thank everyone else at CUBRIC who has helped me during my time here. Firstly, thank you to Gavin for all your help in the lab, firstly with MEG and then with EEG as well. I'm looking forward to bothering you about the OPMs next! A massive thank you to Colette, Nathan, Hannah, Angharad and Laura for helping me with the MEG and EEG data collection. It was hard work and could have easily become a slog, but you all managed to turn it into a series of fun afternoons with friends. Also, thank you to Leandro and Diana for all your help with my analysis and for answering so many emails! And thank you to Matthias for grilling me at the mock vivas each year, in the nicest way possible! The real viva seems a little bit less terrifying after all the practice.

Finally, I'd like to thank my friends and family for their support over the years. To my partner Brendan, thank you for being there for me always and for being incredibly understanding, especially in the last few weeks. A big thank you to Dad, for all the helpful advice over the years about how to be a functional working adult, and to my sister Bethan for teaching me all about action potentials! And a special thanks to Mum, you've been incredible. Not only were you always interested in my work, and listened to whatever problems I was having on any given day, you also let us move in when we had to leave the place we were renting. It took so much stress out of the situation to know we had somewhere to go, so I can say for sure that this thesis is better for all the help you've given. Lastly, a special mention goes to little Ruby and Jasper and the furry cuddles that got me through many hard times. I miss you both loads.

# Contents

# Chapter 1

# Introduction

Functional neuroimaging data are incredibly rich in information, reflecting the enormous complexity of the human brain. By performing complex analysis, it is possible to disentangle the information contained within these datasets to learn about how the brain works, and how its function is affected by disease. One functional neuroimaging technique that has made large contributions to our understanding of the brain is magnetoencephalography (MEG). This is a non-invasive imaging method based on measuring the magnetic fields that are generated by electrical brain activity. It has good spatial resolution and excellent temporal resolution allowing the investigation of brain activity on the millisecond timescale.

The most prominent signals in MEG data are generated by many neurons acting in synchrony, which manifest as oscillations. MEG data is therefore traditionally considered in terms of oscillatory frequency within different frequency bands. However, while oscillations are periodic and thus highly regular, most brain activity appears to be more disorderly. In fact, recent research has indicated that a certain level of irregularity is crucial for healthy brain function, and that too much or too little regularity is associated with mental disorder. This largely ignored aspect of MEG signals has the potential to provide a complementary view of brain function compared to measures of oscillatory activity.

One limitation that is common to all MEG research is a reduced sensitivity to activity that occurs deeper within the brain. Therefore, MEG research has often focused on activity in more superficial brain regions. In recent years, it has been established that it is possible to detect activity within the hippocampus using MEG. However, the spatial resolution of functional images in deep brain structures is reduced due to the lower signal strength from these brain regions. Improvements to

the depth sensitivity of MEG would be highly beneficial for the further study of activity within deep brain structures in health and disease.

The studies described during this thesis were performed with the aim of addressing these limitations of MEG research, through the development of novel analysis methods. The rest of this chapter goes on to introduce concepts surrounding the measurement and analysis of MEG data that are relevant to these studies, and to further illustrate the motivations behind them.

## 1.1 What does MEG measure?

The human brain is composed of billions of interconnected cells, called neurons, which communicate in large networks via the transmission of electrical signals. Neurons receive signals from other connected cells via the transmission of chemicals known as neurotransmitters. Transmission occurs at synaptic connections, which are located on branches called dendrites, as illustrated in Figure 1.1A. When a neurotransmitter is transmitted from the 'presynaptic' neuron, it may be received by a receptor on the 'postsynaptic' neuron. This causes channels to open in the cell membrane which allow ions to enter or exit the cell. This changes the potential difference between the interior and exterior of the neuron, and is referred to as the postsynaptic potential. The flow of ions through the dendrite is known as the primary current, and can be modelled as a current dipole. The movement of charge generates a magnetic field, $b$, as illustrated in Figure 1.1B. MEG (Cohen, 1972) is the non-invasive measurement of these magnetic fields. As the magnetic fields induced by the postsynaptic potential are a direct and immediate result of neuronal activity, MEG has excellent temporal resolution. It is therefore well suited for investigating the fast changing dynamics of brain activity.

The magnetic fields generated by the brain are extremely weak. MEG signals are on the order of $10^{-15}$T, which is approximately $10^{10}$ times weaker than the magnetic field of the Earth. The most commonly used MEG sensors are Superconducting Quantum Interference Devices (SQuIDs), which are highly sensitive magnetic field

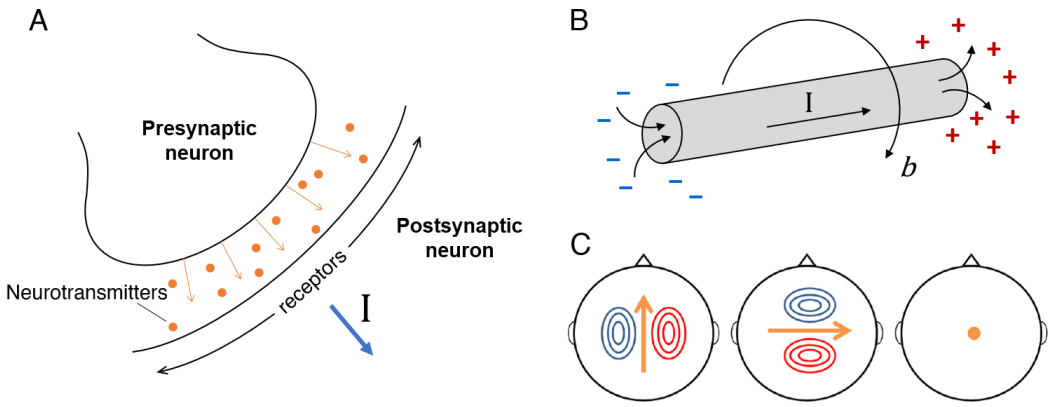


FIGURE 1.1: A) Transmission of neurotransmitters at a synapse, which induces a postsynaptic potential and results in the primary current, *I*. B) An illustration of the primary current flow through a dendrite and the induced magnetic field, *b*. C) An illustration of the magnetic fields detected by MEG for current sources of different orientations (taken from Routley, Hamandi, and Singh, 2017, adapted from Singh, 2006). The left two plots show the field patterns observed for tangentially oriented current dipoles. The plot on the right shows a radial source, which is invisible to MEG sensors. Blue lines indicate negative field (field lines coming out of the scalp) and red indicates positive field (field lines going into the scalp).

sensors that are capable of detecting the tiny fields generated by the brain. However, as the magnetic fields generated by outside sources, such as the Earth's magnetic field or nearby electronic devices, are so much larger than these neural signals, heavy noise suppression is necessary to stop the signals from the brain being overwhelmed. The majority of outside noise is reduced by performing MEG in rooms with magnetic shielding. Further noise suppression is often performed at the sensors. SQuID sensors work by measuring the current induced in one or more pick up coils, which is used to determine the causal magnetic field. Sensors that contain a single pick up coil are called 'magnetometers', whereas those that contain multiple pick up coils are known as 'gradiometers' and have the built-in ability to suppress outside noise signals. One example of a common gradiometer coil configuration is the axial gradiometer. A first order axial gradiometer consists of two coils of opposing current, as shown in Figure 1.2. Gradiometers take advantage of the fact that magnetic field strength decreases with distance from a current source as an inverse square law. Signals from noise sources at a large distance from a given gradiometer will induce similar currents in each loop, whereas the field generated by a source inside the head would more rapidly decrease in strength between the loops, and would induce a larger current in the loop closer to the source. The magnetic field

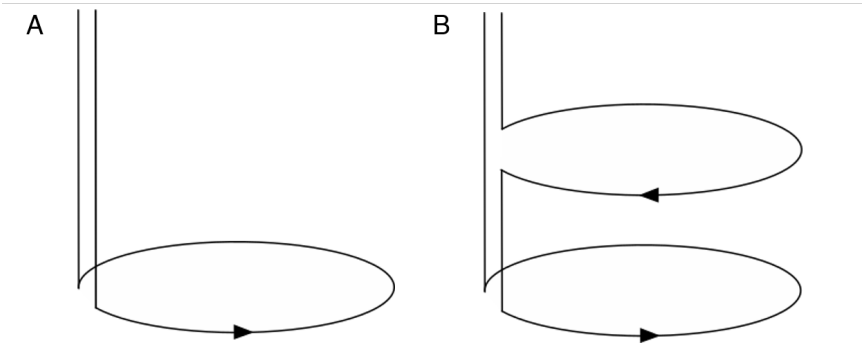


FIGURE 1.2: Coil configurations of a magnetometer (A) and a first order axial gradiometer (B). The arrow heads indicate the direction of induced current flow within each loop.

measured by a SQuID gradiometer is found using the difference between the current induced in each of the pick up loops, and therefore gradiometers are more likely to suppress magnetic fields from sources outside the brain.

Gradiometers with more pick up coil loops can be used to correct for higher order magnetic field gradients. However, this increases the distance between the coil loops (the 'baseline'), which reduces the amount of noise suppressed by the gradiometer. Conversely, using gradiometers with a smaller baseline reduces the sensitivity to sources deeper in the brain. To reach a balance between noise suppression and depth sensitivity, higher order gradiometers can be simulated using software from first order gradiometer measurements (Vrba and Robinson, 2001). To do this, several magnetometers are positioned at a larger distance from the head than the gradiometer sensors. Recordings are taken simultaneously at the gradiometers and these reference sensors. A weighted projection of the reference sensor recordings is then subtracted from the measurements taken at each gradiometer. The use of synthetic higher order gradiometers gives improved noise rejection compared to first order gradiometers, while maintaining the sensitivity to activity within deep brain structures.

Even while using heavy shielding and noise suppression from gradiometers, the fields induced by a single neuron are still too small to be detected at the scalp. However, when large numbers of neurons (approximately 10,000-50,000 (Murakami and Okada, 2006)) fire in synchrony, the fields become measurable using MEG. Therefore, the signals measured by each MEG sensor represent a superposition of signals

originating from large neuron populations. The largest contribution to the MEG signal is thought to be made by pyramidal neurons. This is a common type of neuron, named for the pyramid-like shape of their cell bodies. They are oriented perpendicular to the surface of the brain and so the dendrites of neighbouring cells are aligned roughly parallel to each other. This results in the ionic current underlying postsynaptic potentials flowing in the same orientation across large numbers of cells. The induced magnetic fields can therefore constructively interfere, and the sum of the fields can become measureable by MEG sensors.

Postsynaptic potentials are not the only source of the magnetic fields generated by neuronal activity. Magnetic fields are also generated by the current flow that occurs during 'action potentials'. This term refers to the large and rapid potential difference change that occurs when a neuron 'fires', which transmits along the length of the cell. This results in the transmission of neurotransmitter signals to other neurons connected downstream. However, the magnetic fields induced by action potentials occur over the time scale of a few milliseconds. Therefore, these are unlikely to occur in synchrony across large numbers of neurons, and so are unlikely to produce a measureable magnetic field at the scalp. Also, during an action potential, the ion flow that occurs during the initial potential difference change, or 'depolarisation', is quickly followed by the 'repolarisation' of the cell, where the ion flow reverses. As the action potential transmits along the length of the cell, this results in a repolarisation ion flow following close behind the depolarisation ion flow. The induced magnetic fields are equivalent to those produced by two current sources that are located very close together but flowing in opposite directions, which can be modelled as a quadripole. The magnetic fields induced by a quadripolar generator drop off very quickly with distance (Singh, 2006). Therefore, the magnetic fields generated by action potentials are unlikely to contribute to the MEG signal.

### 1.1.1 Limitations of MEG

The sensitivity of MEG is not uniform across the cortex. As shown in Figure 1.1C, MEG is insensitive to the fields produced by radial sources, i.e. current flow that is oriented perpendicular to the scalp. In a spherical conductor, the induced fields by a radial current source would be completely invisible to MEG sensors, and the

sensitivity of MEG is still greatly reduced for radial current in more realistic head models (Jongh et al., 2005). MEG is also less sensitive to activity originating deeper in the brain, as magnetic field strength drops off rapidly with distance from the source.

The most commonly used MEG sensors, Superconducting Quantum Interference Devices (SQuIDs), need to be held in a fixed sensor array where they can be cooled by liquid helium. Subjects are required to remain completely still during scanning to remain stationary relative to the sensors. A relatively new type of sensor, called the Optically Pumped Magnetometer (OPM) has reduced these practical issues with MEG, as these can operate at room temperature and can be placed directly on the scalp (Boto et al., 2018). However, these are not yet widely used in MEG research. All MEG data collection for studies in this thesis was performed using SQuIDs.

## 1.2 Source reconstruction

While MEG recordings can be directly analysed, in what is known as sensor space analysis, this gives little information about the location of the underlying activity. However, it is possible to estimate the distribution of current across the brain. This is known as source localisation or source reconstruction.

### 1.2.1 The forward problem

Once the magnetic fields have been measured across the surface of the head, the next challenge is to convert the two dimensional field map into a three-dimensional reconstruction of the activity within the brain. The first step to achieving this is to calculate the expected fields that would be measured for a current dipole of known magnitude and location. This is known as solving the 'forward problem'.

To spatially localise brain activity, it is necessary to model the expected magnetic field measurements for current dipoles at many different locations in the brain. The brain is split up into small volume elements, called voxels, which are usually a few $mm^3$ in size. By solving the forward problem for a current dipole within each voxel, a matrix known as the 'lead field', $\mathbf{L}$, is obtained. Each row of the lead field matrix contains the expected field strengths measured at each detector due to a unit current

dipole within a different voxel. With small enough voxels, it can be assumed that any field distribution at the sensors, due to current density distribution, $\mathbf{Q}$, can be modelled by a weighted sum of the field maps contained in the lead field, as written in equation 1.1.

$$\mathbf{B}(t) = \underline{\mathbf{L}}\mathbf{Q}(t) \tag{1.1}$$

The calculation of the field maps contained within the lead field depends on the way in which the electromagnetic properties of the head are modelled. There are many different ways of modelling the head, which vary in complexity. The simplest methods model the head as a spherical conductor, which can be used to obtain analytical solutions for the expected magnetic fields. Other, more realistic methods of modelling the head include the boundary-element method (BEM) and the finite-element method (FEM). BEM models the head as a series of two-dimensional surfaces that split up areas of different conductivity, usually using anatomical MRI data to create realistic surfaces. FEM divides the head model using three-dimensional shapes rather than surfaces, and so can be used to produce more complex models. Magnetic fields are almost unaffected by the media they pass through, and so a sufficiently realistic magnetic forward model can be calculated based on a head model composed of a single conductive compartment (Huang, Mosher, and Leahy, 1999). Throughout this thesis, the magnetic forward model has been calculated using BEM with a single-shell head model.

### 1.2.2 The inverse problem and beamforming

The inverse problem involves going backwards from the measured field distribution to the current density distribution in the brain, i.e. localising activity based on MEG or EEG data. Ideally, we would solve the equation 1.2 to calculate the current distribution from a given set of field measurements.

$$\mathbf{Q}(t) = \underline{\mathbf{L}}^{-1}\mathbf{B}(t) \tag{1.2}$$

However, for any given field distribution, there are an infinite number of possible current distributions, as magnetic fields can cancel out if there are current sources

flowing in opposite directions. The result of this is that the lead field matrix is a singular matrix and so the inverse doesn't exist. Therefore, there is no perfect solution to the inverse problem; it is said to be 'ill-posed'. To produce a single estimation of the current distribution across the brain, inverse solutions need to make realistic assumptions about brain activity.

One popular method of source reconstruction, that has been used widely and successfully in MEG research, is beamforming. Beamforming uses a spatial filter to minimise the total power calculated across the whole brain, while keeping the power coming from the location of interest (Van Veen et al., 1997).

Firstly, the inverse of the lead field in equation 1.2 is replaced by an array of weighting parameters, $W$. Equation 1.3 shows the inverse equation for one voxel, $a$, used to obtain an estimate of the current density distribution, $\mathbf{Q}'$

$$\mathbf{Q}'(a,t) = \mathbf{w}(a)\mathbf{B}(t) \tag{1.3}$$

The weights are defined by minimising the current density outside of voxel $a$, as written in equation 1.4, where the lower case $\mathbf{l}$ denotes the lead field vector corresponding to single voxel, $a$.

$$\min_{w}(\mathbf{Q}'^{2}) \; subject\; to\; \mathbf{w}(a)\cdot\mathbf{l}(a) = 1 \tag{1.4}$$

The constraint $\mathbf{w}(a)\cdot\mathbf{l}(a) = 1$ comes from the fact that the lead field is the model of magnetic field or electric potential distribution due to unit current flow at $a$. If $\mathbf{L}$ is substituted into equation 1.3 instead of the vector containing the MEG measurements, we should calculate a current flow of 1A at $a$. Solving for $\mathbf{w}$ yields the expression in equation 1.5.

$$\mathbf{w}(a) = \frac{\mathbf{C}^{-1}\mathbf{l}(a)}{\mathbf{l}^{T}(a)\mathbf{C}^{-1}\mathbf{l}(a)} \tag{1.5}$$

$C$ is the matrix of covariance, which is a measure of the similarity between the MEG measurements across sensors. The accuracy of the beamformer weights is dependent on obtaining an accurate estimate of the covariance. The error in the covariance matrix can be reduced by calculating the covariance based on the maximum possible number of recorded samples (Brookes et al., 2008).

Covariance matrices calculated from MEG data are often close to singular, which can also lead to unreliability in the calculation of the weights. To counter this, beamformers can be regularised by replacing the covariance matrices with the regularised covariance, $\mathbf{C}_r$, as in equation 1.6.

$$\mathbf{C}_r = \mathbf{C} + \mu\nu^2\mathbf{I} \tag{1.6}$$

$\nu^2\mathbf{I}$ represents the noise covariance matrix, where $\nu$ is the uncorrelated noise power at the sensors and $\mathbf{I}$ denotes the identity matrix (Brookes et al., 2008). $\mu$ is the regularisation parameter, which is a tunable quantity. By increasing the regularisation parameter, the covariance matrix is more strongly affected by regularisation. This results in smoother functional images that have higher SNR but reduced spatial resolution. Throughout this thesis, the regularisation parameter was kept constant at $\mu = 0.05$.

**Vector beamforming**

As shown in Figure 1.1, the magnetic field measurements at the sensors depend on the orientation of the current. Therefore, the calculated lead fields depend on the orientation of the modelled current dipoles. A vector lead field, $\mathbf{l}_{vec}$, is calculated by finding the expected field strengths for a dipole in three orthogonal directions at each voxel, $a$.

$$\mathbf{l}_{vec}(a) = \begin{bmatrix} l_{x1} & l_{y1} & l_{z1} \\ l_{x2} & l_{y2} & l_{z2} \\ & \vdots & \\ l_{xN} & l_{yN} & l_{zN} \end{bmatrix} \tag{1.7}$$

However, as the fields produced by radial current sources are invisible to MEG, the MEG sensors only measure a two-dimensional projection of the fields generated by the brain. Therefore, it makes no physical sense to include a magnetic lead field with three dimensions. The weakest component must be removed, at each voxel, to produce two-dimensional lead fields. Equation 1.3 can then be solved twice to estimate the components of current at each voxel along each remaining direction.

This process can be used to estimate the magnitude and direction of the current within each voxel, and is known as vector beamforming.

#### Scalar beamforming

Functional images with higher SNR and improved spatial resolution can be produced if the orientation of the current source within each voxel is accurately estimated and used in the calculation of the lead field (Sekihara et al., 2004). Beamformers which use a single estimated current dipole orientation for which to model the lead fields for each voxel are known as scalar beamformers. For each voxel, the most likely orientation of the dipole is estimated by finding the direction along which there is the highest variance in current. This can be found by obtaining an initial estimate of the source power using a vector lead field and then using principal component analysis to find the orientation along which the source power exhibited maximum variance (Brookes et al., 2008). Scalar lead fields can then be calculated by multiplying the vector lead fields by the unit vector aligned with the estimated orientation of the current within each voxel.

#### Normalisation

The SNR of beamformer images decreases with depth. This means that towards the centre of the brain, functional images are often dominated by noise power which overwhelms activity of interest (Vrba and Robinson, 2001). The beamformer weights can be normalised to counteract this, for example by dividing the weights by their vector norm (Cheyne et al., 2007).

#### Pros and cons of beamforming

There are a number of advantages of beamforming. It requires no a priori information about the number of sources or their positions or orientations. The use of a spatial filter also serves to suppress outside noise (Vrba, 2002). The main limitation of beamforming is that the algorithm assumes that activity at each location in the brain is temporally uncorrelated. This means that activity occurring in perfect synchrony at multiple areas of the brain will be suppressed by the beamformer algorithm.

Another limitation of beamformer images, which is common to all inverse solution algorithms, is that the spatial resolution is fundamentally limited by the number of MEG sensors used (Singh, 2006). MEG studies will often estimate current at thousands of locations in the brain. However, most MEG systems have only a few hundred sensors. This produces an underdetermined system which limits the number of unique, uncorrelated activity timecourses which can be detected. This leads to MEG functional images being 'blurry', where activity originating from a single location can be dispersed in an image. This phenomenon is known as source leakage. MEG functional images have a maximum spatial resolution of around a few millimetres (Barratt et al., 2018).

## 1.3 Source analysis

Once the inverse problem has been solved, and the current distribution across the brain has been estimated, the activity at each location can be analysed to interrogate its spatio-temporal properties. This is known as source analysis, or source space analysis (as opposed to sensor space analysis). This section briefly introduces some features of brain activity which have been previously investigated via MEG source analysis and which have served as a starting point for the analysis methods developed in this thesis.

### 1.3.1 Virtual sensors

One common approach to source analysis is to start by reconstructing activity timecourses at each location in the brain, which can be produced at the same temporal resolution as the recorded data. These are often referred to as 'virtual sensor' timecourses as they give an estimate of what would be recorded by an MEG sensor implanted at that location. The generation of these is a necessary step for many analysis methods.

### 1.3.2 Oscillations

Oscillatory activity has been observed in the brain since the earliest EEG recordings (Berger, 1929). Oscillations compose some of the most prominent features in EEG

and MEG data and thus have been the subject of much research. It has been found that activity within different frequency ranges is associated with different aspects of brain function, levels of arousal and disease states. Therefore, oscillatory activity is often considered in terms of discrete frequency bands. There are no fixed boundaries to these frequency bands, but previous studies have generally split oscillatory activity in the 1-100Hz range roughly into the following bands: the delta band (1-4Hz), the theta band (3-8Hz), the alpha band (8-13Hz), the beta band (13-30Hz) and gamma band oscillations (>30Hz). A full discussion of the functional role of oscillations will not be covered here. However, one purpose of oscillations that is of relevance to this thesis is that the synchronisation of oscillatory activity is thought to provide a mechanism for the communication between brain regions (Fries, 2005).

### 1.3.3 Neural 'irregularity'

Information theory states that periodic activity, such as oscillations, are low in information content, whereas the most information is encoded in completely random (white) noise, as this is entirely unpredictable (Shannon, 1948). The amount of information carried by a signal can be quantified using measures of signal entropy. More 'irregular', high entropy signals are less predictable and therefore carry more information, whereas more regular, low entropy signals are more predictable and carry less information.

The irregular, constantly fluctuating activity present in the brain even when it is supposedly 'at rest' is less often studied than oscillatory signals and is often dismissed as neural 'noise'. However, recent research suggests that irregular activity is crucial for the brain to process information (Deco, Jirsa, and McIntosh, 2011; Protzner et al., 2010; Takahashi, 2013; Garrett et al., 2013). It has been shown that neural irregularity changes throughout the lifespan (McIntosh et al., 2014), and is altered in patient groups. Activity that is either too regular or too variable is associated with disorder (Protzner et al., 2010; Takahashi, 2013; Brookes et al., 2015; Ghanbari et al., 2015).

While the physiological role of irregularity in the brain is not certain, it is possible that it is related to levels of synchronisation between cortical regions, i.e. connectivity. The synchronisation of oscillatory activity, which is highly regular, is currently

the most promising mechanism for connectivity between brain regions (Schnitzler and Gross, 2005; Fries, 2005; Donner and Siegel, 2011; Brookes et al., 2011a; Hillebrand et al., 2012; Tewarie et al., 2019). In contrast, it is thought that local information processing performed within segregated brain regions is associated with signals that contain high levels of information and therefore are more irregular (Tononi, Sporns, and Edelman, 1994; Friston, Tononi, and Edelman, 1996). However, recent studies have hinted at a more complex role of irregularity in the brain. Links have been found between the functional connectivity and signal complexity exhibited by a region (Wang et al., 2018; Ghanbari et al., 2015), but the direction of the relationship has been found to depend on the time scale over which the complexity was calculated. It has been suggested that complexity at high frequencies is more associated with local processing, whereas complexity at low frequencies is associated with more distributed processing between brain regions (Vakorin, Lippe, and McIntosh, 2011; McIntosh et al., 2014; Wang et al., 2018).

The 'irregularity' of a signal can be quantified using measures of entropy. There are many methods which have been proposed for measuring the entropy of neuronal signals (Garrett et al., 2013). However, the majority of these measure entropy over long signal epochs. In contrast, rank-vector entropy (RVE) can show how the entropy of an activity timecourse changes over time (Robinson et al., 2013), giving timecourses with the same temporal resolution as the original signal. RVE has been shown to distinguish the activity of schizophrenia patients from healthy controls, and to give complementary information to that given by measures of oscillatory activity (Brookes et al., 2015). RVE therefore shows promise as a measure for investigating neuronal irregularity that can take advantage of the high temporal resolution of MEG data.

### 1.3.4 Complexity

Entropy measures are maximal for completely unpredictable, random signals (i.e. white noise). However, the complexity of brain activity emerges from the interplay between the information processing performed by segregated brain regions and the integration between these brain regions (Tononi, Sporns, and Edelman, 1994). There are a number of measures which have been developed to quantify signal complexity

(Tononi, Sporns, and Edelman, 1994; Costa, Goldberger, and Peng, 2005). Such measures show low complexity for completely regular or completely random signals, whereas higher complexity is associated with signals that contain 'meaningful structural richness' (Grassberger, 1991). For example, Multi-Scale Entropy (MSE) exhibits higher complexity values for signals with a 1/f power spectrum, which exhibit complex structures across a range of time scales, compared to white noise time-courses (Costa, Goldberger, and Peng, 2005).

Confusingly, the term complexity has also been used to refer to different quantities related to signal entropy, including RVE. The justification for this is that RVE measures temporal fluctuations in the rate of information within a signal, rather than the information contained within a whole signal (Robinson et al., 2013). However, in contrast with the previously mentioned complexity measures, RVE increases monotonically with the level of randomness in a signal. Therefore, to avoid confusion, the term 'irregularity' has been used throughout this thesis to refer to levels of neuronal RVE.

### 1.3.5 Resting state functional connectivity

While the brain consists of regions that are specialised for specific functions, communication of information between these brain regions is fundamental to cognition. This communication is often investigated in terms of functional connectivity, which refers to finding the statistical dependence between activity in spatially separate brain regions. One area of research that is growing in popularity is concerned with the brain networks that are active even while participants are at rest (Heuvel and Pol, 2010). One resting state network, known as the default mode network (DMN), has even been shown to be more active when participants are at rest compared to during a task (Raichle et al., 2001). Alterations in resting state networks have been found in a variety of mental disorders, including epilepsy (Koelewijn et al., 2015), autism spectrum disorder (Hull et al., 2017; Fan et al., 2018), schizophrenia (Friston et al., 2016), Alzheimer's disease (Stam et al., 2006) and others. The ability to investigate brain function using resting state data is ideal as the experiments are simple to set up and perform, and so are suitable for all participant groups, including children and patient groups.

Research on resting state functional connectivity began with PET and fMRI studies. However, in recent years, MEG has been used to investigate the electrophysiological activity underlying the network communication. MEG studies have detected functional connectivity that show high similarity to those found in fMRI studies by measuring the synchronisation of oscillatory activity (Brookes et al., 2011a; Hillebrand et al., 2012). One popular functional connectivity measure that has measured network connectivity with the highest level of consistency between healthy participants is oscillatory amplitude envelope correlation (AEC) (Brookes et al., 2011a; Hipp et al., 2013). This method defines functional connectivity as the synchronisation of amplitude fluctuations of oscillatory activity in discrete frequency bands. It has been used to detect alterations in network connectivity in a variety of patient groups (Andreou et al., 2015; Koelewijn et al., 2015; Koelewijn et al., 2019; Dima et al., 2020).

## 1.4 Multi-modal imaging

While most functional imaging research is carried out using a single imaging technique, often the combination of different modalities can provide complementary information due to their different relative sensitivities.

### 1.4.1 MEG and fMRI

Blood Oxygen Level Dependent functional Magnetic Resonance Imaging, or BOLD fMRI, is an alternative non-invasive method of measuring brain activity. It works by measuring an increase in the oxygen level present in the blood surrounding areas of active cortex (Ogawa et al., 1992). It is a highly popular functional imaging technique due to its excellent spatial resolution (approximately 1mm). However, it lacks the temporal resolution of MEG and EEG as the haemodynamic response is an indirect and delayed effect of neuronal activity.

A limitation of fMRI research is that the coupling between neuronal activity and the resulting BOLD response is complex and still not fully understood (Singh, 2012;

Hall et al., 2014). Therefore, the understanding that can be gained from fMRI functional images is currently limited. Unfortunately, MEG and fMRI cannot be measured simultaneously, but studies implementing the same task during MEG and fMRI scans have begun to elucidate the neurovascular relationship (Hall et al., 2014). Some studies have found spatial overlap between task-related oscillatory power changes and BOLD activation. An increase in BOLD signal was found to be associated with a desynchronisation of oscillations in the alpha and beta frequency bands, leading to decreased power in these bands, but a synchronisation at higher, gamma band frequencies (Singh et al., 2002; Moradi et al., 2003; Brookes et al., 2005). In studies investigating the temporal correlation between BOLD timecourses and oscillatory power envelopes, negative correlation has been observed with power in the alpha and beta bands, whereas positive correlation has been observed with gamma band power (Mukamel et al., 2005; Zumer et al., 2010; Conner et al., 2011). However, other studies have found inconsistencies in these relationships. For example, it has been found that gamma amplitude increases in the visual cortex vary with certain properties of a visual stimulus, such as spatial frequency and colour, whereas the BOLD response does not (Muthukumaraswamy and Singh, 2008; Muthukumaraswamy and Singh, 2009; Swettenham, Muthukumaraswamy, and Singh, 2013). These findings indicate that the coupling between the BOLD signal and underlying neuronal activity is complex and that measures of oscillatory activity alone may not be sufficient to describe the relationship.

### 1.4.2 MEG and EEG

Electroencephalography (EEG) (Berger, 1929) is the measurement of the electrical potentials generated by neuronal activity. Both EEG and MEG signals are mostly generated by postsynaptic potentials in pyramidal neurons. However, whereas MEG signals are generated by ionic current within neurons, the electric potentials detected by EEG are generated when ions exit neurons into the 'extracellular milieu'. When lots of ions of the same charge enter into the extracellular milieu together, the resulting electric potential may conduct to the scalp. This process is known as volume conduction. If an EEG electrode is in contact with the scalp nearby, a change in the potential difference between the electrode and a reference electrode may be detected.

While the same underlying neuronal activity is the source of both EEG and MEG signals, there are differences between the properties of the magnetic fields and electric potentials measured at the scalp. MEG can achieve better spatial resolution than EEG as electric potential measurements at the scalp are distorted due to the inhomogeneous conductivity of the head, whereas magnetic fields are relatively unaffected (Baillet, 2017). Therefore, EEG is rarely measured in MEG studies. However, EEG has the potential to provide complementary information beyond that available from MEG alone. For example, while MEG is insensitive to radial sources, EEG is most sensitive to radial sources and least sensitive to those parallel to the scalp. EEG also has greater sensitivity to deeper sources (Jongh et al., 2005). It has been found in many previous studies that source reconstruction using combined MEG and EEG, or MEEG, can give improved localisation accuracy than either modality alone (Dale and Sereno, 1993; Fuchs et al., 1998; Baillet et al., 1999; Ko and Jun, 2010; Babiloni et al., 2001; Liu, Dale, and Belliveau, 2002; Sharon et al., 2007; Henson, Mouchlianitis, and Friston, 2009; Hong et al., 2013; Aydin et al., 2015; Chowdhury et al., 2015). A more detailed discussion of the potential complementarity of MEG and EEG is given in chapter 6.

## 1.5 Thesis overview

In **chapter 2**, Rank-Vector Entropy (RVE) is used to measure the variability of simulated pink noise and real resting state MEG data. The tunable parameters of the measure are optimised to maximise temporal resolution and the correlation between RVE and oscillatory amplitude. In **chapter 3**, the relationship between neuronal activity and the associated haemodynamic response is investigated by relating the RVE of MEG signals to the BOLD response. In **chapter 4**, Multi-scale rank-vector entropy (MRVE) correlation is introduced as a novel method of measuring functional connectivity. This is then used to detect resting state connectivity in healthy participants that are consistently strong across participants and that vary across temporal scale. In **chapter 5**, MRVE correlation is used to investigate functional connectivity alterations in patients that are at genetic risk of developing neurodevelopmental disorders, such as schizophrenia. The effects of removing eye movement artefacts

on the resulting connectivity measurements are also examined. In **chapter 6**, an attempt is made to improve upon the depth sensitivity of MEG by performing source reconstruction using simultaneous MEG and EEG, with the aim of localising activity within the medial temporal lobe (MTL).

# Chapter 2

# Optimising neuronal irregularity measures

In recent years, a growing number of studies have found alterations in the 'irregularity' of brain activity associated with disease, aging, and cognitive tasks (Garrett et al., 2013). However, there has been no investigation of how to optimise irregularity measures to utilise the excellent temporal resolution of MEG data. Rank-vector entropy (RVE) was developed by Robinson et al., 2013 to observe the spatio-temporal dynamics of neuronal signal irregularity, and can be used to calculate irregularity timecourses that retain the temporal resolution of MEG data. In this chapter, the RVE of simulated pink noise and resting state MEG data was calculated while varying two of the method's tunable parameters: the decay time constant, $\tau$, and the sliding window length, $W$. It was found that altering these parameters affected the SNR and temporal resolution of the resulting RVE timecourses. A biphasic relationship was also found between RVE and oscillatory amplitude of MEG signals across all parameter sets. Negative correlation was found with lower frequency bands (delta-beta), which was strongest with beta band amplitude. In contrast, a positive correlation was found between RVE and gamma band amplitude. The choice of parameter set was found to affect the strength of these relationships, and optimal parameter sets were identified that gave the strongest positive ($\tau$=0.04s, $W$=4) and negative ($\tau$=0.06s, $W$=5) relationships between RVE and oscillatory amplitude.

## 2.1 Introduction

As the electric and magnetic fields generated by individual neurons are extremely weak, much of MEG and EEG signal analysis concentrates on activity that is synchronised across large neuron populations, such as low frequency oscillatory activity. This synchronised activity produces signals that are strong enough to detect at the scalp due to the constructive interference of the generated fields. However, considering only this high amplitude activity offers an incomplete view of brain function. The other, less studied aspect of MEG and EEG signals is the constantly fluctuating, seemingly 'random' activity present even when the brain is supposedly at rest. These signal components consist of a superposition of many lower power signals generated by smaller neuron groups acting independently. Such complex signals are often dismissed as neural noise but this irregularity is thought to be vital for healthy brain function (Deco, Jirsa, and McIntosh, 2011; Garrett et al., 2013). It has been shown that neural irregularity changes throughout the lifespan (McIntosh et al., 2014; Shumbayawonda et al., 2019), and is altered in patient groups, where activity that is either too regular or too variable is associated with mental health and neurological disorders (Protzner et al., 2010; Mizuno et al., 2010; Catarino et al., 2011; Takahashi, 2013; Brookes et al., 2015; Ghanbari et al., 2015; Monge et al., 2015; Bosl, Loddenkemper, and Nelson, 2017; Hall, 2017).

Entropy can quantify the irregularity of a signal by giving a measure of its 'unpredictability'. More irregular signals have larger entropy whereas more rhythmic signals, such as oscillations, have lower entropy. There are many possible ways of estimating signal entropy (Garrett et al., 2013). However, few of these can take advantage of the good spatial and excellent temporal resolution of MEG functional images (Robinson et al., 2013). In many EEG and MEG studies of neuronal irregularity, entropy has only been calculated at the sensor level, limiting the spatial information that can be gained. Entropy is also often only calculated over long signal epochs, giving no information about fluctuations in entropy over shorter time scales. One measure which was designed to capture the spatio-temporal properties of irregularity in the brain is Rank-Vector Entropy (RVE) (Robinson et al., 2013). RVE is a derivative of Shannon entropy (Shannon, 1948) that has a built-in ability to provide

a dynamic time-course of signal entropy, retaining the signal's original temporal resolution. It is also computationally efficient, is calculated from broadband activity time-courses, and is independent of signal amplitude (Robinson et al., 2013).

Recent studies have begun to show that RVE can provide insight into brain activity in health and disease, beyond what can be learned from more conventional measures. In healthy participants, Robinson et al., 2013 found that the evoked response after a frequent auditory stimulus was associated with a decrease in RVE. An increase in RVE was also detected after hearing rare stimuli, which began after the evoked response and persisted after any observed changes in spectral power. Brookes et al., 2015 investigated the relationship between RVE and oscillatory activity further, and found a biphasic relationship between RVE and oscillatory amplitude at three locations in the brain, where entropy correlated negatively with low frequency amplitude ($\lesssim 50Hz$), but positively with the amplitude of gamma band activity ($\gtrsim 50Hz$). RVE has also been shown to detect transient increases in the entropy of brain activity in schizophrenia patients during tasks, compared to healthy controls (Brookes et al., 2015). The measure was also found to be sensitive to reductions in entropy due to epileptiform activity (Hall, 2017).

An additional benefit of RVE, compared to other entropy measures, is the low number of tunable parameters that must be chosen (Robinson et al., 2013). However, there are several quantities that can be tuned to alter the properties of calculated RVE time-courses, such as the temporal resolution and the length of the sliding window used in the calculations. No investigation has yet been made into the effects of varying these parameters, and so it is unclear whether there are parameter choices that would optimise the ability of RVE to detect changes in neuronal irregularity. In this study, a range of values for each parameter were used to calculate the RVE of simulated pink noise, and the effects of varying these parameters on the resulting entropy time-courses were assessed. The RVE of resting state MEG virtual sensor time-courses was then calculated to further investigate the relationship between RVE and oscillatory amplitude across frequency bands. It was investigated whether the biphasic relationship found previously (Brookes et al., 2015) could be replicated and how this varies spatially across the brain. The effect of parameter

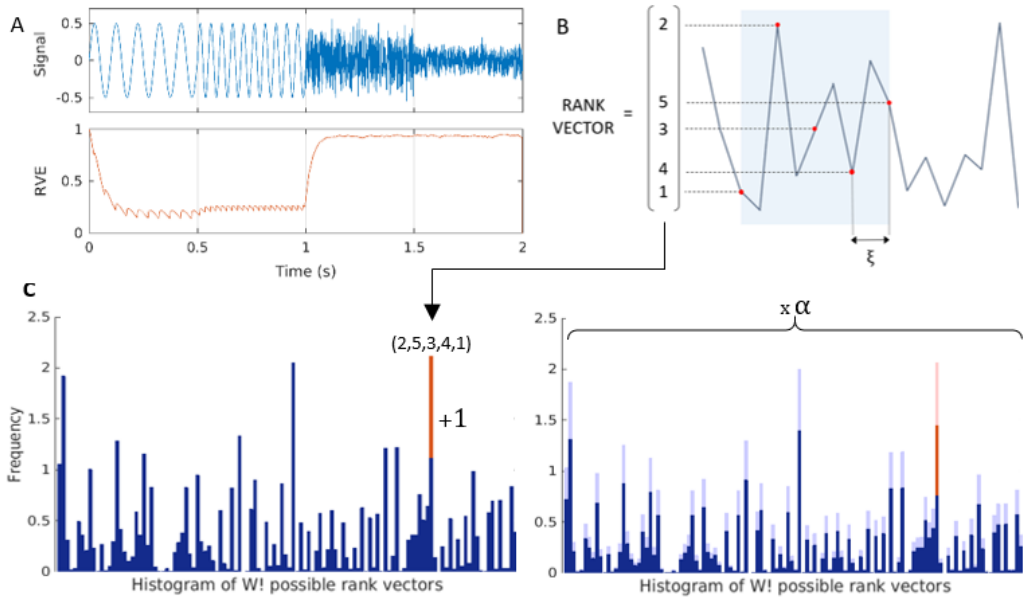


FIGURE 2.1: A) An example signal composed of sinusoidal and white noise components and the resultant RVE time-course. B) Illustration of an example rank-vector calculation. A sliding window of $W = 5$ points is taken, each separated by lag $\xi = 2$. These are then sorted in size, and converted to their original position in the window. C) An example rank-vector frequency distribution with a bin corresponding to each possible rank-vector. The left plot shows the distribution used to calculate the entropy at a time point at which the signal state is defined by rank-vector (2,5,3,4,1). The right plot illustrates the 'leaky integrator' which is applied before moving on to the next time point to introduce temporal resolution to the RVE measure. The distribution is multiplied by the constant factor, $\alpha$, to reduce the effects of states previously observed in the signal on future entropy calculations.

choice on the relationship between entropy and oscillatory amplitude was also examined. The 'optimal' set of values was then sought empirically both to maximise temporal resolution of the entropy time-courses, and to give the strongest relationship between RVE and oscillatory amplitude.

## 2.2 Methods

### 2.2.1 RVE

#### Method

The RVE method was first described by (Robinson et al., 2013). At each time point in a signal, $t$, a window of $W$ points is taken. Each is separated by a lag, $\xi$, where $f_s$ represents the sample rate, and $f_c$ is the lowpass frequency applied to the data.

$$\xi = \frac{f_s}{2f_c} \tag{2.1}$$

Therefore, the values taken to form each sliding window may be sampled at a lower frequency than the signal sample rate. For example, with a sampling frequency of $f_s = 600$Hz and a lowpass frequency of $f_c = 150$Hz, the sliding window values would be separated by a lag of $\xi = 2$. The lag would increase to $\xi = 4$ when data are recorded at a sample frequency of $f_s = 1200$Hz but filtered at the same lowpass frequency. This lag is introduced to avoid oversampling the signal. Any signal can be sampled at the Nyquist rate of $2f_c$ without any loss of the information contained within the signal (Robinson et al., 2013). Sampling at a higher frequency than this would lead to sampling at a higher frequency than any signal components containing information, which can artificially lower the calculated entropy values.

The $W$ points of the sliding window are ordered in size, and then converted to the position they originally held in the window. This is the 'rank-vector' associated with this time point, and is illustrated graphically in Figure 2.1b.

In a histogram showing the frequency distribution of all $W!$ possible rank-vector states, the frequency of the bin associated with the calculated rank-vector is increased by one. The state probability distribution, $P$, is calculated by dividing the histogram by the sum of the frequencies over all bins. This can then be used to calculate the Shannon entropy, $H$, at this time point using equation 2.2 (Shannon, 1948).

$$H(t) = \frac{1}{ln(W!)}(-P(t) \cdot ln(P(t))) \tag{2.2}$$

The multiplication by the constant $k = \frac{1}{ln(W!)}$ constrains the possible RVE values to the range of 0-1. Lower entropy values are obtained when the probability distribution shows bias towards a smaller number of states, indicating that there are patterns in the signal that occur relatively more frequently, and thus that the signal is less 'random' and more predictable.

Before the entropy calculation for the next time point is carried out, the frequency distribution is multiplied by constant factor $\alpha$, where $\tau$ is the decay time constant.

$$\alpha = e^{-1/\tau f_s} \tag{2.3}$$

This 'leaky integrator' is introduced so that RVE has a limited 'memory' of the

signal patterns that occurred previously in the signal, which allows RVE to detect changes in entropy over time. Without it, RVE calculations at each time point would represent the cumulative entropy over the signal up to that time point.

During this thesis, the $W$ points were taken going forward in time from sample $t$. However, the position of the sliding window, relative to sample $t$, can be varied. For example, for real time signal analysis it may be desirable to define the sliding window going backwards in time from the most recent sample. However, this would not affect the resulting RVE time-course, except for introducing a slight temporal shift.

#### Parameter selection

The value chosen for the decay time constant, $\tau$, determines the sensitivity of the RVE measure to fast changes in signal irregularity. As $\alpha$ will decrease with $\tau$, the effect of states found at previous time points will drop off more quickly with time when a smaller decay time constant is used. Thus, a smaller window of the signal before a given time point will have a significant effect on the entropy value calculated. The result of this is that the RVE measure will respond more quickly to changes in signal irregularity.

The sliding window length, $W$, determines the number of states that RVE can distinguish between. A longer window length will mean that there are more possible rank-vectors (the total number possible is $W!$) so the RVE measure will have higher 'state resolution'. However, this also means that the state frequency histogram is larger and will take longer to populate. Therefore, larger values of $W$ require the use of larger decay time constants, and so temporal resolution will suffer. Using a longer window also increases the computation time as each rank-vector must be compared to more possible states to find its corresponding histogram bin.

### 2.2.2 Data and analysis

#### MEG data acquisition

Resting state MEG data were collected as part of the '100 Brains' UK MEG Partnership project using a whole head 275-channel CTF axial gradiometer system. An additional 29 reference channels were recorded for noise cancellation purposes and

the primary sensors were analysed as synthetic third-order gradiometers (Vrba and Robinson, 2001). Subjects were seated upright in the magnetically shielded room with their head supported with a chin rest to minimize movement. Head localisation was performed at the beginning and end of each scan, using three fiducial markers attached to the nasion and the right and left preauricular sites.

Five-minute MEG scans were performed for 183 participants at a sample rate of 1200Hz. Inclusion criteria ensured all participants were aged 18-65, had completed or were undertaking a degree, had normal or corrected-to-normal vision, and had no history of neurological or neuropsychiatric disorder. Handedness was not used as an exclusion criterion. Handedness data were collected for 95 subjects in the cohort, 94 of whom were right handed. Subjects had been asked to rest and fixate their eyes on a central red fixation point, presented on either a CRT monitor or LCD projector.

Structural T1-weighted MRI scans were also acquired for each participant using a 3T General Electric or Siemens MRI scanner with a 1mm isotropic FSPGR/MPRAGE pulse sequence. Co-registration was performed manually between the MEG and MRI coordinate spaces; the fiducial locations were kept fixed relative to each participant's nasion, left and right ears and so could then be identified and marked on their MRI scan.

**Pre-processing and analysis**

A $4^{th}$ order two pass bandpass filter of 1-150Hz was applied to the MEG data, before downsampling to 600Hz, using the CTF 'newDs' function. Datasets were cut into 2 second epochs, which were each visually inspected and removed if they contained any major artefacts. No bandstop filter was used to remove 50Hz mains noise as the gradiometers and the beamformer spatial filter both suppress noise from sources which are at a large distance from the head.

To perform analysis in source space, MEG virtual sensor timecourses were obtained using a scalar LCMV beamformer (Van Veen et al., 1997) using FieldTrip (Oostenveld et al., 2011). Voxel locations were defined in MNI152 template space (Fonov et al., 2009) on a $6mm^3$ grid. These coordinates were then transformed to fit each participant's anatomical MRI. Thus, the voxel locations used for each participant were in the same location in template space. Lead fields were calculated using

a 'localspheres' head model, which models the head as a set of overlapping spheres (Huang, Mosher, and Leahy, 1999).

A bandpass filter was used to filter the data into eleven frequency bands (1-4, 3-8, 8-13, 13-30, 40-60, 60-80, 80-100, 100-120, 120-140, 140-160 and 60-140Hz). Covariance matrices were obtained using the narrow band data in each of these frequency bands, as well as using the broadband pre-processed data filtered between 1-150Hz. For all frequency bands, beamformer weights were normalised using the vector norm (Hillebrand et al., 2012). The virtual sensor current timecourses, concatenated over all epochs, were then calculated at each voxel for each frequency band.

RVE time-courses were calculated from the broadband, 1-150Hz current timecourses using a range of values for $\tau$ and $W$. Oscillatory amplitude envelopes were calculated using the timecourses for each of the ten narrower frequency bands by taking the absolute magnitude of the analytic signal using the 'hilbert' MATLAB function. The RVE time-courses and oscillatory amplitude envelopes were then downsampled to 2Hz, as it has been found previously that the synchronisation of oscillatory amplitude envelopes can be observed over slow time scales (Brookes et al., 2011a).

For each subject, oscillatory frequency band and set of RVE parameters, the Pearson correlation between the RVE and oscillatory amplitude envelopes was found at each voxel, and was converted to a z-score using the Fisher transform. To determine whether each correlation was significant, the 95% confidence interval of the z-scores was found across participants, at each voxel, using the 'tinv' MATLAB function. Voxels at which this interval did not span zero were taken to exhibit a significant relationship. The average z-score was taken at all voxels where this was the case and transformed back to a Pearson correlation coefficient.

#### Simulated data

MEG data was simulated by generating signals of pink noise, which are noise signals that exhibit a $1/f$ relationship on a power spectrum. This is similar to the spectrum of 'background' MEG data in the absence of peaks due to high amplitude oscillatory activity. Pink noise signals were simulated using the 'pinknoise' MATLAB function.

Signals were assigned a sample rate of 600Hz in accordance with the real MEG data and were filtered with a 1-150Hz bandpass filter. No downsampling was performed on the pink noise signals as the $1/f$ relationship is observed independently of sample rate (i.e. the signals are scale free).

## 2.3 Results

### 2.3.1 Optimising the temporal resolution of RVE on simulated data

First, the RVE of simulated pink noise was calculated to investigate how the choice of tunable parameters would affect the properties of the calculated irregularity time-courses. Optimal parameter combinations were then found by finding the value of $\tau$ which maximised the temporal information content of the RVE timecourses for each value of $W$.

Figure 2.2 shows an example pink noise signal and the corresponding RVE time-courses calculated using an array of values for $\tau$ and $W$. It can be seen that increasing $W$, for a given value of $\tau$, gives entropy time-courses with a lower mean value, and lower amplitude of fluctuations around the mean. On the other hand, decreasing $\tau$ was found to decrease the mean entropy value, but increase the amplitude of fluctuations around this mean value. It was also found to decrease the amount of time taken for the algorithm to 'warm up', indicating higher temporal resolution. However, using the lowest $\tau$ value with the longer window lengths led to a loss of the shape of the waveform.

To optimise the RVE parameters for temporal resolution, the lower limit on the decay time constant was found that can be used with each $W$ that still retains the entropy waveform. As a lower value of $\tau$ also increases the amplitude of entropy fluctuations, the lowest $\tau$ that will give an accurate measure of the entropy should give the RVE time-course with the maximum variance. Figure 2.2c shows the standard deviation of the RVE of pink noise signals, calculated using a range of values for $\tau$ for each window length, $W$. For each combination of parameters, RVE was found for 100 pink noise signals with a length of 20000 samples. Standard deviation was calculated using the second half of each RVE time-course, to avoid the 'warm up' period, and average values were taken across the 100 iterations. For each

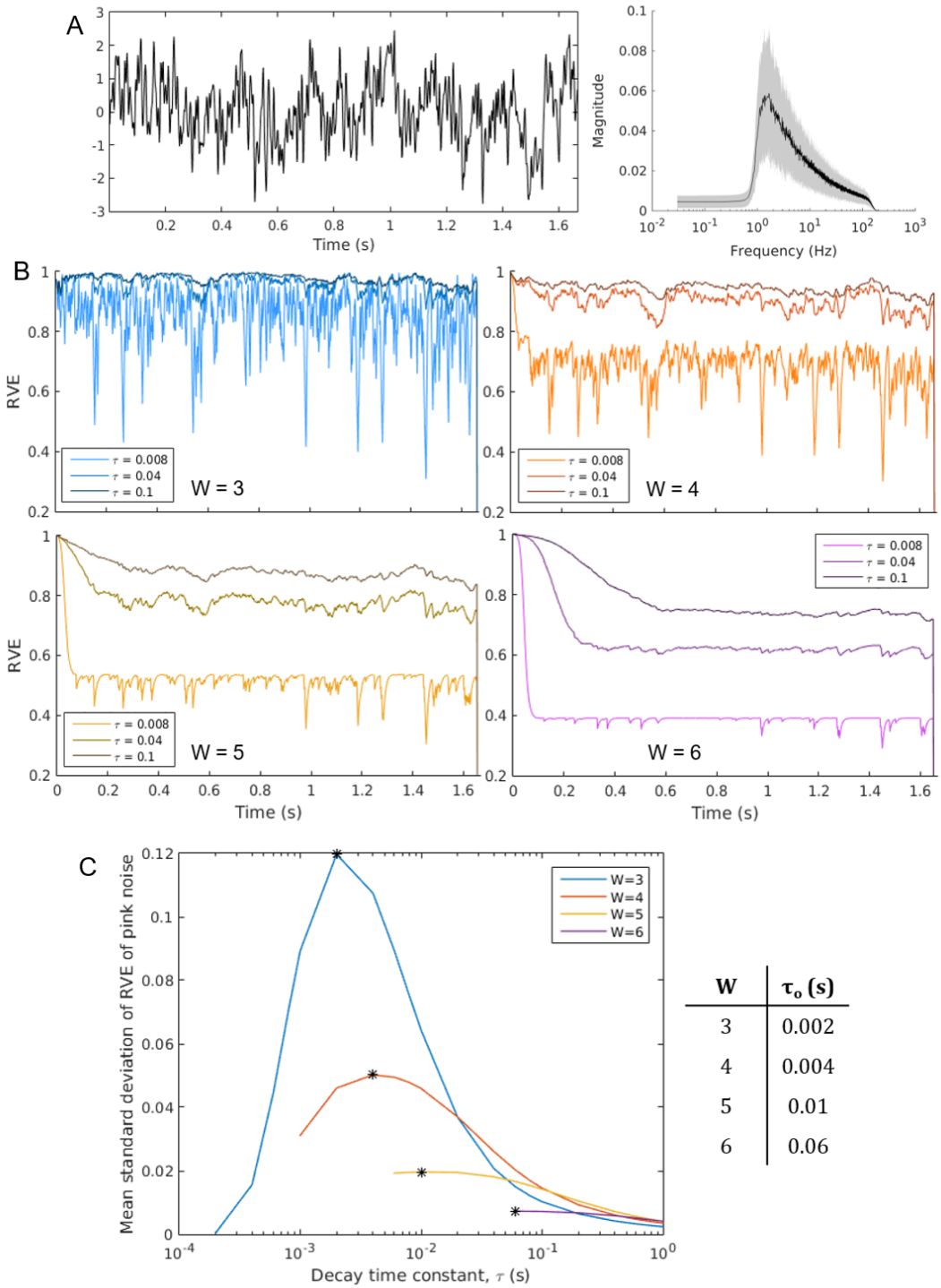


| W | $\tau_o$ (s) |
|---|---|
| 3 | 0.002 |
| 4 | 0.004 |
| 5 | 0.01 |
| 6 | 0.06 |

FIGURE 2.2: A) An example pink noise signal with the average Fourier spectrum, where the error band shows the standard deviation. B) The corresponding RVE time-courses calculated using a range of decay time constants, $\tau$, and sliding window lengths, $W$. C) The mean standard deviation of the RVE of 100 pink noise signals, with the peak for each value of $W$ marked by a black star. The corresponding $\tau$ values are given in the table.

window length, an optimal value for the decay time constant, $\tau_o$, was found that maximised the standard deviation of the RVE time-courses. These values are given in Figure 2.2c.

### 2.3.2 Optimising the relationship between RVE and MEG oscillatory amplitude

It was then investigated how RVE relates to oscillatory amplitude envelopes calculated from real MEG data to determine how irregularity relates to more classical measures of oscillatory activity. The effects of varying the RVE parameters were also assessed, and optimal parameter sets were found that maximised the strength of the relationship with amplitude in each frequency band.

The relationships between RVE and oscillatory amplitude in each frequency band were found for a range of values of $\tau$ and $W$. It was found that using a sliding window length of $W = 6$ was highly computationally expensive so a maximum value of $W = 5$ was included in the analysis.

Figure 2.3 indicates the combination of parameters for each frequency band that gives the strongest correlation anywhere in the brain. For all parameter sets, amplitude in lower frequency bands negatively correlates with entropy (<60Hz) and higher frequency band amplitude positively correlates (>60Hz). The strongest negative correlation was consistently found with beta band amplitude, whereas the strongest positive correlation was found with amplitude in the wide, 60-140Hz gamma band. Across the narrow gamma bands, the strongest positive correlation was found with 100-120Hz band amplitude.

However, the strength of the correlations varied with different parameter sets. For the five lowest frequency bands, the parameter set that maximised the absolute correlation was consistent: $\tau = 0.06$ and $W = 5$. The optimal parameter sets for correlation with the gamma frequency bands (>60Hz) varied. It can be seen in Figure 2.4 that for many parameter combinations there is a frontal peak in correlation between RVE and gamma band oscillatory amplitude, but that this is not visible for all parameter sets. This suggests that the choice of RVE parameters should depend on the frequency of activity of interest.

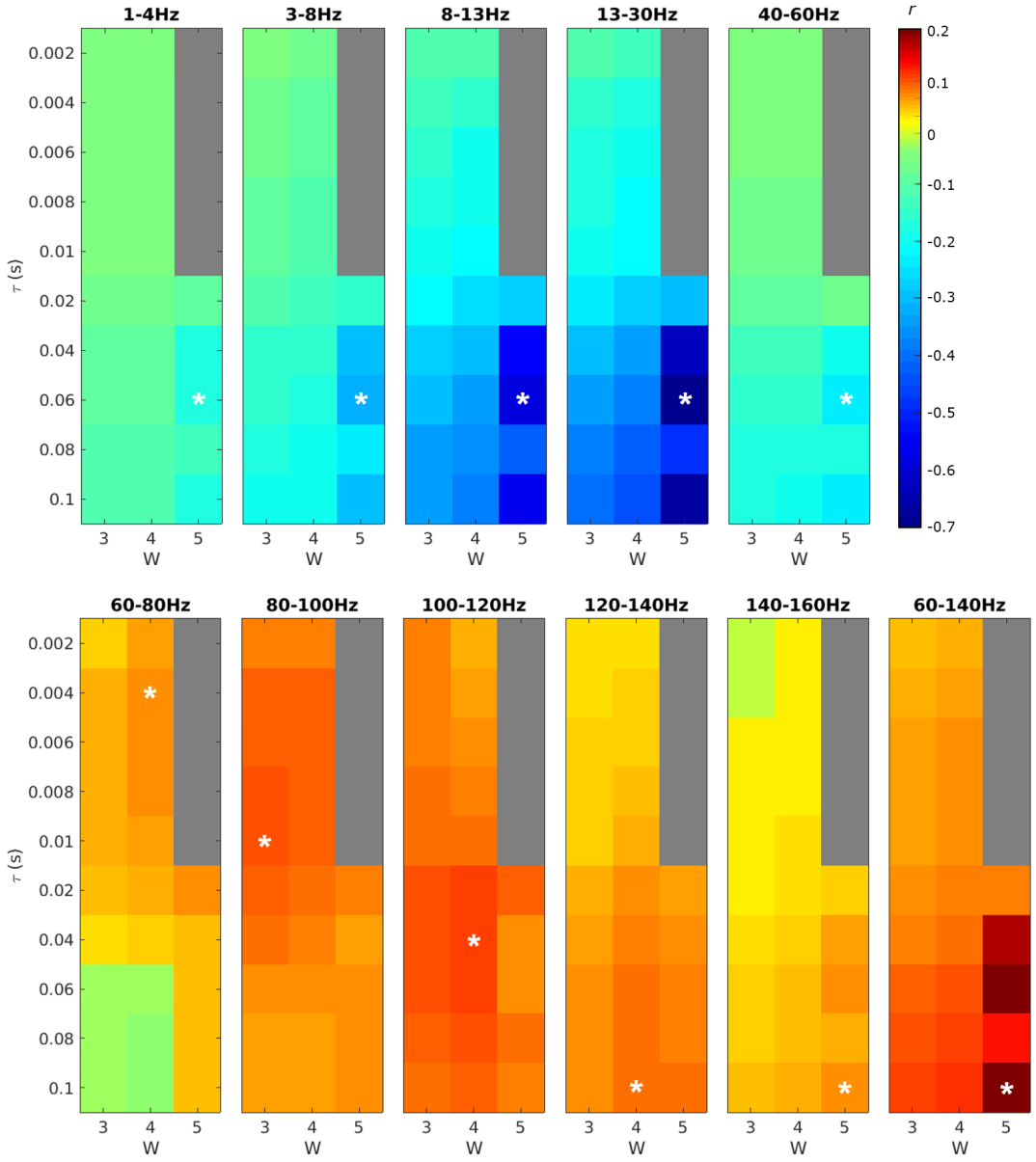


FIGURE 2.3: Optimising the relationship between RVE and oscillatory amplitude. The colour plots show the strongest correlation values obtained between RVE and oscillatory amplitude for each combination of RVE parameters, $\tau$ and $W$, taken from the voxel of maximum absolute mean correlation across subjects for each parameter set and frequency band. White asterisks indicate the parameter set that yielded the strongest correlation for each frequency band, and grey indicates an inappropriate parameter combination (gave an insufficiently populated state frequency distribution).

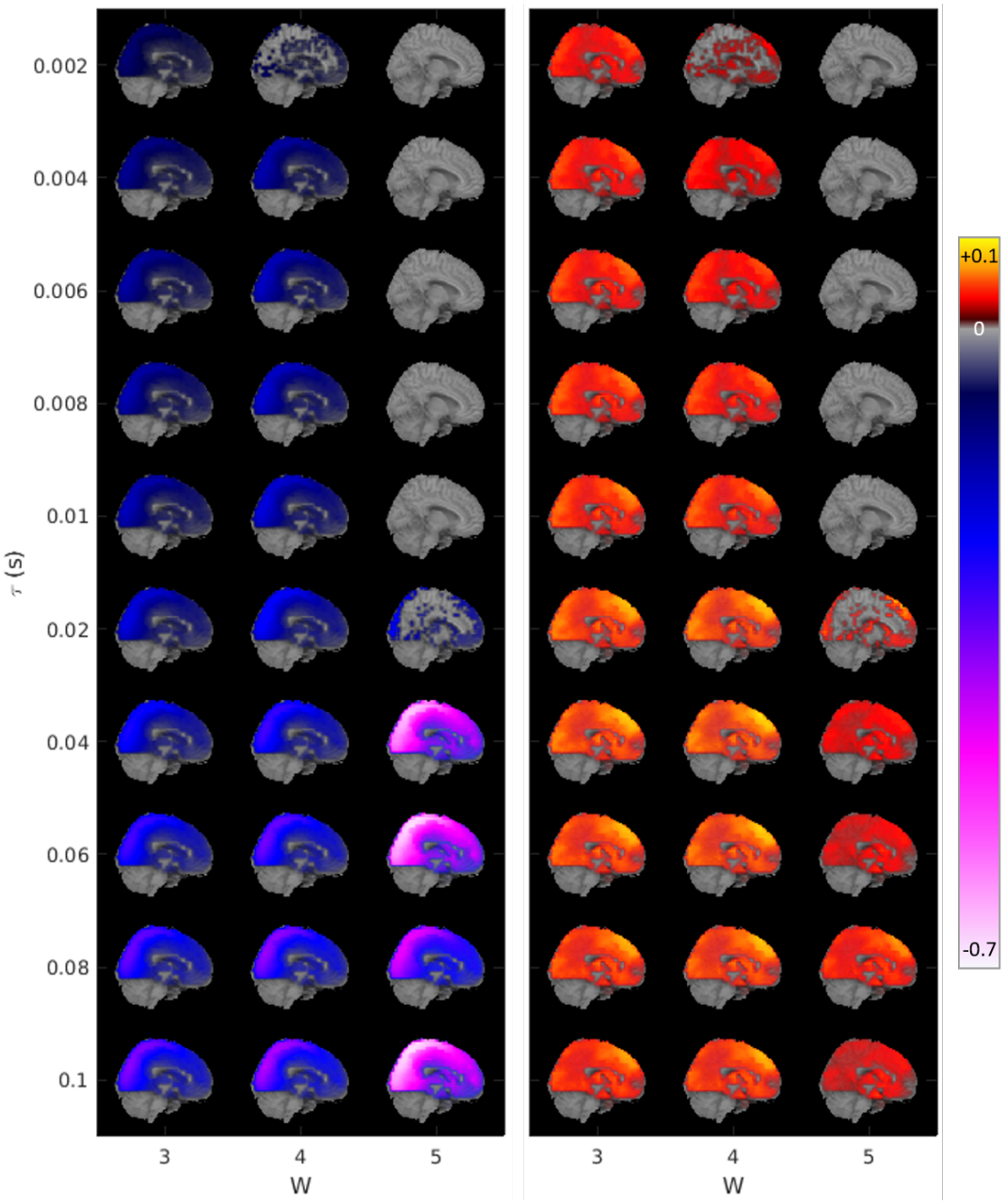


FIGURE 2.4: The correlation between RVE and oscillatory amplitude in the beta band (left) and 100-120Hz gamma band (right), for a range of RVE parameter combinations. Pearson correlation coefficients are displayed on a template brain as indicated by the colour bar. Warmer colours indicate positive correlation and cooler colours indicate negative correlation.

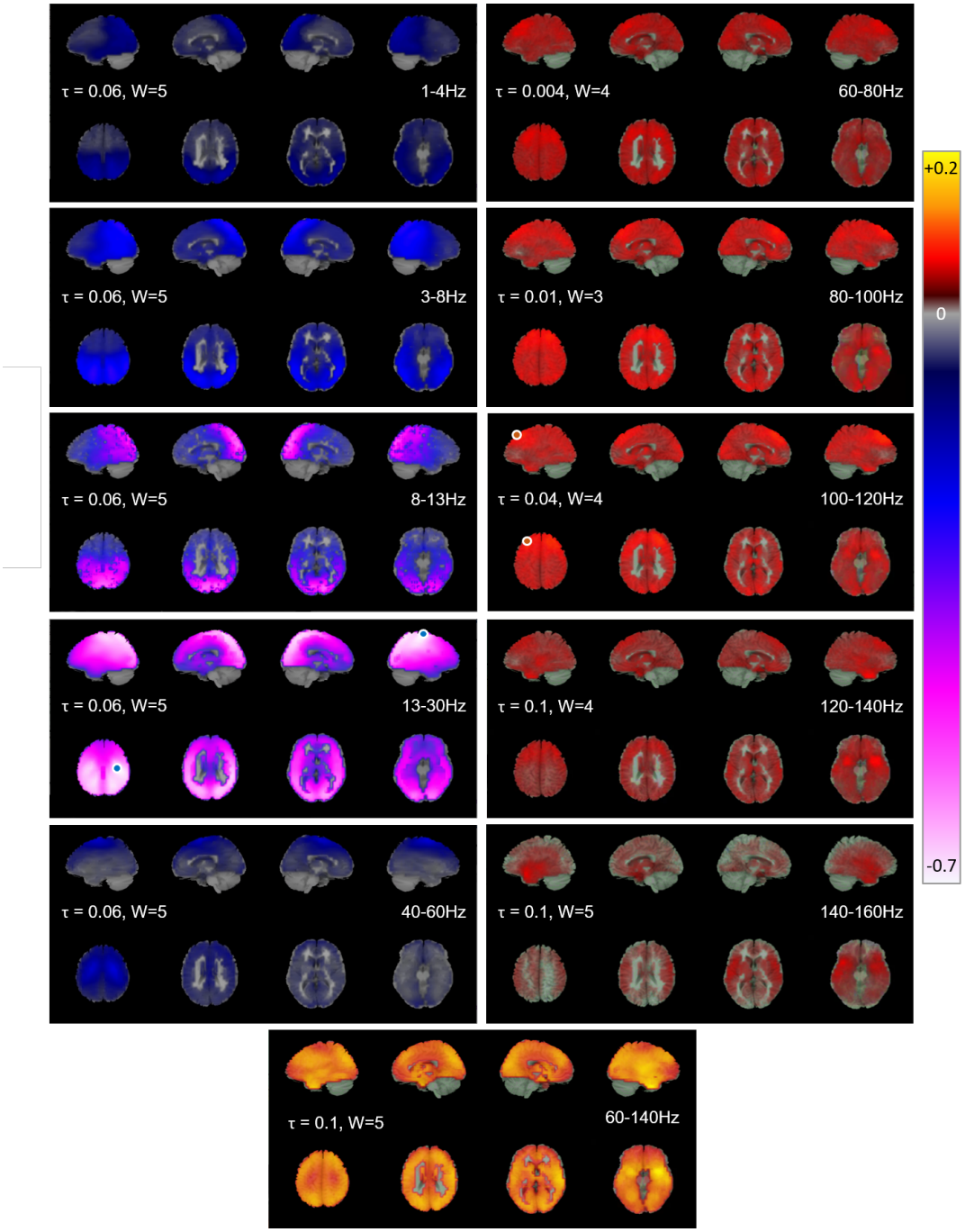


FIGURE 2.5: Correlation between RVE and oscillatory amplitude. RVE parameters chosen to give maximal correlation for each frequency band. Warmer colours indicate positive correlation and negative correlation is represented by cooler colours. Voxels are indicated that showed strongest negative correlation with beta band amplitude and the strongest positive correlation with 100-120Hz gamma band amplitude.

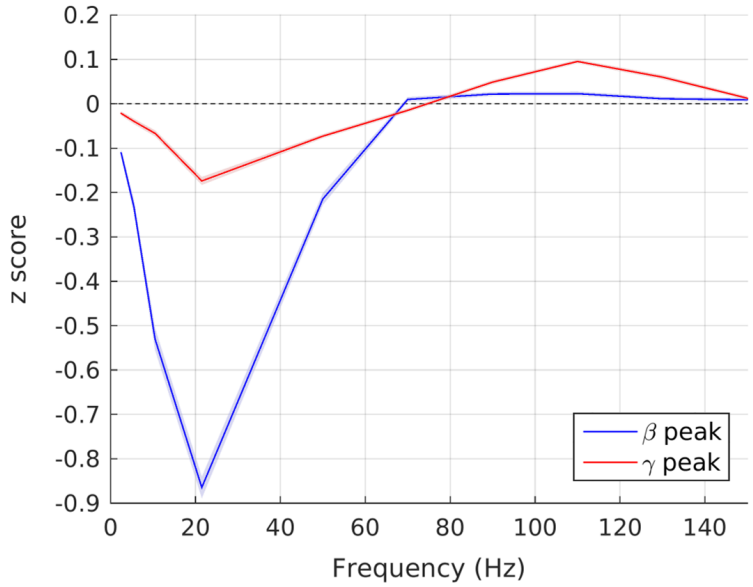


FIGURE 2.6: Average correlation between RVE and oscillatory amplitude as a function of frequency at the voxels of peak mean correlation with beta and 100-120Hz amplitude. RVE parameters chosen to give maximal correlation for each frequency band. Error bands show the standard error on the mean across participants.

Figure 2.5 shows the relationship between RVE and oscillatory amplitude in each frequency band during the resting state, using the parameter set that maximises the correlation strength with amplitude for each frequency. The strongest negative correlation values are found between RVE and beta band amplitude bilaterally in the primary motor cortex and superior parietal lobe, and in the right precuneus. The strongest positive correlation was found in the middle temporal gyrus between RVE and amplitude in the wide gamma, 60-140Hz band. The strongest positive correlation with 100-120Hz band amplitude was found in the right superior and left middle frontal gyri.

Figure 2.6 shows the relationships between RVE and oscillatory amplitude at the voxels of peak negative and positive correlation (marked on Figure 2.5). The same general shape of the biphasic relationship as found by (Brookes et al., 2015) can be seen at both voxels. However, at the voxel where negative correlation is strongest, the positive correlation with gamma band amplitude is relatively weak. The reverse is true at the voxel of peak positive correlation with 100-120Hz amplitude, where the negative correlation with beta band amplitude is weaker.

## 2.4 Discussion

In this study it was found that the amplitude, waveform and temporal resolution of RVE time-courses are dependent on the chosen parameter values of the decay time constant, $\tau$, and sliding window length, $W$.

By examining the RVE of simulated pink noise, it was found that reducing the value of $\tau$ increased the temporal resolution of the resulting entropy timecourse. However, for each value of $W$, reducing $\tau$ below a critical value resulted in a loss of the waveform. This critical value was smaller for shorter window lengths, suggesting that to maximise the temporal resolution of the calculated RVE, the smallest possible values of $W$ and $\tau$ should be selected that will maintain the waveform ($W = 3$, $\tau = 0.002s$). However, these smaller parameter values also gave RVE timecourses with high amplitude fluctuations, indicating that entropy calculations using these parameter values would be more sensitive to noise. These results suggest that the selection of RVE parameters should be based on the desired properties of the entropy timecourses, and that the values of $\tau$ and $W$ should be chosen in combination.

The irregularity of resting state MEG data was then investigated, and a consistent biphasic relationship between RVE and oscillatory amplitude was found across all parameter sets. RVE was found to show strong negative correlation with oscillatory amplitude below 60Hz, particularly with the alpha and beta bands, and to correlate positively with gamma band amplitude. The direction of the relationship with each frequency band was also found to be consistent across the brain. This replicates the findings of Brookes et al., 2015 where the correlation between RVE and oscillatory amplitude was investigated during tasks. The strong negative relationship with alpha and beta band amplitude is potentially unsurprising as oscillatory synchronisation in these frequency bands have been suggested as a mechanism underlying resting state connectivity (Engel and Fries, 2010; Brookes et al., 2011a; Hillebrand et al., 2012). In contrast, an increase in entropy is thought to indicate an increase in local cortical processing (Tononi, Sporns, and Edelman, 1994; Friston, Tononi, and Edelman, 1996; Brookes et al., 2015). This suggests that oscillatory activity and irregularity measures, when used together, could give complementary views of cortical integration and segregation, respectively. Subsequent chapters will investigate the

extent to which alterations in RVE are driven by oscillations and whether RVE can provide new information beyond that given by measures of oscillatory amplitude.

The strength of the relationship between RVE and oscillatory amplitude in each frequency band was found to vary spatially. By observing the areas of strongest correlation in Figures 2.4 and 2.5, it seems that the spatial distribution of the correlation values may have been partly driven by the signal strength in each frequency band. The strongest negative relationships with alpha and beta band amplitude were observed towards the back of the brain in the sensorimotor cortex, parietal lobe and visual cortex, consistently across parameter choices. These areas have been previously shown to exhibit high alpha and beta band power during the resting state (Hillebrand et al., 2012). Also, for certain parameter combinations, a peak in correlation between RVE and narrow-band gamma amplitude was observed in the prefrontal cortex, which was strongest for 100-120Hz amplitude. It is known that areas of the default mode network, including the medial prefrontal cortex, show increased gamma band power during rest compared to that measured during tasks (Miller, Weaver, and Ojemann, 2009; Ossandon et al., 2011). This may suggest that, for frequency bands up to the beta band, high resting state power is associated with signal regularity, whereas higher resting state gamma band power is associated with higher signal entropy.

The strongest positive relationship was observed between RVE and amplitude in the wide, 60-140Hz gamma band. This suggests that RVE may more closely represent the sum of gamma activity across a wide bandwidth than the activity in a particular narrow frequency band. However, the stronger relationship may also be observed because activity in the gamma band generally has lower SNR, due to the 1/f power spectrum of neuronal activity. By describing the high frequency activity across a wider range using one amplitude envelope, this may combine information from the activity in the narrower bands and thus increase SNR. While the correlation values are higher between RVE and broadband gamma, there is also a loss of the spatial variation in the correlation values that can be seen between RVE and amplitude in the narrow gamma bands. For example, the medial prefrontal peak in correlation that was observed between RVE and narrow band gamma amplitude can't be seen in

the wide-band correlation map. This suggests that wide gamma bands may be useful in maximising SNR, but that narrow gamma bands contain distinct information about brain activity, and so it may be beneficial to examine them individually.

The lower limits on $\tau$ that were established by the simulation test generally agreed with the parameter combinations that were found to be appropriate for calculating RVE of MEG data, i.e. those that maintained a populated state frequency distribution. It was found that RVE of MEG data could be reliably calculated for $\tau \geqslant 0.004$ when $W = 4$ and for $\tau \geqslant 0.04$ when $W = 5$. For $W = 5$, this was a larger critical $\tau$ value than was found in the simulation analysis. While the reason for the slight difference is unknown, there are a number of potential causes. Firstly, the MEG data signals were much longer than the pink noise signals used in the simulation test. With RVE being calculated at more time points, the probability increases of reaching a situation where a state histogram bin is vacant. Alternatively, the difference could be due to the properties of the signals. For example, it would be more likely to find an empty state bin when calculating RVE of a signal with low entropy. This is due to a higher frequency of occurrence of a small number of states, meaning that other states must occur less often. This may suggest that higher temporal resolution could be obtained when measuring RVE of signals of high entropy, as a smaller value of $\tau$ could be used for a given window length, $W$. However, while it was found to be possible to calculate RVE at higher temporal resolution, the parameter values that optimised the relationship between entropy and oscillatory amplitude were generally larger than the minimum possible. This suggests that the optimisation of this relationship required a balance to be reached between increasing the temporal resolution (smaller $\tau$ and $W$) and SNR (larger $\tau$ and $W$) of the RVE timecourses.

A limitation of this study is the confined parameter space included in the analysis. The value of $W$ that would optimise correlation with oscillatory amplitude could have been larger than 5. However, a priority was placed on limiting the computation time of the RVE calculation, and so larger window lengths were not considered. The frequency of the lowpass filter applied to the data, $f_c$, is also technically a tunable parameter of the RVE method, which would alter the sampling lag, $\xi$. As the value of the lag is dependent on the lowpass frequency applied to the data, the choice

of lowpass frequency therefore decides the length in time that the sliding window spans. In this chapter, RVE was only calculated using broadband data, where the lowpass frequency of the bandpass filter applied to the data was not reduced below the Nyquist frequency, $f_N = \frac{f_s}{2}$, where $f_s$ denotes the sample rate of the downsampled data. However, by reducing the lowpass frequency, the sliding window at each time point would be generated using a larger sampling lag, $\xi$, which would cause the sliding window to extend over a longer period of time. The current RVE methodology is limited to measuring irregularity at a single time scale. However, varying the lag could give a view into the properties of neuronal irregularity over a range of time scales. The calculation of multi-scale entropy (MSE) has previously been shown to be useful in the analysis of neuronal complexity, and to reveal different properties of irregularity measured at different time scales (Costa, Goldberger, and Peng, 2005). Chapter 4 investigates whether multi-scale RVE can provide additional information about irregularity in the brain compared to the current RVE methodology.

A further limitation is that the definition of an 'optimal' RVE calculation is not universal, as the best parameter choices could be dependent on the activity of interest. The optimisation methods used here were entirely empirical and so could provide little insight into the mechanisms that determine the optimal parameter values. It is therefore uncertain how these values would vary when calculating RVE of neuronal signals with different spectral content, for example during sleep (Achermann and Borbely, 1997) or in many patient groups (Uhlhaas and Singer, 2010; Little and Brown, 2014; Zijlmans et al., 2013). It is also unknown whether parameter choice could affect the sensitivity of RVE to alterations in neuronal irregularity due to disease or experimental conditions. However, this analysis does highlight the fact that the choice of parameters used in the RVE calculation influences the resulting irregularity measurements, and that the activity of interest and the desirable properties of the entropy timecourses should be considered when selecting the parameter set. For example, if the activity of interest is expected to be sustained over a long period of time, such as during tasks with a blocked design, it may be beneficial to use a longer decay time constant to maximise SNR, as high temporal resolution may be less important in this case. Alternatively, if the signal of interest has high SNR, such as an evoked response or high amplitude oscillation, then it may be possible to use a

shorter decay time constant to maximise the temporal information given by the entropy timecourse. It may also be beneficial to use a short decay time constant if the activity of interest is expected to give a quick, transient change in entropy, such as an epileptic spike (Hall, 2017). In this case, a shorter time constant may be necessary for the change in entropy to significantly affect the rank-vector frequency histogram. To extend this analysis, it may be beneficial for future work to investigate the ability of RVE to detect transient changes in entropy when using different parameter sets. For example, this could be investigated by calculating the RVE of noise signals with embedded oscillatory segments of varying lengths. This could further help to inform appropriate RVE parameter choices for different tasks and paradigms.

## 2.5 Conclusion

RVE was found to exhibit a biphasic relationship with the oscillatory amplitude of MEG signals, replicating the findings of Brookes et al., 2015 during resting state recordings. The direction of the relationship with each frequency band was also found to be consistent across the brain and across all RVE parameter sets. One 'optimal' parameter set was found that maximised the strength of the negative correlation with oscillatory amplitude in frequency bands below 60Hz. This combination of parameters will now be used in all further entropy calculations during this thesis. However, the parameters that maximised the correlation strength with oscillatory amplitude were not consistent across the higher frequency bands. It was also found that there were alternative parameter sets that could give entropy timecourses with higher temporal resolution, suggesting that the optimal parameter set could be dependent on the brain activity of interest. For the remainder of this thesis, it will be established whether RVE can provide insight into brain function in health and disease, beyond that which can be learned from oscillatory activity.

# Chapter 3

# The irregularity of neuronal activity explains the BOLD response

The coupling between the haemodynamic activity observed by BOLD fMRI and neural function is not entirely understood, and is known to depend on multiple factors. In previous studies, it has been found that the fMRI BOLD response exhibits a complex relationship with oscillatory neuronal activity. BOLD exhibits positive temporal correlation with activity in the gamma band and negative correlation with activity in the alpha and beta frequency bands. This pattern is similar to the relationship between the oscillatory amplitude and rank-vector entropy (RVE) of MEG virtual sensor timecourses, which was presented in chapter 2. Therefore, in this chapter, it was investigated whether MEG RVE could explain the BOLD response. During a movie task, a relationship was found between the BOLD response and MEG signal entropy that varied in direction across the brain. Positive correlation was found in task-activated areas, while negative correlation was observed within the default mode network, which remained after correction for source leakage. In contrast, the relationship between MEG RVE and MEG oscillatory amplitude was found to be consistent in direction across the brain for each frequency band. The relationships between RVE and oscillatory amplitude were found to be consistent with the findings presented in chapter 2. Negative correlation was found with amplitude at lower frequencies (<50Hz) and positive correlation was found with amplitude in the gamma bands (>50Hz). These findings suggest that the regions composing the default mode network exhibit atypical neurovascular coupling; while BOLD activation

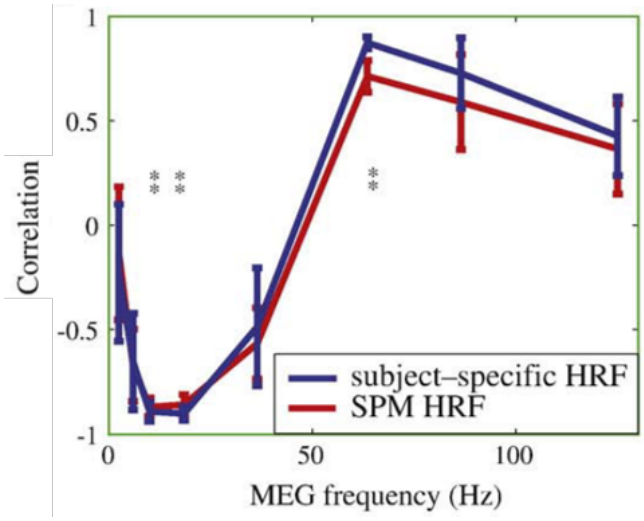


FIGURE 3.1: Taken with permission from Zumer et al., 2010: temporal correlation between bandpass filtered MEG signals (convolved with HRF) and BOLD signal from visual cortex, during a visual task.

in task activated regions is associated with an increase in high frequency, irregular activity, an increase in BOLD response within the default mode network is associated with more regular, low frequency activity.

## 3.1 Introduction

The relationship between the haemodynamic activity observed by BOLD fMRI and neuronal function, i.e. neurovascular coupling, is not entirely understood. It is known to differ between participants, and also to vary within individuals over time, with disease and respiration changes, and spatially across the brain (Singh, 2012; Hall et al., 2014). While functional images created by measuring the BOLD response have excellent spatial resolution, without a definite idea of what the BOLD response represents, these images cannot be assumed to purely reflect neuronal function, and so the understanding we can gain from them is limited.

Previous studies have investigated the relationship between the BOLD response and oscillatory neuronal activity across frequency bands. Across studies, a consistent relationship has been observed, an example of which is shown in Figure 3.1 (Zumer et al., 2010). The BOLD signal exhibits negative temporal correlation with oscillatory power envelopes at low frequencies. The strongest negative relationships

are observed with oscillatory activity in the alpha and beta frequency bands. In contrast, the BOLD response has been found to correlate positively with activity in the gamma band ($f \gtrsim 50$Hz). This general relationship has been found consistently across different locations in the brain and across studies that have utilised different electrophysiological imaging methods, including MEG (Zumer et al., 2010), intracranial depth electrodes (Mukamel et al., 2005) and electrocorticography (ECoG) (Conner et al., 2011).

Interestingly, this follows a similar pattern to the relationship between oscillatory amplitude and the rank-vector entropy (RVE) of MEG signals, which was found previously by (Brookes et al., 2015) and was replicated in chapter 2 (see Figure 2.5). Therefore, in this chapter, an investigation was carried out into the existence of any temporal correlation between BOLD fMRI and the RVE of MEG timecourses. The relationship between oscillatory power and entropy was also investigated further, to see whether the relationship found in chapter 2 would be replicated during a visual task.

## 3.2 Methods

### 3.2.1 Data acquisition and processing

MEG and BOLD fMRI data were obtained for 16 participants (7 female, mean age: 27) who each watched the same 20-minute clip of the movie 'Skyfall' during each session. The order of the scans was randomly counter-balanced, and the scans were carried out on separate days for each participant. MEG data were recorded as in chapter 2 at a sample rate of 1200Hz. An anatomical MRI was also obtained for each participant, to allow coregistration of the MEG and fMRI data, using an FSPGR sequence with 1mm isotropic voxel resolution.

Offline, the MEG data were downsampled to 600Hz and a bandpass filter of 1-150Hz was applied. Visual inspection of the data was then performed in 2 second epochs, and sections containing artefacts were removed. The data were then filtered into six frequency bands for analysis of oscillatory amplitude: 1-4, 3-8, 8-13, 13-30, 40-60 and 60-140Hz. For each of these frequency bands, a scalar LCMV beamformer (Van Veen et al., 1997) was used to construct virtual sensor timecourses in template

space at voxels on a 6mm$^3$ grid, as in chapter 2. Current timecourses were also produced using broadband data (1-150Hz) for entropy analysis.

The fMRI data were collected using a GE Sigma 3T scanner with a gradient-echo BOLD EPI sequence of 600 volumes. Data were collected with a repetition time (TR) of 2000ms (corresponding to a sampling rate of 0.5Hz), and an isotropic voxel resolution of 2mm. The fMRI data were pre-processed using a pipeline that included motion correction (MCFLIRT), spatial smoothing (SD=4.25mm kernel), despiking using a median replacement filter and a temporal highpass filter of 0.01Hz. The fMRI data were then spatially normalised to the same template space as the MEG virtual sensors, and were resampled to the same 6mm$^3$ grid. The BOLD timecourse from each voxel was also converted to the percentage deviation from the mean BOLD signal at that voxel.

### 3.2.2 Analysis

Rank vector entropy timecourses (RVE) were calculated from the broadband MEG virtual sensor timecourses at each voxel as described in chapter 2 section 2.2.1 (Robinson et al., 2013). These were subsequently downsampled from the sample rate of 600Hz to 2Hz, and the BOLD signals were upsampled to the same sample rate. A highpass filter of 0.5Hz was then applied to all BOLD and RVE signals. This was applied as signal epochs of 2s were removed during the MEG data cleaning process. This precluded the investigation of signal components with a period longer than the length of these epochs. One BOLD and one entropy timecourse was thus produced for each voxel, for each participant, in a common space so that signals from each voxel could be compared across modalities and participants.

Average RVE and BOLD timecourses were then found for each voxel by taking the mean values across participants at each time point. The average RVE was then convolved with the SPM HRF, and the first and last 50 time points of each entropy and BOLD signal were trimmed to avoid any artefacts due to edge effects. Finally, the Pearson's correlation between the BOLD and convolved RVE was found at each voxel.

Oscillatory amplitude timecourses were then obtained for each narrow frequency band, as in chapter 2, by taking the magnitude of the analytic signal of the virtual

sensor timecourses. These were also downsampled to 2Hz and averaged across participants at each voxel. The correlation between the averaged RVE and oscillatory amplitude timecourses were then found at each voxel for each frequency band.

## 3.3 Results

### 3.3.1 The relationship between RVE and the BOLD response

Figure 3.2 indicates areas where the correlation between the mean RVE and BOLD timecourses was calculated to be significant ($p < 0.05$, FDR corrected for multiple comparisons using the 'fdr' function in the EEGLAB toolbox (Delorme and Makeig, 2004)). A widespread positive correlation can be seen in the occipital and parietal lobes, whereas negative correlation is observed in the precuneus, medial prefrontal cortex, and left angular gyrus. These areas are thought to be core functional hubs of the default mode network (DMN) (Andrews-Hanna, Smallwood, and Spreng, 2014).

However, some of this negative correlation could be artefactual due to MEG source leakage. While the spatial resolution of fMRI is excellent, MEG functional images are always blurred to some extent due to the ill-posed nature of the inverse problem. The number of sensors used is low compared to the number of voxels and so there is insufficient information to recreate independent current timecourses at each voxel. Activity originating in one location could therefore be observed in MEG functional images across multiple voxels (Colclough et al., 2015). In the case of this study, if MEG signals from the visual cortex (active during the movie task) have blurred into the precuneus (inactive during the movie task), then a spurious negative correlation could be observed with the BOLD response, as source leakage does not affect fMRI signals.

To test whether the negative correlation is genuine, virtual sensors were generated at all voxel locations within the precuneus and calcarine (the region of the visual cortex neighbouring the precuneus). Within the precuneus, the voxel was identified where RVE exhibited the minimum correlation with the BOLD response ($z = -0.18 \pm 0.02$). Within the calcarine, the voxel where RVE showed maximum correlation with the BOLD signal was taken ($z = 0.41 \pm 0.02$). For each participant,

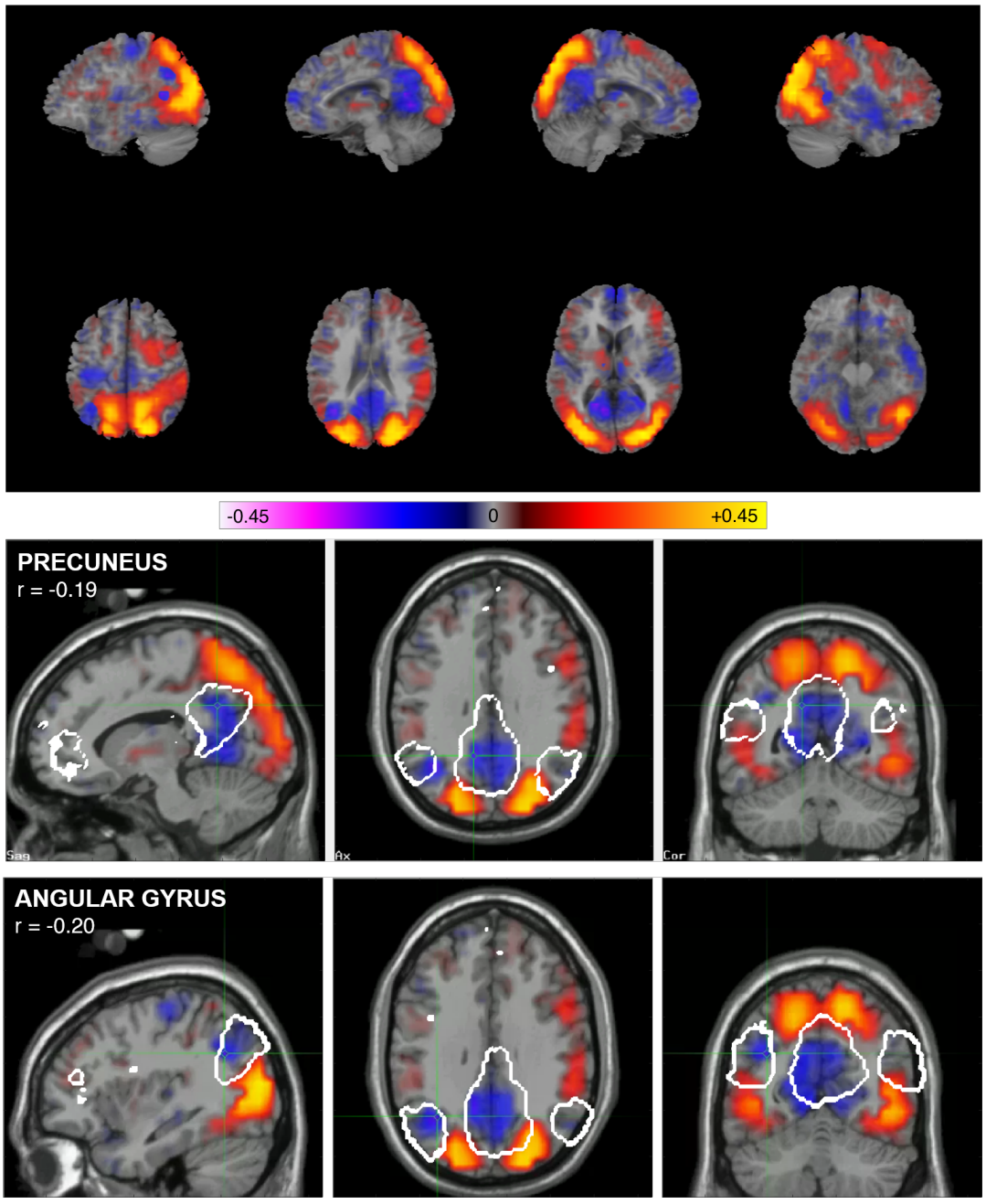


FIGURE 3.2: Correlation of average RVE and BOLD signals during a movie task, thresholded at p<0.05 (with FDR correction for multiple comparisons). Warm colours indicate positive correlation as indicated by the colour bar. The slices in the bottom rows intersect the largest negative peaks in the left precuneus and angular gyrus. The default mode network as measured by Smith et al., 2009 is outlined in white.

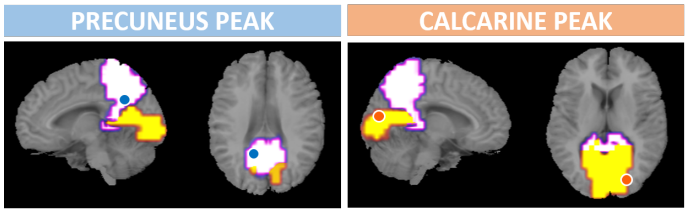


| | $z_p$ | $z_c$ |
|---|---|---|
| With correction | -0.17±0.02 | +0.41±0.02 |
| Without correction | -0.18±0.02 | +0.41±0.02 |

FIGURE 3.3: Fisher transformed correlation between RVE and BOLD at the voxels showing the strongest correlation within the precuneus, $z_p$, and the calcarine, $z_c$, with and without correction for source leakage. The two voxel locations are indicated on a template brain, with the precuneus region of the AAL atlas shaded in white, and the calcarine shaded in yellow.

the two timecourses from these voxels were then symmetrically orthogonalised (Colclough et al., 2015) to remove any correlation between them due to source leakage. The RVE of these orthogonalised timecourses were then calculated and downsampled to 2Hz, and the average entropy timecourse across participants at each voxel was convolved with the HRF. The mean BOLD signal timecourse from each voxel was then correlated with the corresponding corrected RVE timecourse. The resulting z-scores are shown in Figure 3.3. It was found that the negative correlation in the precuneus remained when the virtual sensor timecourses were orthogonalised, suggesting that this was not a spurious effect of source leakage.

### 3.3.2 The relationship between RVE and oscillatory amplitude

Figure 3.4 maps the correlation across the brain between the hilbert envelopes of each frequency band and entropy during the movie paradigm. Areas of strongest correlation are mostly confined to the occipital lobe, but a consistent biphasic relationship is seen across the brain, where lower frequency bands negatively correlate with entropy, and higher frequency bands positively correlate. This is consistent with the relationship found by Brookes et al., 2015 and with the results presented here in Chapter 2 Figure 2.5. The 'crossover' band is seen to be around 40-60Hz, where significant correlation was not observed consistently across the brain. For this frequency band, peaks in negative correlation were found in the somatosensory cortex and middle frontal gyrus.

Table 3.1 provides a summary of the directional relationships that RVE has exhibited with the BOLD response and the oscillatory amplitude of MEG signals at low

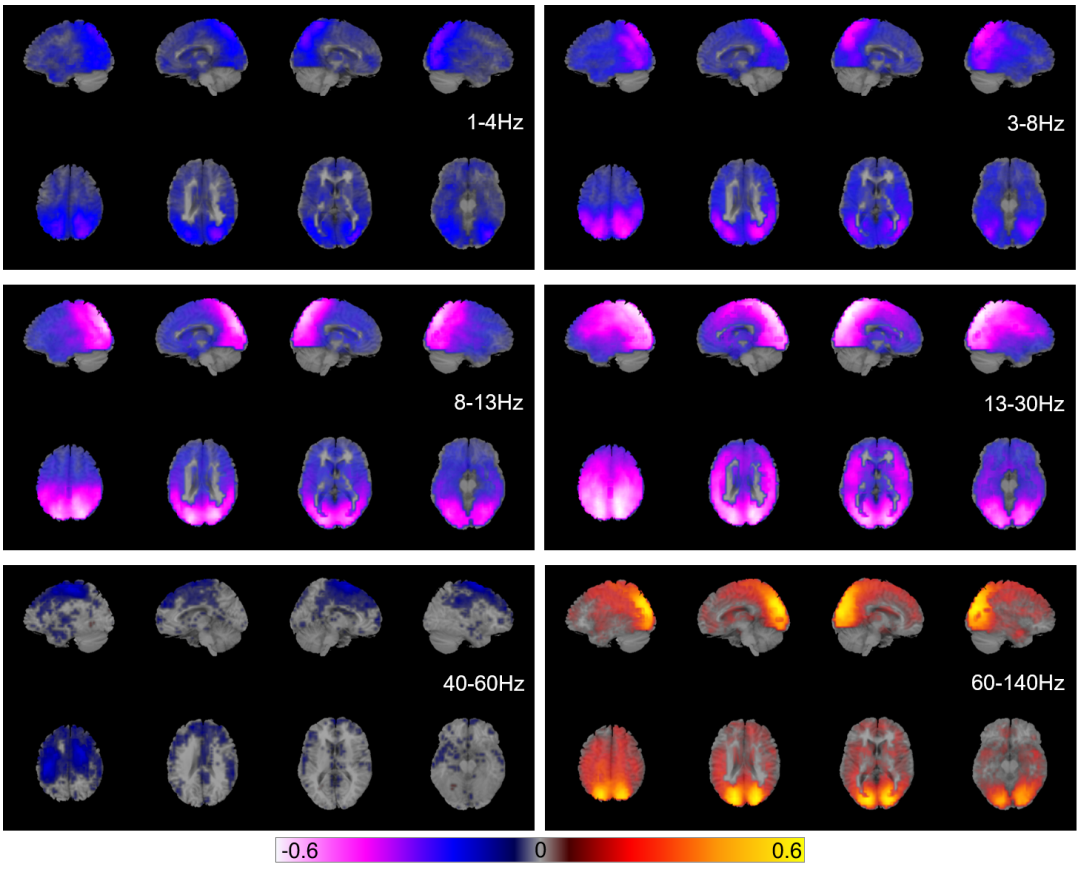


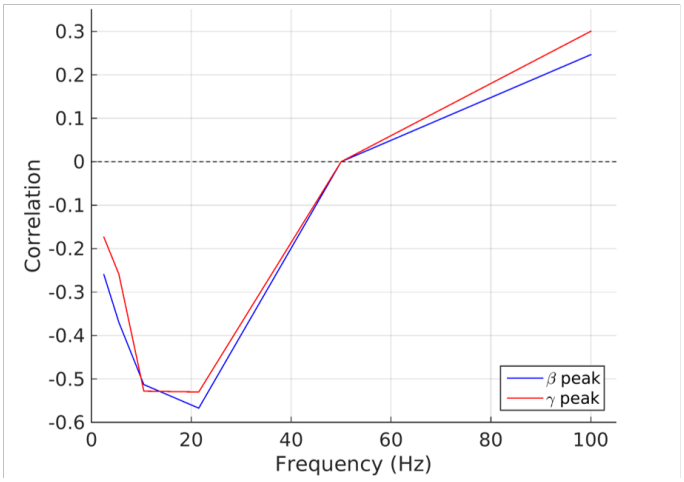


FIGURE 3.4: The above colour plots show the temporal correlation between average RVE timecourses and oscillatory amplitude envelopes during the movie paradigm, for each frequency band. Pearson's r coefficients are plotted on a template brain as indicated by the colour bar. The line plot below shows the average correlation as a function of frequency at the voxels of peak correlation with the 13-30Hz and 60-140Hz bands.

| | BOLD | Low frequency amplitude (<60Hz) | High frequency amplitude (>60Hz) |
|---|---|---|---|
| DMN | − | − | + |
| Occipital | + | − | + |

TABLE 3.1: A summary of the directional relationships found with RVE in regions active during the movie watching task (occipital) and within the default mode network (DMN).

(<60Hz) and high (>60Hz) frequencies, within task-activated areas and the default mode network.

## 3.4 Discussion

This study has found a significant and spatially varying relationship between the irregularity of MEG signals and the BOLD fMRI response during a passive movie watching task. The positive correlation observed in the visual cortex and parietal lobe indicates that a larger BOLD response is associated with more irregular neuronal activity in task-activated areas. In contrast, a negative correlation between the BOLD response and MEG RVE was found within the functional hubs of the DMN (Andrews-Hanna, Smallwood, and Spreng, 2014). Within these regions, a larger BOLD signal was associated with more regular, low entropy activity during movie watching. This relationship remained after calculating the RVE of orthogonalised MEG virtual sensor timecourses in the precuneus and calcarine. This suggests that the negative correlation observed in the precuneus was not spurious due to MEG source leakage (Colclough et al., 2015). The spatial variance of the relationship between MEG RVE and the BOLD response contrasts with the correlation between RVE and oscillatory amplitude, which was consistent in direction across the brain for each frequency band. These findings point to atypical, and potentially inverted, neurovascular coupling within functional hubs of the DMN compared to within task-active areas.

From this analysis alone, it is difficult to gain insight into the nature of the brain activity underlying this relationship. However, both the BOLD response (Logothetis, 2003) and neuronal entropy (Tononi, Sporns, and Edelman, 1994; Wang et al., 2018)

have previously been linked to regional levels of local information processing. This is supported by the positive correlation found in areas which would have been active during the movie task. The relationship found within the DMN is more puzzling. However, it is well established that the DMN shows a decrease in BOLD signal during tasks; the so-called negative BOLD response (Raichle et al., 2001). The prevailing theory is that this decrease is due to neural inhibition (Sten et al., 2017). The negative correlation found here between the BOLD response and RVE implies that a decrease in the BOLD signal in these regions would be accompanied by an increase in neuronal irregularity, which indicates a reduction in neuronal synchrony (Brookes et al., 2015) and may suggest a decrease in cortical integration in these regions (Tononi, Sporns, and Edelman, 1994). A number of studies in recent years have detected resting state connectivity between DMN nodes in the alpha and beta frequency bands (Pasquale et al., 2010; Brookes et al., 2011a; Hillebrand et al., 2012). Therefore, one explanation of the observed results could be that the task-related reduction in BOLD and the associated neuronal entropy changes within the DMN are driven by the suppression of this network connectivity. Future work could test this hypothesis by investigating how the BOLD response and neuronal irregularity relate to functional connectivity in these frequency bands.

This could be investigated by altering the levels of functional connectivity measured across the brain using a hypercapnic challenge. It has been found previously that lower functional connectivity, as measured using fMRI, is associated with higher levels of $CO_2$ in the bloodstream (Golestani et al., 2016). It could be determined whether the negative correlation between RVE and BOLD is driven by the suppression of functional connectivity by seeing how the relationship varies while participants inhale air containing $CO_2$ in different proportions.

The general biphasic relationship between the RVE and Hilbert envelopes of MEG signals was shown to be consistent with the relationship found in chapter 2 during the resting state (see Figures 2.5 and 2.6). Negative correlation was found with oscillatory amplitude in all frequency bands up to the beta band, implying that activity at lower frequencies is more regular regardless of task. In contrast, positive correlation was found with amplitude in the high gamma band (60-140Hz), suggesting that high frequency activity is consistently more variable. This is consistent with

low frequency oscillatory activity being synchronised across larger neuron populations than gamma band activity, which is more associated with local processing (Pfurtscheller and Lopes, 1999). However, while the direction of the relationship remained consistent for each frequency band across the brain, the areas of strongest correlation differed to those found during the resting state. The strongest correlation was found within occipital and parietal regions during the movie task, except for the correlation between RVE and low gamma band amplitude (40-60Hz). This contrasts with the findings presented in chapter 2, where the area of strongest correlation depended on frequency band. This is consistent with the prediction made in section 2.4 that the strongest correlation is observed in areas with the highest levels of task related activity, potentially due to higher SNR.

In this chapter, the relationship between gamma band amplitude and the RVE of MEG signals was investigated using a broad high gamma band as this frequency band exhibited the strongest positive correlation with RVE in chapter 2. However, it may have also been interesting to again investigate the relationship between RVE and oscillatory amplitude in narrow frequency bands. Evidence from recent studies suggests that there is a dissociation between the functional roles of narrow- and broadband visual gamma activity (Bartoli et al., 2019). It was also found in chapter 2 that narrow gamma band amplitude exhibited relationships with RVE that varied in strength and topography between frequency bands. Future work could therefore determine whether this variation is also observed during the movie task, to determine whether RVE exhibits different relationships with narrow- and broadband visual gamma amplitude, and whether the relationship varies between narrow gamma bands.

The relationship between the BOLD response and oscillatory amplitude was not directly investigated here. However, in the visual cortex, the RVE of MEG signals was found to correlate positively with both gamma band oscillatory amplitude and the BOLD response. This is seemingly consistent with the findings of previous studies that have found a positive relationship between gamma band amplitude and the BOLD response in task-active areas (Mukamel et al., 2005; Zumer et al., 2010). However, previous research has also indicated that the relationship between gamma band amplitude and the BOLD signal is complex; it has been found that increases

in gamma amplitude in the visual cortex vary with certain properties of a visual stimulus, such as spatial frequency and colour, whereas the BOLD response does not (Muthukumaraswamy and Singh, 2008; Muthukumaraswamy and Singh, 2009; Swettenham, Muthukumaraswamy, and Singh, 2013). It is unclear from this analysis whether the RVE of MEG signals exhibits a closer relationship with the BOLD response than gamma band oscillatory amplitude, or whether the same decoupling would be observed if the properties of the visual stimulus were varied. This relationship could potentially be probed further by using a visual stimulus with more controlled properties, such as gratings with known spatial frequency. However, the visual stimulus must maintain temporal structure in order to allow the direct correlation of activity between the MEG and fMRI scanning sessions.

The temporal structure afforded to the data by the movie watching task allowed the analysis of group level cross-modality relationships, which could not be assessed using a resting state paradigm, for example. However, a limitation of MEG-fMRI studies is that the relationship between neuronal activity and the BOLD response can only be examined in regions where activity variations are time-locked with the stimulus. It may be possible to investigate how the relationship varies across the whole brain, and using stimuli without clear temporal structure, by recording simultaneous EEG and fMRI. However, EEG has inferior spatial resolution compared to MEG, and so an EEG-fMRI study may not allow the investigation of how the neurovascular relationship varies across the brain in as such high spatial detail. It may therefore be difficult to examine distinct relationships in neighbouring brain regions, such as the precuneus and the calcarine sulcus.

One of the benefits of the simple movie task is that it would be easy to perform even in challenging patient populations, and so future work could investigate whether alterations in the relationships found here could act as potential biomarkers of mental disorder. However, it may first be beneficial to also investigate variance in the relationships within healthy cohorts. It has been found previously that the BOLD response to movie watching varies with age (Petroni et al., 2018). Neurovascular coupling has also been found to vary between participants of different ages (Fabiani et al., 2014). The haemodynamic response is also known to vary between people, as well as across the brain in individual subjects (Zumer et al., 2010; Singh, 2012;

Hall et al., 2014). However, the cohort here was predominantly young adults, and a single canonical HRF was kept constant across all participants and at all voxels. It is therefore unclear how the relationships observed here would vary in a cohort of a different age range or when using a different HRF. This could limit the ability to assess how the relationships may be altered in patient groups, as it is uncertain how robust they would be across healthy participants of all ages.

One limitation of this study is that the 0.5Hz highpass filter applied to the RVE and BOLD timecourses may have removed relevant neural information from the BOLD signals. fMRI timecourses contain slow fluctuations at a range of lower frequencies and are often filtered into frequency bands within the range of 0.01-0.25Hz (Kalcher et al., 2014; Yuen, Osachoff, and Chen, 2019). The MEG data cleaning method used here precluded the inclusion of these low frequency components in this analysis. However, it may be possible to investigate the impact of slow fluctuations on the relationships found here by using an alternative cleaning method that does not involve removing signal epochs. For example, ICA could be used to identify and remove artefactual signal components without removing epochs of the data.

Another limitation is that, while the oscillatory amplitude of the MEG signals is measured across a range of frequencies, RVE measures entropy at only a single temporal scale. This is due to the fixed width of the RVE sliding window, which defines the frequency of activity that is visible to the RVE measure. However, other measures of signal complexity have been developed and have shown that brain activity contains recurring patterns across a range of time scales, which can result in different entropy measurements depending on the time scale considered (Costa, Goldberger, and Peng, 2005). The RVE method described by Robinson et al., 2013 measures irregularity at the shortest possible time scale given the sampling rate of the MEG data. It could be beneficial to measure RVE at a range of coarser temporal scales to further investigate the correlates of neuronal irregularity.

## 3.5 Conclusion

This chapter has presented further evidence that RVE is a valuable metric for investigating the time resolved irregularity of neuronal activity. The relationship between the RVE of MEG signals and the BOLD response was found to be inverted within the functional hubs of the DMN compared to task-activated areas. This suggests that the coupling between the BOLD response and the properties of the underlying neuronal activity varies across the brain during movie watching. These findings suggest caution when interpreting BOLD signals as they cannot be assumed to have a consistent relationship with the properties of neuronal activity.

The results in this chapter also indicated a potential relationship between neuronal entropy and network connectivity, and so the next chapter will investigate whether neuronal entropy can be used to measure functional connectivity. The RVE method will also be extended beyond a single temporal scale to investigate how neuronal irregularity, and functional connectivity, vary across time scales.

# Chapter 4

# Measuring functional connectivity using neuronal irregularity

Recent studies have shown how MEG can reveal spatial patterns of functional connectivity using frequency-specific oscillatory coupling measures and that these may be modified in disease. However, there is a need to understand both how repeatable these patterns are across participants and how these measures relate to the irregularity of neural activity seen in healthy brain function. In this study, we used Multi-scale Rank-Vector Entropy (MRVE) to calculate the dynamic timecourses of signal irregularity over a range of temporal scales. The correlation of MRVE timecourses was then used to detect functional connections in resting state MEG recordings that were robust over 183 participants and varied with temporal scale. We compared these MRVE connectivity patterns to those derived using the more conventional method of oscillatory amplitude envelope correlation (AEC) using methods designed to quantify the consistency of these patterns across participants. Using AEC, the most consistent connectivity patterns, across the cohort, were seen in the alpha and beta frequency bands. At fine temporal scales (corresponding to 'scale frequencies', $f_S$ = 30-150Hz), MRVE correlation detected mostly occipital and parietal connections. These showed high similarity with the networks identified by AEC in the alpha and beta frequency bands. The most consistent connectivity profiles between participants were given by MRVE correlation at $f_S$ = 75Hz and AEC in the beta band. The physiological relevance of MRVE was also investigated by examining the relationship between connectivity strength and local irregularity. It was found that local activity at frequencies $f_S \gtrsim$ 10Hz becomes more regular when a region exhibits high levels of resting state connectivity, as measured by fine scale MRVE correlation

($f_S \sim$ 30-150Hz) and by alpha and beta band AEC. Analysis of the EOG recordings also revealed that eye movement affected both connectivity measures. Higher levels of eye movement were associated with stronger frontal connectivity, as measured by MRVE correlation. More eye movement was also associated with reduced occipital and parietal connectivity strength for both connectivity measures, although this was not significant after correction for multiple comparisons.

## 4.1 Introduction

In recent years, MEG has revealed much about the electrophysiological underpinnings of connectivity in the brain. The direct view of neuronal activity provided by MEG and its excellent temporal resolution have allowed the investigation of frequency-specific communication (Brookes et al., 2011a; Hillebrand et al., 2012; Hipp et al., 2013) and dynamic changes in connectivity on the millisecond timescale (Baker et al., 2014; O'Neill et al., 2017). Alterations in MEG connectivity have also been detected in patient groups (Van Dellen et al., 2014; Ghanbari et al., 2015; Brookes et al., 2016; Hamandi et al., 2016; Engels et al., 2017; Boon et al., 2017). However, to be clinically useful, connectivity research must progress from group level analysis to the characterisation of individual subjects. To make meaningful comparisons between connectivity profiles of individuals, robust connectivity measures are needed that give consistent results for subjects with the same pathology.

Several recent studies have found that many commonly used techniques for measuring functional connectivity in MEG lack repeatability between healthy subjects, and even show inconsistency over repeated scans of the same subject (Wens et al., 2014; Colclough et al., 2016; Liuzzi et al., 2017). Colclough et al., 2016 found that the method that gave the most consistent connectivity was oscillatory amplitude envelope correlation (AEC), using symmetric orthogonalisation to remove spurious zero-lag correlation between timecourses due to signal leakage (Colclough et al., 2015). The repeatability of connectivity given by any alternative methods could therefore be compared to AEC to assess the extent to which it can add to our understanding of cortical communication in health and disease.

The irregularity of neural activity has been found to be altered in patient groups, where activity that is either too regular or too variable is associated with mental disorder (Protzner et al., 2010; Mizuno et al., 2010; Brookes et al., 2015; Takahashi, 2013; Fernández et al., 2013; Monge et al., 2015; Ghanbari et al., 2015; Mateos et al., 2018). Also, while the physiological role of irregularity in the brain is not certain, it is possible that it is related to levels of synchronisation between cortical regions, i.e. connectivity. The synchronisation of oscillatory activity, which is highly regular, is currently the most promising mechanism for connectivity between brain regions (Schnitzler and Gross, 2005; Fries, 2005; Donner and Siegel, 2011; Brookes et al., 2011a; Hillebrand et al., 2012; Tewarie et al., 2019). However, it is thought that local information processing performed within segregated brain regions is associated with signals that contain high levels of information and therefore are more irregular (Tononi, Sporns, and Edelman, 1994; Friston, Tononi, and Edelman, 1996). This would lead to the hypothesis that the irregularity of signals from a cortical region would be related to the levels of connectivity it exhibits with other brain areas. Therefore, measures of irregularity and oscillatory activity may be sensitive to complementary aspects of functional connectivity.

There is evidence for a relationship between neural irregularity and functional connectivity in the literature. One fMRI study found a correlation between the complexity of BOLD signals and functional connectivity (Wang et al., 2018) i.e. the correlation of activity in spatially separate neuron populations. Age related connectivity changes have also been shown to covary with the irregularity of EEG and MEG signals (Vakorin, Lippe, and McIntosh, 2011; McIntosh et al., 2014) and in an EEG study applying graph theory to functional networks, irregularity was found to correlate with network node centrality (Mišić et al., 2011).

The irregularity of neural activity can be quantified using entropy measures, where more disordered and irregular signals have larger entropy, and more regular signals have lower entropy. RVE is a derivative of Shannon entropy (Shannon, 1948) that has a built-in ability to provide a dynamic timecourse of signal entropy, retaining the signal's original temporal resolution (Robinson et al., 2013) (for more details see chapter 2). The relationship between irregularity and neural synchronisation, and the desirable qualities of RVE, suggest that RVE could be an alternative

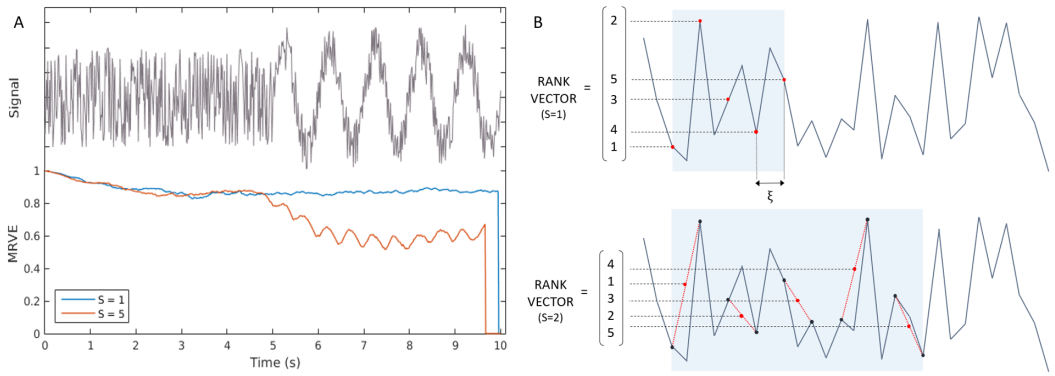


FIGURE 4.1: A) An example signal composed of white noise with an embedded 1Hz sinusoid (above), with the corresponding MRVE timecourses calculated at two temporal scales (below). $S = 1$ represents a fine time scale and a coarser scale is shown by $S = 5$. B) Graphical illustration of example rank-vector calculations for RVE (above), equivalent to the MRVE rank vector at scale factor $S = 1$, and MRVE at $S = 2$ (below). Both calculations are made with window length, $W = 5$, and lag, $\xi = 2$. For $S = 2$, the window of $W = 5$ points is found by taking the average values of 5 consecutive pairs of points.

measure to use in functional connectivity analysis that is not limited to the consideration of oscillatory activity.

RVE, and many other entropy measures, measure signal irregularity at a single temporal scale. However, it has been shown that neural activity contains recurring patterns that occur across a range of such scales (Costa, Goldberger, and Peng, 2005). It is not certain what these correspond to physiologically, however it is thought that activity at coarser scales is associated with long range, distributed information processing, while more local processing is captured at finer scales (Vakorin, Lippe, and McIntosh, 2011).

To utilise the in-built temporal resolution that is specific to RVE, a multi-scale extension of RVE (MRVE) was introduced. Figure 4.1A shows an example signal composed of a white noise component followed by an oscillation superimposed with low amplitude white noise. This is accompanied by the corresponding MRVE timecourses calculated at two different temporal scales. The entropy measure at the finer scale is dominated by the high frequency, high entropy noise. In contrast, at the coarser time scale MRVE is able to detect the regularity of the low frequency oscillation. An MRVE timecourse (at any scale) can be calculated from MEG virtual sensor timecourses at any number of required voxels, allowing for a direct comparison with dynamic oscillatory measures.

In this study, MRVE was used to reconstruct functional connectivity patterns, assess how repeatable these patterns are across a cohort of healthy volunteers and investigate how these patterns vary with temporal scale. We then compared connectivity profiles measured by MRVE correlation with those derived using amplitude envelope correlation (AEC). We also compared the robustness of MRVE correlation, and whether it provides extra information over standard methods, by comparing connectivity patterns derived at multiple entropy time scales with those derived from AEC in multiple frequency bands. The physiological relevance of irregularity was then investigated by examining the relationships between MRVE, oscillatory amplitude and regional connectivity strength. Finally, the effects of eye movement on the measured connectivity were investigated in an analysis of EOG recordings.

## 4.2 Methods

### 4.2.1 Data acquisition

All data analysed here were recorded at CUBRIC as part of the '100 Brains' UK MEG Partnership project (see Chapter 2 section 2.2.2 for more details). Participants also underwent a magnetic resonance imaging (MRI) session to aquire a T1-weighted 1mm anatomical scan, using an inversion recovery spoiled gradient echo acquisition (3T, General Electric).

### 4.2.2 Pre-processing

All data were downsampled to 600Hz from the original sample rate of 1200Hz, and a 1-150Hz bandpass filter was applied. Datasets were cut into 2 second epochs, which were each visually inspected and removed if they contained any major artefacts.

To perform analysis in source space, MEG virtual sensor timecourses were obtained in template space using a scalar LCMV beamformer (Van Veen et al., 1997) as described in chapter 2 section 2.2.2. Covariance matrices were obtained using the broadband pre-processed data filtered between 1-150Hz, as well as for activity within ten narrower frequency bands (1-4, 3-8, 8-13, 13-30, 40-60, 60-80, 80-100, 100-120, 120-140 and 140-160Hz). The current timecourses were then calculated at each

voxel for each frequency band, which could be used to calculate irregularity and oscillatory amplitude timecourses.

### 4.2.3 MRVE

The RVE method was first described by (Robinson et al., 2013), and was outlined here in chapter 2 section 2.2.1. The calculation of MRVE at each scale is identical to the calculation of RVE, except that each instance of the sliding window is formed from a 'coarse-grained' version of the raw signal. For a given scale factor, $S$, at each time point in the signal, $t$, $W$ consecutive, non-overlapping windows of $S$ points are taken starting at $t$, where each value is separated by lag $\xi$ (as defined in section 2.2.1 equation 2.1). Then, the values in the sliding window are found by taking the average of the data points within these windows. This is written in Equation 4.1, where $\boldsymbol{y_t}$ is the window found at time point $t$.

$$y_{t,j} = \frac{1}{S} \sum_{i=t+(j-1)S+1}^{t+jS} x_i \quad for\, 1 \leq j \leq W \tag{4.1}$$

This is then converted to the rank-vector, as illustrated in Figure 4.1B for example scale factors $S = 1$ and 2. At scale factor $S = 1$, this is the equivalent vector to that used in standard RVE. As the rank-vector calculated is dependent on the scale factor used, a separate entropy timecourse is generated for each value of $S$.

The time scale examined by MRVE is determined by the effective sample frequency of the values in $\boldsymbol{y_t}$. This 'scale frequency', $f_S$, is determined by the scale factor, where a higher value of $S$ correspond to a coarser sampling rate and therefore a lower value of $f_S$ (Courtiol et al., 2016). Equation 4.2 relates the scale factor to $f_S$ to aid in the interpretation of MRVE and its relationship with oscillatory measures.

$$f_S = \frac{f_c}{S} \tag{4.2}$$

For a given scale frequency, the values in $\boldsymbol{y_t}$ will be taken with the same effective sample frequency regardless of the sample rate of the data. This is ensured by the use of the lag, $\xi$. Before the coarse graining is performed, this ensures that samples are taken at the highest frequency of any signal components that could contain information (i.e. the lowpass frequency of the filter applied to the data, $f_c$).

### 4.2.4 Functional connectivity

90 nodes were selected by taking one voxel timecourse to represent each region of the AAL atlas (Tzourio-Mazoyer et al., 2002). The selection was performed for each participant and for each frequency band, identifying all voxels in each AAL region and finding the virtual sensor time course with the highest variance within the region. This voxel was chosen as an estimate of the timecourse exhibiting the maximum SNR within the region. To avoid the detection of spurious connections due to signal leakage, the zero-lag correlation between all 90 timecourses was removed by symmetric orthogonalisation (Colclough et al., 2015). This resulted in 90 orthogonal timecourses for each participant and frequency range, which were then used to calculate MRVE and oscillatory amplitude timecourses.

MRVE was calculated using the broadband, 1-150Hz virtual sensor timecourses, using a window length of $W = 5$ and a decay time constant of $\tau = 0.07s$. Timecourses were calculated for 25 scale factors between $S = 1 - 150$, with corresponding scale frequencies ranging from $f_S = 1 - 150$Hz. Oscillatory amplitude envelopes were found by taking the magnitude of the analytic signal of the timecourses obtained for each of the aforementioned narrow frequency bands, as in chapter 2. Functional connectivity was then measured as described by Koelewijn et al., 2019. The MRVE and Hilbert envelope timecourses were de-spiked to remove artefactual temporal transients using a median filter, and downsampled to 1 Hz. The first 50 samples were then trimmed to remove the MRVE 'warm-up' period while the histogram populates, and a window of samples at the end was removed, the length of which was defined by the length in time of the longest sliding window used in the MRVE calculation, corresponding to the largest scale factor.

Functional connectivity matrices were calculated separately for MRVE at each scale, and for oscillatory amplitude within each narrow frequency band by correlating each of the 90 timecourses from each participant with all others. The correlation values were then normalised by converting them to Z-scores using the Fisher transform. These were variance-normalised to correct for the effects of the varying timecourse lengths between participants, due to the removal of data epochs containing artefacts (Koelewijn et al., 2019). Without such normalisation, datasets

which have had more epochs removed may exhibit spuriously high correlation between the calculated amplitude and entropy envelopes due to their shorter length. Significant connections were determined by first ranking connections in order of strength for each participant, where the strongest connection was given the value 1 and the weakest given value 0. For each connection, the mean rank value was then found across participants. 'Valid connections' were taken as those with a mean rank above a threshold of 0.8, indicating that these connections are consistently among the strongest across participants. This threshold is arbitrary, however it has been shown previously to be a suitable threshold for detecting robust resting state network connections using AEC (Koelewijn et al., 2019).

## 4.3 Results

### 4.3.1 MRVE correlation

MRVE correlation was then used to measure functional connectivity and the connections were found that were consistently among the strongest across subjects. Figure 4.2 shows the location and number of the valid connections found for scale frequencies, $f_S$ = 1-150Hz. At higher scale frequencies, i.e. at finer temporal scales, most connections are found in occipital and parietal regions. As shown in Figure 4.3A, the maximum number of connections was found at $f_S$ = 75Hz. However, there is a second peak in the number of valid connections found at $f_S$ = 10Hz, where more frontal connections are seen. Cumulatively across all scales, valid connections were detected between 254 different pairs of nodes.

The valid connections found using AEC are also shown in Figure 4.2. Valid connections were found within four frequency bands. The most valid connections were seen in the beta band, giving the same number as for $f_S$ = 75Hz using MRVE correlation. Across all frequency bands, valid connections were detected between 248 different node pairs.

Figure 4.3C shows the connectivity networks plotted on a template brain for the MRVE scale frequencies that exhibit peaks in the number of connections detected ($f_S$ = 10, 75Hz), and for the AEC frequency bands that exhibit the most valid connections (1-4, 8-13, 13-30Hz). It can be seen in Figure 4.3C that the MRVE correlation

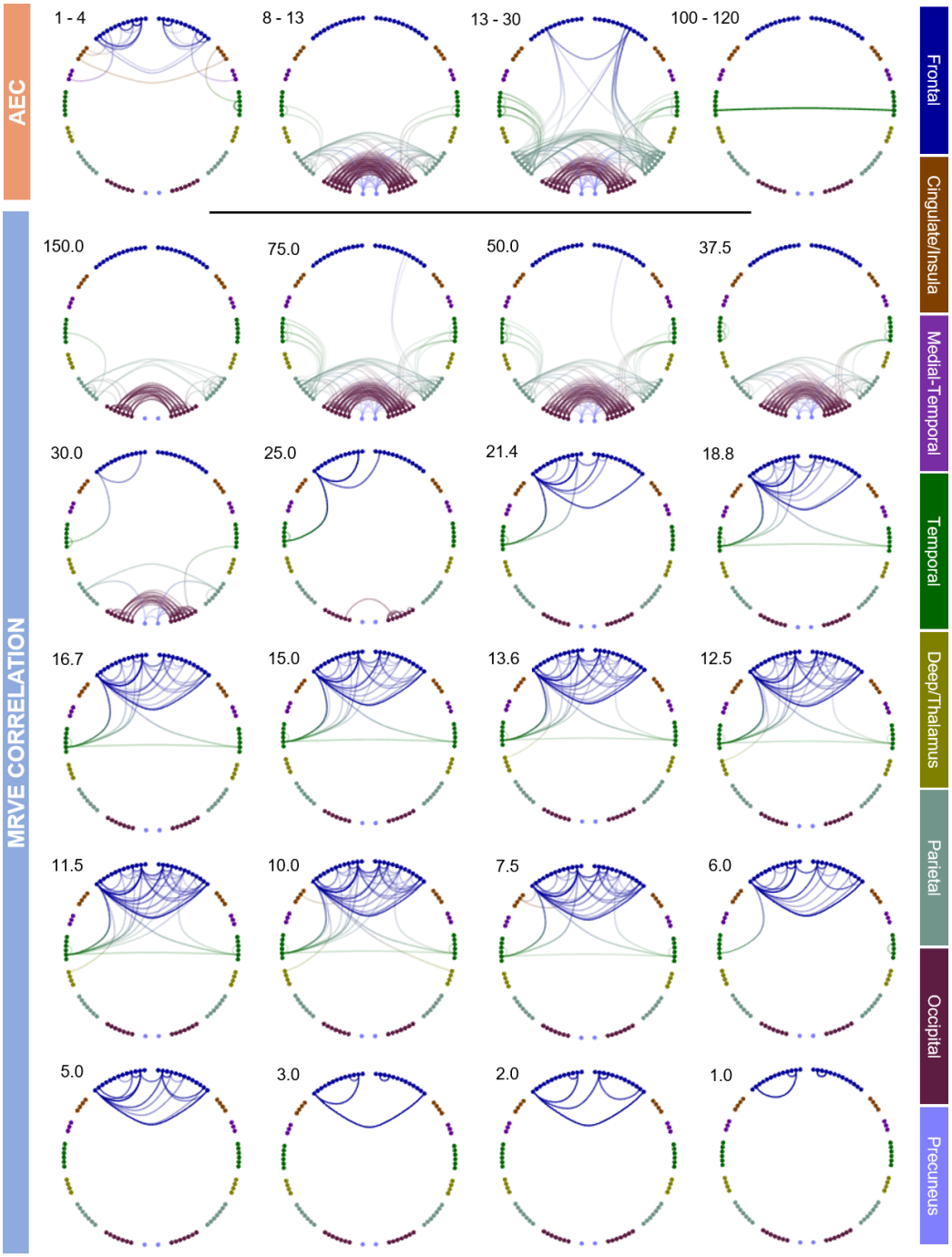


FIGURE 4.2: Valid connections (mean rank $>$ 0.8) found using AEC correlation for four frequency bands (above) and MRVE correlation for a range of time scales (below). Each point represents an AAL region and each line represents a connection. The AEC frequency band or MRVE scale frequency is given in Hz in the top left corner of each plot. The key on the right indicates the colour of the connections that originate in each brain region. No valid connections were found using AEC in the 3-8, 40-60, 60-80, 80-100 or 140-160Hz frequency bands.

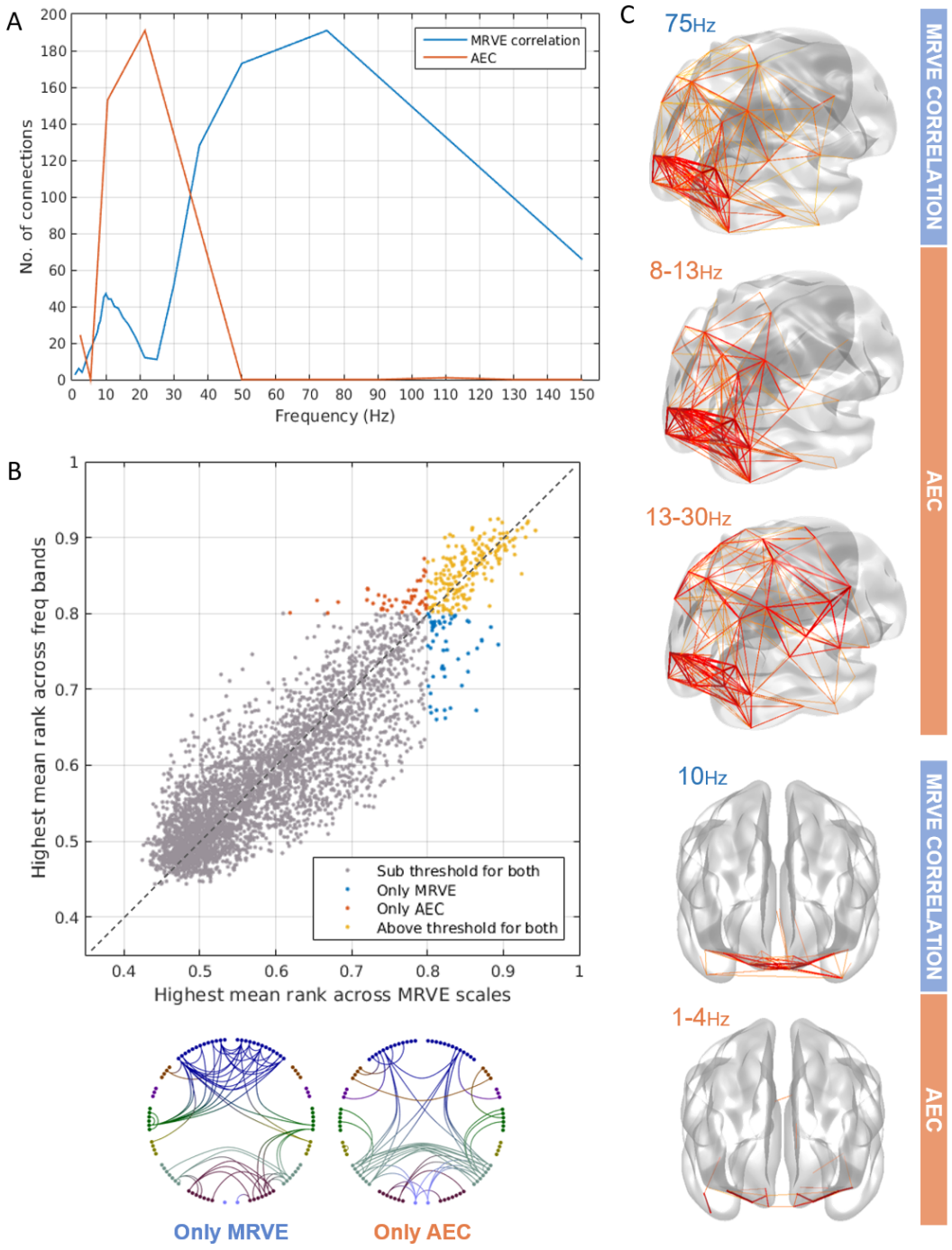


FIGURE 4.3: A) The number of valid connections found for each scale frequency using MRVE correlation and each frequency band using AEC. B) The highest mean rank of each connection across all frequency bands vs. all scale frequencies, where the colour indicates whether the connection is detected by both MRVE correlation and AEC, detected by neither, or detected by only one of the methods. Circle plots show the connections that are only detected as valid by either MRVE correlation or AEC. C) Valid connections plotted on a template brain for MRVE scale frequencies $f_S = 75$Hz and 10Hz and AEC frequency bands 1-4Hz, 8-13Hz and 13-30Hz.

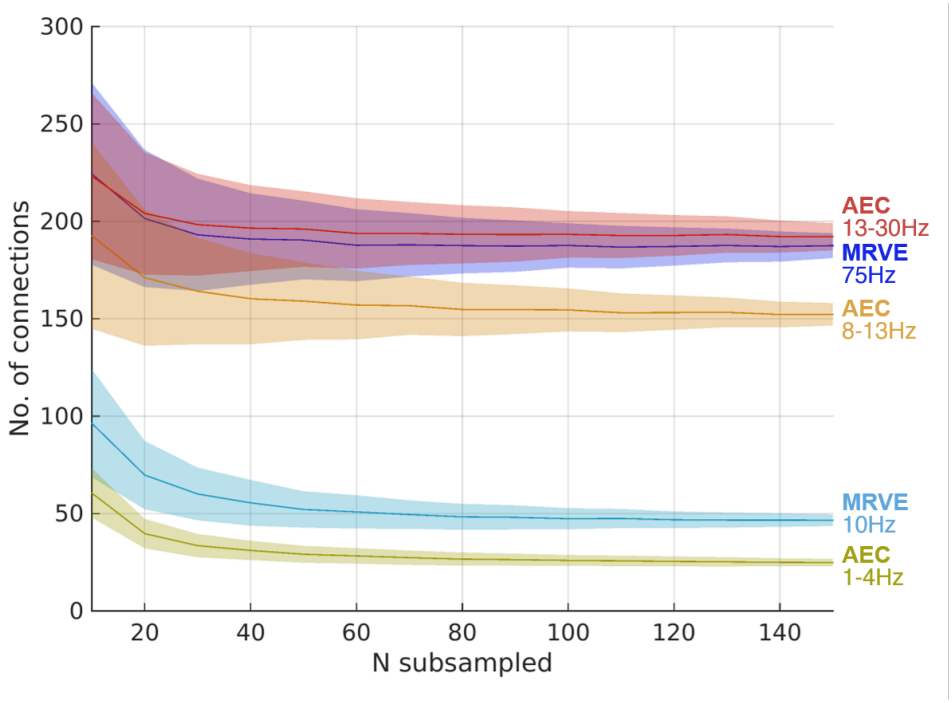


FIGURE 4.4: Analysis of the robustness of the connectivity measures given by AEC and MRVE correlation to varying sample size as measured by bootstrapping. The mean number of valid connections are shown over 1000 sub-samples of size $N$, randomly sampled with replacement. Error bands show the standard deviation.

connectivity profile at $f_S$ = 75Hz exhibits high similarity to the posterior networks found using alpha and beta band AEC. It can also be seen that the connections detected using MRVE correlation at $f_S$ = 10Hz are located at the very front of the brain, showing similarity to the delta band AEC network.

It was then investigated whether MRVE correlation could provide novel information about functional connectivity compared to AEC analysis. Firstly, it was seen whether each method could detect unique connections that were not deemed valid by the alternate method. To determine this for each connection, the highest mean rank was taken across all scale frequencies for MRVE and across all frequency bands for AEC. Those with a highest mean rank above the threshold of 0.8 for either method were taken as detectable by the corresponding connectivity measure. Figure 4.3B shows the highest mean rank values for each connection plotted against each other. Those connections that are 'unique' to each method are then shown plotted between the AAL nodes. 200 connections are visible to both MRVE correlation and AEC across all scales and frequency ranges, leaving 54 connections (21%) that can only be seen using MRVE correlation, and 49 (19%) that can only be seen using AEC.

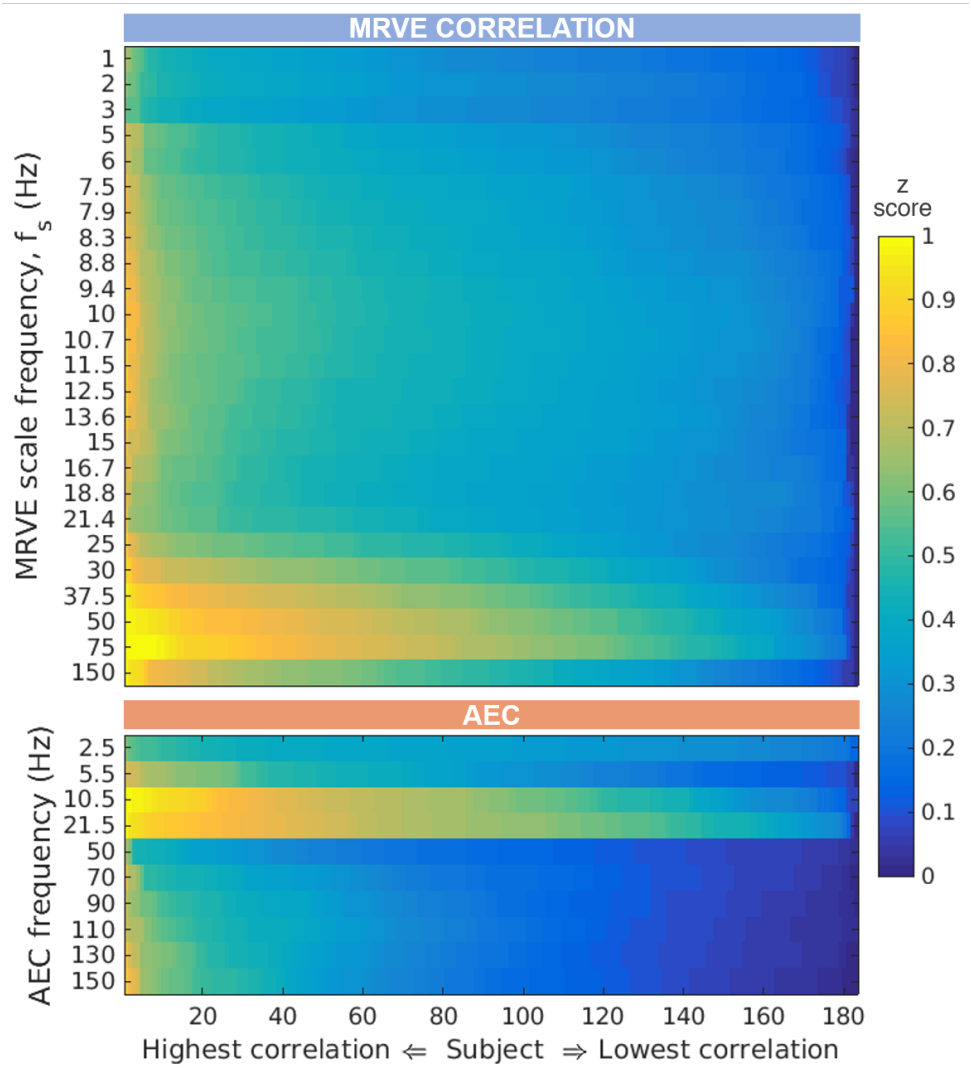


FIGURE 4.5: Analysis of the inter-participant consistency of the connectivity measures given by AEC and MRVE correlation. The consistency across subjects was found by correlating the vectorised $z$ score connectivity matrices of individual subjects with the average connectivity pattern across all subjects. The colour plots show the resultant *pattern-correlation* coefficients for each subject, sorted by correlation strength, for each MRVE scale frequency and AEC frequency band. AEC bands are represented by the frequency at the midpoint between the limits of the frequency range.

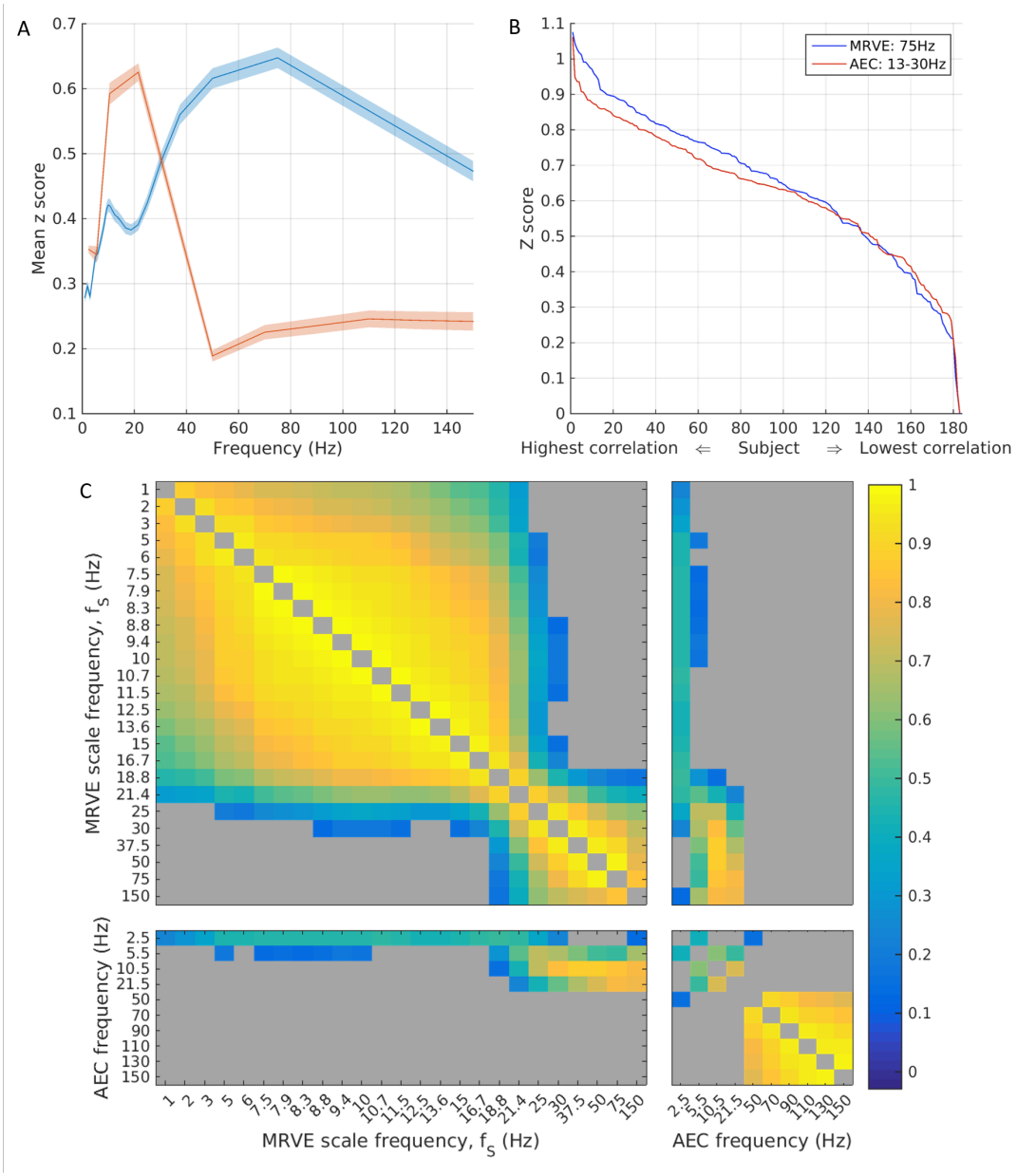


FIGURE 4.6: Analysis of the inter-participant consistency of the connectivity measures given by AEC and MRVE correlation. A) The *pattern-correlation* coefficients shown in Figure 4.5 wwere transformed to $z$ scores and averaged over subjects for each scale frequency and frequency band. Error bands show the standard deviation over 1000 sub-samples of $N = 90$. B) Sorted *pattern-correlation* coefficients, calculated as in Figure 4.5 for MRVE scale frequency $f_S$ = 75Hz and beta band AEC. C) Cross-correlation plot illustrating the within-participant consistency in *pattern-correlation* coefficients between scales and frequency bands. For each pair of scale frequencies and frequency bands, the Pearson correlation between the *pattern-correlation* z-scores was found across participants. Grey indicates a non-significant relationship ($\alpha = 0.05$, FDR corrected for multiple comparisons).

**Robustness of connectivity measures to sample size**

The robustness of each connectivity measure to the participant sample size was determined using bootstrapping. Sub-samples were taken from the cohort of 183 participants by simple random sampling with replacement. The sub-sample size, $N$, ranged from 10-150 participants. The number of valid connections was found for each sub-group taken, over 1000 tests per sub-group size. It can be seen in Figure 4.4 that the average number of connections found was less stable when using fewer participants in the analysis for both MRVE correlation and AEC. The average number approximates to the number of connections detected using the whole cohort (as shown in Figure 4.3A) when using $N \gtrsim 60$. However, for both MRVE correlation and AEC, the variance in the number of valid connections detected was found to be larger when fewer participants were included. For $N \lesssim 60$, a smaller sample was also associated with more connections detected on average.

**Consistency of connectivity patterns across participants**

The consistency of the connectivity profiles between individuals was then investigated. The average connectivity profile for each frequency band and scale frequency was taken by vectorising the mean $z$ score connectivity matrix, before the conversion to ranks. This profile was then correlated with the equivalent vector of $z$ scores obtained for each participant individually. For very robust networks that are highly reproducible across subjects, this method will give consistently high *pattern-correlation* with the average connectivity profile. However, the distribution of correlation coefficients will be, on average, lower for a network that shows high variability across participants. Each *pattern-correlation* coefficient is represented in the colour plot shown in Figure 4.5. For each scale factor and frequency band, these have been sorted in descending order. Consistent high correlation with the average connectivity patterns can be seen for MRVE correlation for scale frequencies 50 and 75Hz, and for alpha and beta band AEC.

To further quantify the robustness of each connectivity measure, the mean correlation with the average connectivity profile was found for each scale frequency and frequency band (i.e. the average was taken from each column on the colour

plot). These average *pattern-correlation* values are shown in Figure 4.6A, with error-bands generated by bootstrapping, using 1000 sub-samples of group size $N = 90$. The highest mean *pattern-correlation* was found for MRVE correlation, $f_S$=75Hz ($r = 0.5089 \pm 0.0004$), followed by beta band AEC ($r = 0.4980 \pm 0.0003$), suggesting that these two connectivity profiles were the most reproducible across subjects.

The *pattern-correlation* values (as shown in Figure 4.5) were then compared for MRVE correlation at $f_S$ = 75Hz and beta band AEC. The sorted *pattern-correlation* values for these frequencies are shown in Figure 4.6B. It appears that MRVE correlation at $f_S$ = 75Hz gives individual profiles that are slightly more similar to the average connectivity profile than beta band AEC. The *pattern-correlation* values were then compared in a permutation test, where the group assignment was randomised between 75Hz MRVE and beta band AEC over 10,000 permutations. However, it was found that there was no significant difference between the *pattern-correlation* values (p=0.344) for each connectivity measure.

**Within-participant consistency in pattern-correlation coefficients between scales and frequency bands**

It was then investigated whether the *pattern-correlation* coefficients calculated for each participant were related between scale frequencies and frequency bands. For example, it would be interesting to determine whether those participants who exhibited high similarity to the mean connectivity profile for one frequency also exhibited high *pattern-correlations* for other frequencies. For each pair of scale frequencies and frequency bands, the correlation between the *pattern-correlation* z-scores was found across participants (with the participant order held constant, in contrast with Figure 4.5). The resulting Pearson correlation coefficients are shown in Figure 4.6C.

No negative correlations were found between any frequency pairings, within or between connectivity measures. This indicates that there are no frequencies for which a high *pattern-correlation* indicates that a participant is more likely to have a lower *pattern-correlation* for another scale frequency or frequency band.

Strong positive correlations were found between the *pattern-correlation* vectors at a range of high MRVE scale frequencies, and also between low scale frequencies, with a crossover frequency of approximately 20Hz. This indicates that participants

exhibiting high *pattern-correlation* at one high scale frequency are also likely to show high similarity to the mean connectivity profile for other scale frequencies above 20Hz. The same can be seen for scale frequencies below 20Hz. However, the *pattern-correlations* exhibited by each participant at high scale frequencies have no relationship with their low scale frequency *pattern-correlation* coefficients.

For AEC, the strongest relationships between *pattern-correlation* vectors are found across the frequency bands in the gamma range (>40Hz). Positive relationships are also observed between *pattern-correlation* vectors corresponding to the lower frequency bands, the strongest of which is found between alpha and beta band *pattern-correlation*. As was observed for MRVE correlation, no relationships were found between the high and low frequency ranges.

Some relationships were also observed between the two connectivity measures. A strong positive correlation was observed between *pattern-correlation* vectors corresponding to high scale frequency MRVE correlation and alpha and beta band AEC. A weaker relationship was also found between the lower MRVE scale frequencies and delta band AEC. Interestingly, these relationships correspond to frequency pairings where high similarity was observed between the average connectivity profiles, as seen in Figure 4.2. This suggests that there is high within-subject similarity between connectivity profiles calculated by MRVE correlation at $f_S$ =75Hz and AEC profiles in the alpha and beta bands, in participants exhibiting high *pattern-correlations* for these frequencies.

**Predicting MRVE connectivity from AEC connectivity**

The amount of variance in the MRVE correlation that could be explained by AEC was then calculated using a multiple regression model. For each scale and frequency band, the correlation matrices for each participant were again converted to a column vector and then concatenated with those from all other participants to produce a single vector of connectivity values for that scale or frequency range. The fraction of the variance in the MRVE connectivity vectors that could be explained by the AEC vectors was then calculated using the model in equation 4.3, where $i$ represents each frequency band, $N_f$ is the number of frequency bands used in the model and $x_i$ represent the regression coefficients. This was implemented using the 'fitlm' MATLAB

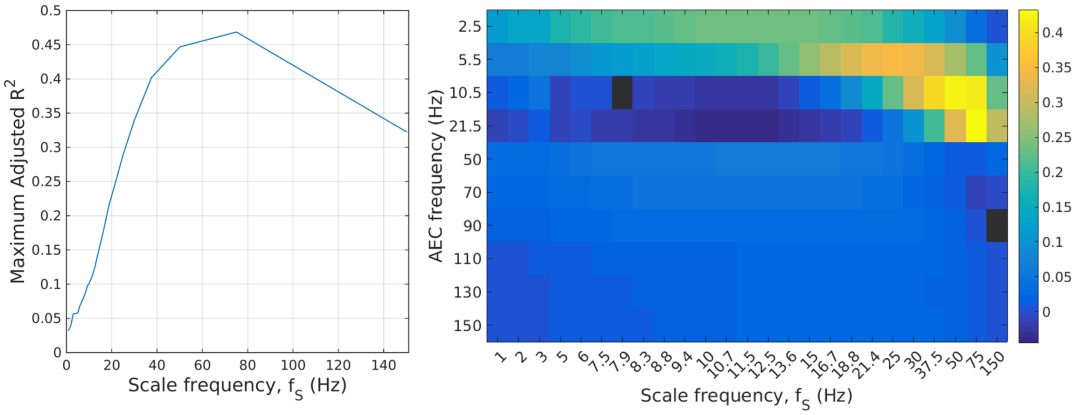


FIGURE 4.7: (left) The maximum adjusted $R^2$ obtained across all possible multiple linear regression models for each scale frequency. (right) Colour plot showing regression coefficients, where each column represents the coefficients obtained using MRVE correlation at the given scale frequency as the response variable. AEC bands are represented by the frequency at the midpoint between the limits of the frequency range. Black indicates that the corresponding AEC frequency was not included as a predictor variable in the optimal regression model (maximising adjusted $R^2$).

function.

$$MRVE\ correlation \sim 1 + \sum_{i=1}^{N_f} x_i AEC_i \tag{4.3}$$

The adjusted $R^2$ value found for each scale factor is shown in Figure 4.7. The adjusted $R^2$ value was considered to determine which combination of frequency bands would best explain the MRVE connectivity, as the highest adjusted $R^2$ values are obtained when the model only includes predictor variables which add explained variance beyond that which would be expected by chance. However, it was found that the highest adjusted $R^2$ values for each scale frequency were achieved when the AEC connectivity vectors from all frequency bands were incorporated in the model, except for $f_S$ = 7.9Hz when the alpha band was excluded, and for $f_S$ = 150Hz when the 80-100Hz band was excluded.

### 4.3.2 Temporal correlation between MRVE and oscillatory amplitude envelopes

The relationship between entropy and oscillatory amplitude was then investigated. At each voxel in the brain, the temporal correlation between MRVE timecourses and oscillatory amplitude envelopes was found across scale frequencies and frequency bands. Average $z$-scores are shown on a template brain in Figure 4.8.

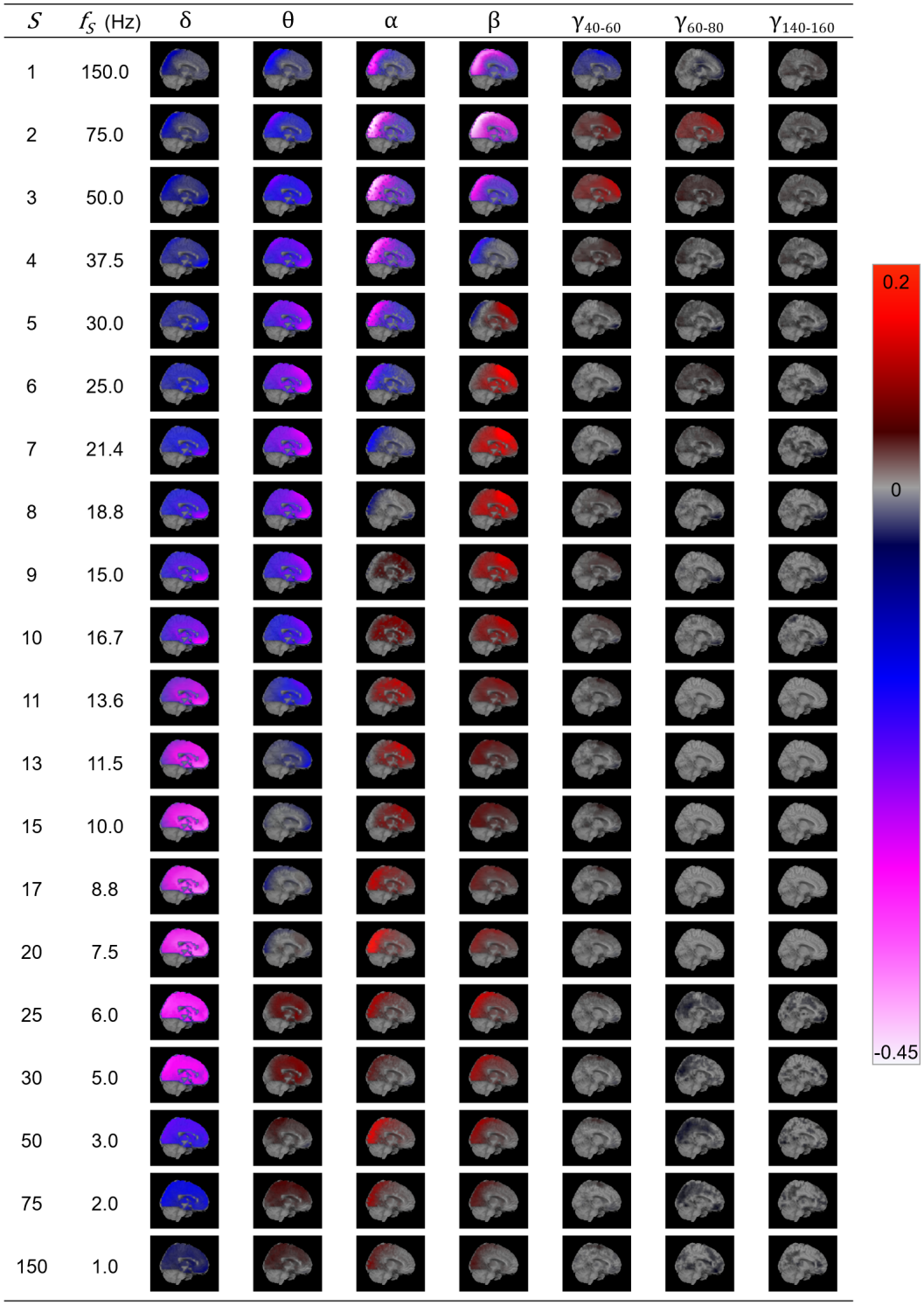


FIGURE 4.8: The temporal correlation between MRVE timecourses and oscillatory amplitude envelopes for scale frequencies $f_S$ = 1-150Hz and frequency bands 1-4Hz ($\delta$), 3-8Hz ($\theta$), 8-13Hz ($\alpha$), 13-30Hz ($\beta$), 40-60Hz ($\gamma_{40-60}$), 60-80Hz ($\gamma_{60-80}$) and 140-160Hz ($\gamma_{140-160}$). The temporal correlation coefficient was found at each voxel for each participant and transformed to a z-score by applying the Fisher transformation. The 95% confidence interval was found for the $z$-scores calculated across all participants for each voxel. Average Pearson correlation values were found at each voxel where $z = 0$ lay outside of this confidence interval and displayed on a template brain as indicated by the colour bar.

The relationship is shown to be dependent on the MRVE scale frequency and oscillatory frequency band, however the direction is generally consistent across the brain for each combination. At high scale frequencies ($f_S$ = 50-150Hz), MRVE shows a strong negative correlation with power in the alpha and beta frequency bands, where the strongest relationship is seen between MRVE at $f_S$ = 75Hz and beta band amplitude in the occipital and parietal regions. At $f_S$ = 50-75Hz, a weak positive correlation with gamma band amplitude is also observed, which is strongest in frontal and temporal regions. At mid to lower scale frequencies ($f_S$ = 1-25Hz), MRVE shows a negative correlation with delta band amplitude but a positive correlation with power in the alpha and beta bands. However, the areas in which the strongest positive correlation is observed varies with scale frequency and differs between the two frequency bands. The strongest positive correlation was observed between MRVE at $f_S$ = 21.4Hz and beta band amplitude in frontal and temporal regions. However, positive correlation was also observed in occipital and parietal regions between alpha and beta band amplitude and MRVE for $f_S$ = 1-8.8Hz.

### 4.3.3 The relationship between MRVE magnitude, oscillatory amplitude and connectivity strength

The overall connectivity 'strength' was then estimated for each AAL region. This was done for each node by finding the sum of the correlation coefficients indicating the connectivity between that node and all other nodes, for each AEC frequency band and each MRVE correlation scale frequency. This gave one connectivity strength value for each AAL region for each participant, for each frequency band and scale frequency used. The average entropy value within each AAL region was then found at each scale frequency for each participant, by taking the average value of the MRVE timecourses from the node voxel used in the connectivity analysis. Figure 4.9 shows the correlation between a vector containing all average entropy values across participants and the corresponding connectivity strength values. The correlation between connectivity strength and average oscillatory amplitude was also found, taken as the mean value of the hilbert envelope for each frequency band.

At high scale frequencies, it was generally found that average entropy negatively

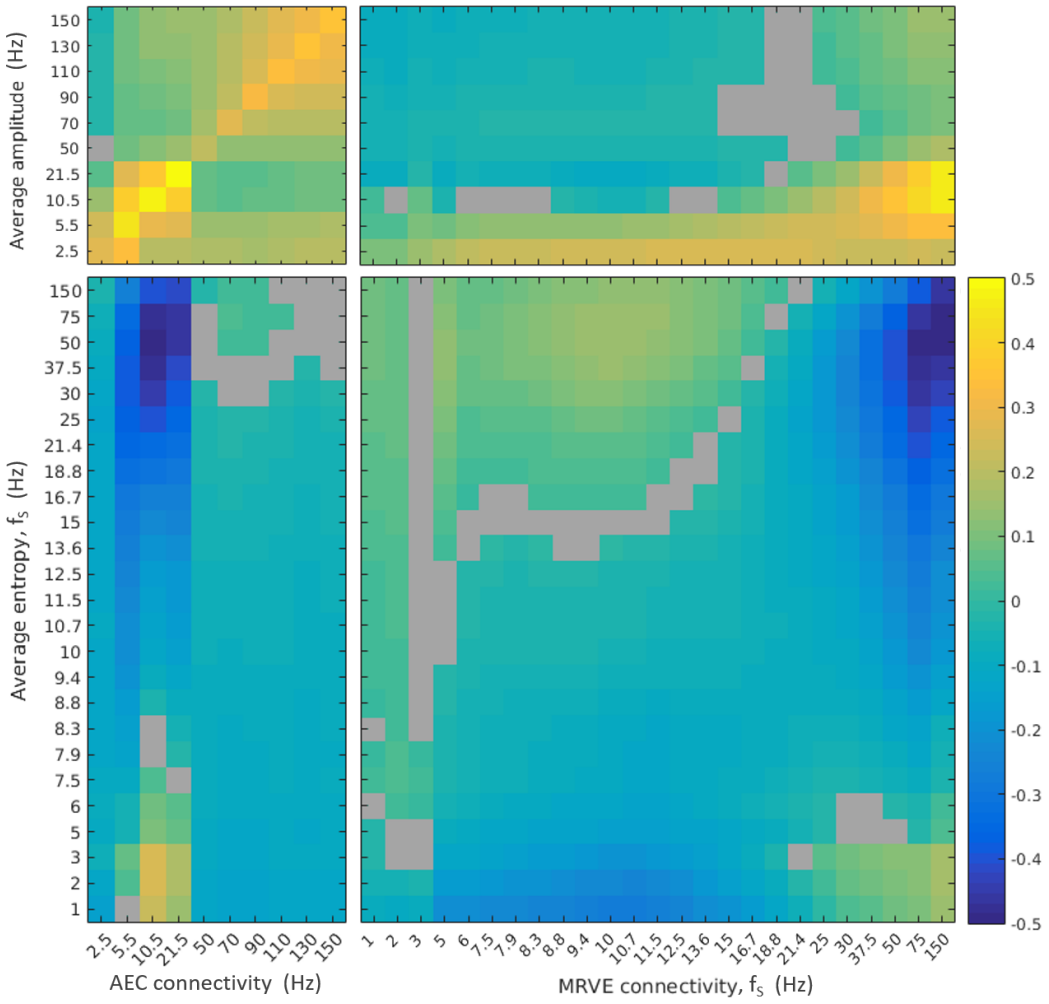


FIGURE 4.9: The correlation between average oscillatory amplitude/entropy and the overall connectivity strength at each voxel as measured by AEC and MRVE correlation. AEC bands are represented by the frequency at the midpoint between the limits of the frequency range. Warm colours indicate positive correlation whereas cooler colours show negative correlation and grey indicates a non-significant relationship.

correlates with connectivity strength. The strongest relationship with MRVE correlation was found between average entropy at $f_S$ = 75Hz and connectivity strength at $f_S$ = 150Hz ($r = -0.66$, $p << 0.001$), whereas the strongest relationship with AEC was found between average entropy at $f_S$ = 50Hz and alpha band connectivity strength ($r = -0.51$, $p << 0.001$). However, a weaker positive correlation was found between average entropy at fine time scales and connectivity at coarser scales, where the strongest correlation was found between average entropy at $f_S$ = 75Hz and connectivity strength at $f_S$ = 10Hz ($r = 0.18$, $p << 0.001$). A positive correlation is also seen between average entropy at very low scale frequencies ($f_S$ = 1-3Hz) and AEC in the alpha and beta bands, as well as with MRVE correlation at the highest scale frequencies. This is strongest between average entropy at $f_S$ = 3Hz and alpha band AEC ($r = 0.26$, $p << 0.001$), and between average entropy at $f_S$ = 2Hz and MRVE correlation at $f_S$ = 150Hz ($r = 0.18$, $p << 0.001$).

In contrast, there was generally a positive relationship between average oscillatory amplitude and connectivity strength. As shown in the top left of Figure 4.9, for AEC connectivity the strongest correlations were found when relating amplitude and connectivity strength within the same frequency band, where the strongest relationship was found for the beta band ($r = 0.49$, $p << 0.001$). Average amplitude also generally showed a positive correlation with connectivity strength as measured by MRVE correlation at fine time scales, where the strongest relationship was found between alpha band amplitude and connectivity strength for $f_S$ = 150Hz ($r = 0.46$, $p << 0.001$).

### 4.3.4 Effects of eye movement on functional connectivity measurements

The frontal location of connections observed for low MRVE scale frequencies and for delta band AEC suggests that they could be spurious due to eye movement. We therefore analysed the EOG recorded with each scan to investigate whether this connectivity could be explained by eye movement artefacts. For each participant, their level of eye movement during the MEG scan was summarised as the standard deviation of the EOG timecourse measuring their horizontal eye movements. However, there was a large difference in scaling between the EOG for the first and second halves of the participant cohort, so the standard deviation values were then

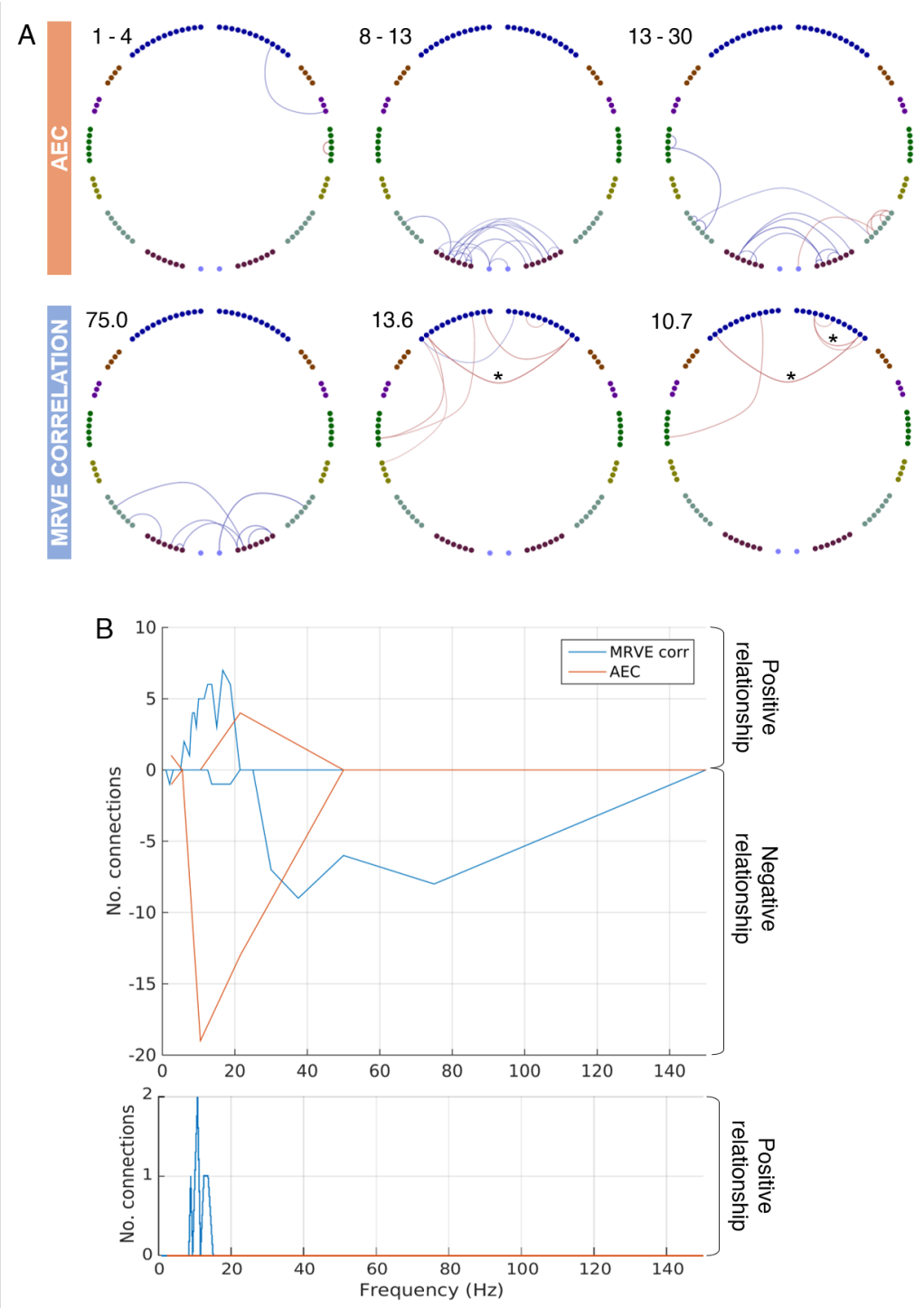


FIGURE 4.10: A) Connections where the EOG standard deviation could explain a significant amount of variance in the connectivity strength across participants ($p < 0.05$). Red indicates a positive relationship and blue indicates a negative relationship. Asterisks mark connections that show a significant relationship after Bonferroni correction. The AEC frequency band or MRVE scale frequency is given in the top left corner of each plot. B) The number of connections showing a significant relationship. The number of connections exhibiting a positive relationship is given above the $x$-axis. The number showing a negative relationship are given below the $x$-axis. The plot above shows the number before correction for multiple comparisons. The plot below shows the number after Bonferroni correction.

converted to Z scores separately for each half of the cohort. For each MRVE scale frequency and AEC frequency band, a linear regression model was used to determine whether a significant amount of variance in the connectivity strength measured across participants could be explained by horizontal eye movement for each valid connection. For low MRVE scale frequencies, a significant positive relationship was found between eye movement and connectivity strength for some frontal connections. For some of these connections, a significant relationship was still found after Bonferroni correction for multiple comparisons. This suggests, as hypothesised, that eye movement could be driving the frontal connectivity detected using MRVE correlation at these scale frequencies. However, no such relationship was found between eye movement and delta band AEC connectivity strength.

In contrast, for alpha and beta band AEC and for MRVE correlation at high scale frequencies ($f_S > 30$Hz) a negative relationship was found between connectivity strength and eye movement for a number of occipital and parietal connections. This suggests that higher levels of eye movement are associated with reduced resting state connectivity in these regions. However, at these frequencies, no connections were found to exhibit a significant relationship after correction for multiple comparisons.

## 4.4 Discussion

The correlation of neural irregularity as measured by MRVE has been used here to detect robust functional connections from MEG recordings, suggesting that this is a viable method for the analysis of resting state connectivity. The existence of robust connections that can only be detected by MRVE correlation also suggests that this method can provide complementary information to that provided by AEC.

By introducing the multi-scale element to the RVE method, it was possible to observe network connections that were present at different temporal scales. The number of valid connections detected and the brain areas they originated from varied with each scale frequency, although it was found that two general patterns of connectivity emerged.

At finer temporal scales ($f_S$ = 30-150Hz), the networks revealed are dominated by occipital and parietal connections, with some fronto-parietal and temporo-parietal connections. Connectivity in these regions during the resting state has been well established in the literature, in both fMRI (Lee, Smyser, and Shimony, 2013) and MEG studies, where connections in these areas have been found in the alpha and beta frequency bands using oscillation-based connectivity measures (Brookes et al., 2011a; Hillebrand et al., 2012).

The relationship between MRVE at fine time scales and oscillatory amplitude in the alpha and beta frequency bands was a recurring feature throughout the analysis here. It was shown that the connectivity profiles revealed by fine scale MRVE correlation and AEC in the alpha and beta bands showed high levels of similarity; the AEC within the alpha and beta frequency ranges made large contributions to the explained variance in the MRVE correlation at $f_S$ = 75Hz, the scale at which most connections were detected. It was also found that fine scale MRVE timecourses exhibited a strong negative correlation with the alpha and beta band amplitude envelopes, and that connectivity strength negatively correlates with average MRVE at this frequency while positively correlating with alpha and beta band amplitude. These findings imply that high levels of alpha and beta band AEC are associated with more regular activity at scale frequencies $f_S$ = 30-150Hz.

It could be that the decrease in irregularity represents a reduction in information processing performed locally within areas showing high levels of inter-regional connectivity. Entropy is maximised when there is the least integration between brain regions, while increased connectivity introduces statistical dependencies from activity in other brain areas and so decreases the 'randomness' exhibited by a region (Tononi, Sporns, and Edelman, 1994).

At coarser temporal scales, a second network pattern emerged consisting of mostly frontal and temporal connections which most closely resembles the AEC network found within the delta band. This similarity was again supported by the regression analysis, where the delta band AEC explained the largest fraction of variance in the MRVE correlation for scale frequencies $f_S = 1 - 13.6$Hz. Although, the overall fraction of the variance that can be explained at these coarser time scales is relatively small, suggesting that MRVE correlation provides more novel information about

connectivity at these scales beyond that which can be observed by AEC.

However, the EOG regression analysis revealed that the MRVE correlation observed at these low scale frequencies may have been driven by artefactual signal components generated by eye movements. A fixation point was used to limit eye movements, but it was found that participants still exhibited horizontal eye movement during the recordings, in agreement with previous resting state research (Fransson et al., 2014). Future work could repeat the analysis outlined here using data that has been cleaned of eye movement artefacts, for example using ICA, to determine whether these frontal connections are still observed. However, it was also found that eye movement may affect the posterior connectivity detected by alpha and beta band AEC and MRVE correlation at high scale frequencies. Although no connections exhibited a significant negative relationship after the correction for multiple comparisons, there is evidence for a relationship between eye movement and resting state activity from several fMRI studies. It has been found that disrupted eye movement due to Parkinson's disease is associated with widespread resting state functional connectivity alterations (Gorges et al., 2013; Gorges et al., 2016). It has also been found that areas within the default mode network show fluctuations in activity that correlate with spontaneous eye movement (Fransson et al., 2014). This could have implications for the study of functional connectivity in patient groups known to exhibit altered eye movements relative to controls, such as schizophrenia (Calkins, Iacono, and Ones, 2008). It is unclear how the removal of ocular signal components during data cleaning would affect the measurement of associated functional connectivity, and therefore the detection of alterations in patients.

Rather than solely relying on data cleaning to remove ocular artefacts, it may be beneficial to understand which factors underlie high levels of eye movement, so that steps can be taken at the scanning stage to avoid their impact on connectivity measurements. For example, it could be investigated whether participants are more likely to exhibit higher levels of eye movement when they are more alert or with increased drowsiness. This is not a question that could be addressed with the current dataset as no measures of alertness were recorded. Previous work may suggest that vertical eye movement would increase as participants become more drowsy, as

the frequency of spontaneous eye closures increases with drowsiness during resting (Ong et al., 2015). However, it has also been found that saccadic movement is quicker in participants who are more alert (Pettersson et al., 2019), suggesting that horizontal eye movement may increase with alertness. Future work could record alertness levels simultaneously with neuroimaging data to investigate their effects on eye movements, and thus resting state connectivity. One measure that is often used to quantify alertness levels is pupil diameter as this is known to decrease, and to fluctuate more, as a participant grows more tired (Lowenstein, Feinberg, and Loewenfeld, 1963). It may also be beneficial to record an electro-oculogram (EOG), which can be used to detect vertical and horizontal eye movements, to observe how these change with alertness levels. If it is found that alertness levels have an effect on the measured resting state functional connectivity, these findings could then inform experimental practice.

It is interesting to note that MRVE correlation for a given scale frequency does not provide the same information about functional connectivity as AEC for an overlapping frequency band. For example, while the frequency band that shows the most connections using AEC ranges from 13-30Hz, scale frequencies in this range are associated with a trough in the number of connections when using MRVE correlation. In fact, the connections that are detected by AEC for each frequency band show low similarity to those found by MRVE correlation with scale frequencies in the same range, as shown in Figure 4.7 by the low regression coeffficients for each MRVE scale frequency seen at equivalent AEC midpoint frequencies. This difference may be because the MRVE scale frequency, as defined in equation 4.2, can't be interpreted in the same way as an oscillatory frequency. While oscillatory frequency is defined as the inverse of the time period of an oscillation, the scale frequency does not assume that activity takes oscillatory form and so can't be defined in the same way. Instead, the scale frequency is an effective sample frequency of the coarse-grained samples in the MRVE sliding window. The benefit of defining the scale frequency in this way is that it is consistent across datasets with different sample frequencies. A given scale factor, $S$, may correspond to different temporal scales when data is recorded with different sample rates or filtered with a different lowpass frequency. However, a given scale frequency, $f_S$, will always give a sliding window with the

same effective sample frequency, regardless of the sample rate or filters applied to the data.

There could be alternative methods of defining the MRVE scale frequency that are more intuitively analogous to oscillatory frequencies. For example, an alternative scale frequency, $f'_S$, could be defined as the inverse of the time period spanned by the sliding window, as in equation 4.4.

$$f'_S = \frac{1}{W\xi S - (\xi - 1)} \tag{4.4}$$

However, when it is defined this way, the scale frequency gains an additional dependency on the number of samples included in the sliding window, $W$. The values of $f'_S$ would therefore vary with the value of $W$. For example, if all other parameters are kept consistent with those used in this analysis, an original scale frequency of $f_S$ =75Hz would correspond to an alternative scale frequency of $f'_S$ = 31.6Hz using $W = 5$, but $f'_S$ = 54.5Hz using $W = 3$. $W$ is a tunable parameter which affects the sensitivity of RVE to small changes in entropy, but it does not affect the temporal scale being examined. This was shown in chapter 2 where it was found that changing $W$ didn't change the general shape of the RVE waveform. Suitable alternative definitions of the MRVE scale frequency must be solely dependent on parameters that are related to the temporal scale being examined.

An investigation was also performed into the relationship between the MRVE and oscillatory amplitude calculated from the same activity timecourses. This relationship was investigated using single scale RVE ($f_S = 150$Hz) in chapter 2. In this chapter, the analysis was extended to investigate the relationship across a range of scale frequencies. MRVE was shown to have a complex relationship with oscillatory amplitude. In general, a positive correlation was found between oscillatory amplitude and entropy timecourses calculated when the MRVE scale frequency approximately overlapped the oscillatory frequency band. In contrast, a negative correlation is seen when the MRVE scale frequency is approximately higher than the lowpass frequency of the oscillatory frequency band. At the finest time scales, this is seen as a biphasic relationship where MRVE shows negative correlation with low frequency amplitude but positive correlation with gamma band amplitude, as seen

in chapter 2. By considering multiple time scales using MRVE, it was found that the correlation between the entropy and amplitude envelopes varies with the entropy scale frequency.

The direction of the relationships between MRVE and oscillatory amplitude were found to be generally consistent across the brain, for each pairing of MRVE scale frequency and oscillatory frequency band. However, the strength of the relationships were often found to vary spatially. For a number of combinations, the correlation was found to be strongest either in occipital and parietal regions, where most functional connections were detected, or in frontal and temporal regions. For example, the negative correlation between beta band amplitude and MRVE at fine scales is strongest in more posterior regions. In contrast, the positive correlation observed for $f_S$ values within the beta frequency range is strongest in anterior regions. This could imply that regional connectivity strength moderates the relationship between the irregularity and oscillatory amplitude of neural activity within that region. Future work could look at whether the same phenomenon is observed during a task, during which different regions would show higher connectivity strength.

### 4.4.1 Limitations

A limitation of this study is that the performance of MRVE correlation was only compared to AEC. AEC was chosen for comparison as it has been shown to give the most consistent results across participants (Colclough et al., 2016). This method was therefore the appropriate benchmark to use in a comparison of the number of robust connections detected by each connectivity measure. However, it could also be interesting to look at how MRVE correlation relates to connectivity measured by techniques that are centred around phase relationships. It has been suggested that an increase in signal regularity facilitates phase relationships between brain regions (Mcdonough et al., 2014) so it could be investigated whether there is similarity between the connections each method can detect and how this would differ from the relationship between MRVE correlation and AEC.

Another constraint on this analysis was the limit on the resolution of scale frequencies that could be used to generate MRVE timecourses. By increasing the low-pass frequency of the filter applied to the data, it would be possible to obtain MRVE

timecourses at finer temporal scales, and at more frequencies within the frequency range investigated here. For example, with a lowpass frequency of 300Hz, MRVE timecourses could be calculated for all frequencies considered here, as well as for $f_S$ = 300Hz, 100Hz, 60Hz etc. Future work could therefore choose the sample rate, lowpass frequency and scale factors used in order to target specific frequencies of interest.

It may also have been beneficial to calculate AEC within a broad gamma frequency band, such as the 60-140Hz band considered in chapter 3. This may have given an increase in SNR which could increase the likelihood of detecting gamma band connectivity. Future studies could therefore aim to detect AEC connectivity in a broad gamma band to investigate how these networks may relate to MRVE correlation networks across scale frequencies.

One methodological decision which may not have been appropriate was the downsampling of the MRVE timecourses before the calculation of the connectivity matrices. AEC is often calculated using downsampled envelopes as it has been found that the amplitude fluctuations underlying AEC connectivity occur over slow time scales (Brookes et al., 2011b). However, this may not be the case for the fluctuations in entropy that underlie MRVE correlation. By downsampling these timecourses it is possible that information was lost which may have provided additional information about connectivity. It may be interesting to repeat the analysis described here without the downsampling of the MRVE timecourses to investigate whether this affects the sensitivity of MRVE correlation to functional connectivity.

It was assumed that the optimal values of the RVE parameters, as established in chapter 2, would also be the optimal parameter choices for MRVE across all temporal scales. It was found in chapter 2 that values chosen for the decay time constant, $\tau$, and the sliding window length, $W$, determined the balance between the SNR and temporal resolution of the RVE timecourses. While it was found in chapter 2 that the choice of parameters didn't affect the shape of the RVE waveform, it may be that different parameter sets could be optimal for maximising the information contained within the MRVE timecourses at each scale frequency. For example, it is possible that MRVE timecourses could vary in SNR between scale frequencies, or that entropy at certain scale frequencies may vary more quickly in time, which would be better

captured by MRVE calculated using higher temporal resolution. By optimising the parameter choices for each scale frequency, future work could determine whether MRVE correlation could give higher sensitivity to functional connectivity than was found in this study.

Leakage correction has shown to be important for measuring reliable AEC (Colclough et al., 2016) and was performed here using symmetric multivariate orthogonalisation. This method has been shown to minimise spurious correlation between virtual sensor timecourses (Colclough et al., 2015). However, the performance of any leakage correction method is dependent on the choice of the timecourses to represents each AAL region. In this study, the voxel corresponding to the timecourse with the maximum temporal standard deviation was chosen as an estimate of the voxel exhibiting the largest SNR. This method could lead to voxels selected from adjacent AAL parcels being in close proximity to each other, and therefore the corresponding current time-courses at these locations could show real correlation (beyond spurious correlation due to source leakage). Any signal orthogonalisation method, including the one used here, would result in signal cancellation in the case of being presented with signals with such zero-lag correlation (Colclough et al., 2015). However, it is worth noting that even if signal components with zero-lag correlation are suppressed, it is still possible to observe correlation between the amplitude envelopes and the MRVE of signals with a relative phase difference.

While the issue of voxels selected in close proximity would affect AEC and MRVE correlation measurements equally, another limitation of this leakage correction method is that a bias towards signals with high SNR may led to missing important information about entropy. For AEC, maximising SNR may be desirable as oscillatory amplitude has been shown to correlate with functional connectivity (Tewarie et al., 2019). In contrast, the MRVE of a signal is independent of its amplitude. Selecting only signals with high amplitude may increase the chances of selecting those with low entropy, as larger groups of synchronised neurons are capable of generating MEG signals with higher amplitude. This could have lead to increased similarity between MRVE correlation networks and those found using AEC. It may be interesting to employ an alternative voxel selection method, that selects voxels on a basis other than SNR, to investigate how this alters the measured MRVE correlation. For

example, timecourses could be taken from voxels at the centre of each AAL region.

It is well established that neuronal irregularity varies with age (McIntosh, Kovacevic, and Itier, 2008; Lippé, Kovacevic, and Mcintosh, 2009; McIntosh et al., 2014; Vakorin, Lippe, and McIntosh, 2011). Functional network activity has also been found to vary over the lifespan, increasing during development (Schäfer et al., 2014; Brookes et al., 2018), and then being disrupted in healthy aging (Andrews-hanna et al., 2007; Vakorin, Lippe, and McIntosh, 2011; Schlee et al., 2012). It may be beneficial to investigate the effects of age on MRVE correlation connectivity profiles, to determine whether they remain consistent between age groups. However, the age distribution of the cohort used here was skewed towards younger participants, where almost 70% of participants (126/183) were in the 18-25 age range. This limited our ability to assess the effects of age on the results presented here. In addition, resting state functional connectivity has previously been shown to differ between the sexes (Weis, Hodgetts, and Hausmann, 2019). However, the participant cohort used here was mostly female (123/183). It is possible that connectivity profiles given by both measures may be less robust when applied to a cohort with more even distributions of age and sex. Although, one MEG study found that resting state power envelope correlation connectomes did not significantly alter with age (Coquelet et al., 2017). Future work could recruit a cohort with more balanced distributions of age and sex to investigate their effects on the reliability of these connectivity measures.

## 4.5 Conclusion

While it is interesting that MRVE correlation has shown promise as a measure of functional connectivity, the true test of its usefulness will be its performance in patient groups. The next chapter will investigate whether MRVE correlation can provide understanding about connectivity changes associated with genetic conditions, in comparison to conventional measures based on the oscillatory components of brain function.

# Chapter 5

# Connectivity and genetic risk of mental health disorder

A number of rare genetic variants, known as copy number variants (CNVs), have been identified that are associated with an increased risk of developing neurodevelopmental disorders (ND). However, the causal mechanisms are largely unknown. Previous findings suggest that alterations in functional connectivity that are observed in neurodevelopmental disorders may also be associated with a number of different ND-CNVs, suggesting that atypical network activity may be a link between the presence of ND-CNVs and disorder risk. Sensitive and robust methods of measuring functional connectivity can help to detect these alterations and aid in our understanding of the mechanisms underlying the increased risk of disorder.

MRVE correlation was introduced in the previous chapter as a method of calculating functional connectivity from MEG recordings, based on the synchronisation of entropy timecourses across temporal scales. In this study, MRVE correlation was used to measure functional connectivity from resting state MEG recordings of ND-CNV carriers. The sensitivity of this measure to connectivity alterations was also evaluated in comparison to oscillatory amplitude envelope correlation (AEC). Connectivity was found to be largely reduced compared to healthy controls, in agreement with previous findings, although some hyperconnectivity was also observed with temporal regions in the right hemisphere. Additionally, the properties of MRVE correlation networks in ND-CNV carriers, as quantified using metrics derived from graph theory, were distinguished from controls with an accuracy of $80.7 \pm 0.6\%$. This gave an 8.1% increase in accuracy compared to when connectivity was calculated using AEC. These results suggest that MRVE correlation can provide additional,

complementary information about alterations in connectivity associated with neurodevelopmental risk compared to that provided by oscillatory based measures.

## 5.1 Introduction

Copy number variants (CNVs) are rare genetic rearrangements where segments of DNA occur an unusual number of times in the genome (Redon et al., 2006). These can be duplications, where a segment is repeated more times than usual, or deletions, where a segment of DNA is not present or occurs fewer times than usual. Many CNVs have no known effects on any observable characteristics, but some are associated with an increased risk of developing certain diseases. For example, some CNVs have a higher incidence in people suffering from neurodevelopmental (ND) disorders, particularly increasing the risk of developing schizophrenia, autism spectrum disorder (ASD) and attention-deficit/hyperactivity disorder (ADHD) (Kirov et al., 2014; Chawner et al., 2019). Little is known about the mechanisms that link the presence of these variants, termed ND-CNVs, to mental health disorder. However, there are few variants associated with specific disorders (Chawner et al., 2019), implying that the effects of the ND-CNVs that contribute to disorder risk may be common between variants. Identifying alterations in brain activity that are associated with a variety of ND-CNVs can help us in identifying these universal mechanisms.

One symptom common to many neurodevelopmental disorders is altered functional connectivity compared to healthy controls. Reduced integration across the cortex has long been thought to underlie the symptoms of schizophrenia (Friston et al., 2016). Abnormal functional connectivity has also been found in patients with ASD (Hull et al., 2017; Fan et al., 2018) and ADHD (De La Fuente et al., 2013). The majority of studies investigating connectivity alterations associated with ND-CNVs have considered only individual variants. Most of these have focused on 22q11.2 deletion syndrome, also known as DiGeorge or velo-cardio-facial syndrome. 22q11.2 deletion is the most common ND-CNV and has the highest associated risk of developing schizophrenia (McDonald-McGinn et al., 2016). The presence of this variant has been found to be associated with disrupted structural and functional connectivity (Debbané et al., 2012; Padula et al., 2015). Structural connectivity alterations have

also been associated with other ND-CNVs studied in isolation, such as variations at 16p11.2 (Berman et al., 2016) and 15q11.2 (Silva et al., 2019). However, little research has been done to investigate functional connectivity alterations associated with the rarer variants.

Some recent evidence has revealed the existence of network connectivity alterations that are common between ND-CNVs. In a recent MEG study, Dima et al., 2019 was the first to investigate the oscillatory basis of atypical functional connectivity in carriers of a range of ND-CNVs. It was found that participants with the genetic variants showed decreased oscillatory amplitude envelope correlation (AEC) within the alpha and beta frequency bands, compared to controls. Similar abnormalities in white matter structures have also been found across a range of variants (Drakesmith et al., 2019).

Another commonality between many neurodevelopmental disorders is altered neuronal entropy. A number of MEG and EEG studies have detected more irregular brain activity in schizophrenia patients compared to controls (Fernández et al., 2013; Brookes et al., 2015). It has been theorised that this increase in irregularity is driven by a reduction in synchronisation between cortical regions due to disrupted integration (Fernández et al., 2013). On the other hand, reduced entropy of EEG signals has been observed in patients with ASD (Catarino et al., 2011; Ghanbari et al., 2015; Bosl, Loddenkemper, and Nelson, 2017). One study also detected reduced irregularity of resting state MEG activity in ADHD patients (Monge et al., 2015). There has been no analysis in the literature of neuronal irregularity in ND-CNV carriers, so it is unclear at present whether alterations in neuronal signal entropy are observed in those at neurodevelopmental risk. MRVE correlation was introduced in chapter 4 as a method of measuring functional connectivity from MEG recordings by measuring the synchronisation of entropy time-courses, and was found to be able to measure robust connectivity patterns in healthy participants. This connectivity measure might, therefore, be an alternative tool for detecting alterations in connectivity that can elucidate atypical irregularity of neuronal activity in ND-CNV carriers.

In this study, MRVE correlation was used to measure functional connectivity in participants with ND-CNVs, compared to controls with no known genetic conditions. The measured alterations in connectivity were then compared to those found

using AEC to determine whether the entropy based measure could provide any complementary information beyond that given by the more established technique. It was also investigated whether MRVE correlation could provide any additional sensitivity to differences between the ND-CNV and control cohorts by classifying the MRVE correlation and AEC network properties as quantified using metrics derived from graph theory.

The effects of the cleaning method used during the data pre-processing stage on the measured connectivity was also examined. ICA is often employed as a semi-unsupervised method of removing artefactual signal components from MEG and EEG data. It was speculated in chapter 4 that connectivity observed in frontal regions may have been spurious due to eye movements, which may have been suppressed if those components of activity had been removed using ICA. However, it is unclear from the literature how using this method affects connectivity measurements compared to when cleaning is performed manually, such as in chapter 4. Therefore, two different cleaning methods were employed - the visual identification of artefacts as used in chapter 4 and a semi-automated method using ICA - to determine whether this choice affects the sensitivity of each measure to connectivity alterations in ND-CNV carriers.

## 5.2 Methods

### 5.2.1 Participants and ethics

42 adults were recruited who each had one of 13 different ND-CNVs, chosen for frequent occurrence in those with neurodevelopmental disorders (22 female, average age $38.5 \pm 12.5$yrs). The frequency of each ND-CNV present in the cohort is shown in Figure 5.1.

Participants were recruited from NHS genetics clinics and support groups within the UK. These participants may have been initially diagnosed for a number of reasons. For example, they may have presented with developmental delay or they may have been a close relation of a person who had a ND-CNV. In some cases, participants may have presented with physical manifestations due to their condition. For

example, participants with a 22q11.2 deletion may have presented with a cleft palate or cardiac abnormalities.

34 of the participants in the ND-CNV cohort had been diagnosed with at least one mental health disorder. Of these, 15 had been diagnosed with neurodevelopmental disorders. 26 of these participants were taking medication for physical, neurological or mood disorders. The most common medications across the cohort were gabapentin, co-codamol and fluoxetine. However, there was a high level of variability in the medications taken between participants and so their effects could not be investigated on functional connectivity. Instead, only effects that were robust across the cohort were investigated. More details regarding the psychiatric assessment of the participants in this cohort, as well as details of the genotyping performed to diagnose the ND-CNVs, have previously been described by Dima et al., 2019. MEG data were collected with written consent from these participants, in accordance with the code of ethics put forward in the Declaration of Helsinki. All procedures were also approved by the South East Wales research ethics committee.

42 age and gender matched controls were selected from the cohort scanned as part of the '100 brains' UK MEG partnership project (22 female, average age 33.3 $\pm$ 9.6yrs). All control participants had no history of neurological or neuropsychiatric disorders. It was assumed that none of the control cohort had any of the ND-CNVs investigated here due to their rarity. Details of the cohort these control participants were sampled from can be found in Chapter 2 section 2.2.2. Data was collected from this group in accordance with procedures approved by the Cardiff University School of Psychology ethics committee.

### 5.2.2 Data and analysis

Five minute resting state MEG data were collected as described in chapter 2 section 2.2.2, and any channels showing excessively high variance were removed. Data were then cleaned of artefacts using two different methods: a visual cleaning procedure and a semi-automated method using ICA. The visual cleaning process first required splitting data into two second epochs. These were each visually inspected and those containing artefacts due to muscular activity or eye movements were removed.

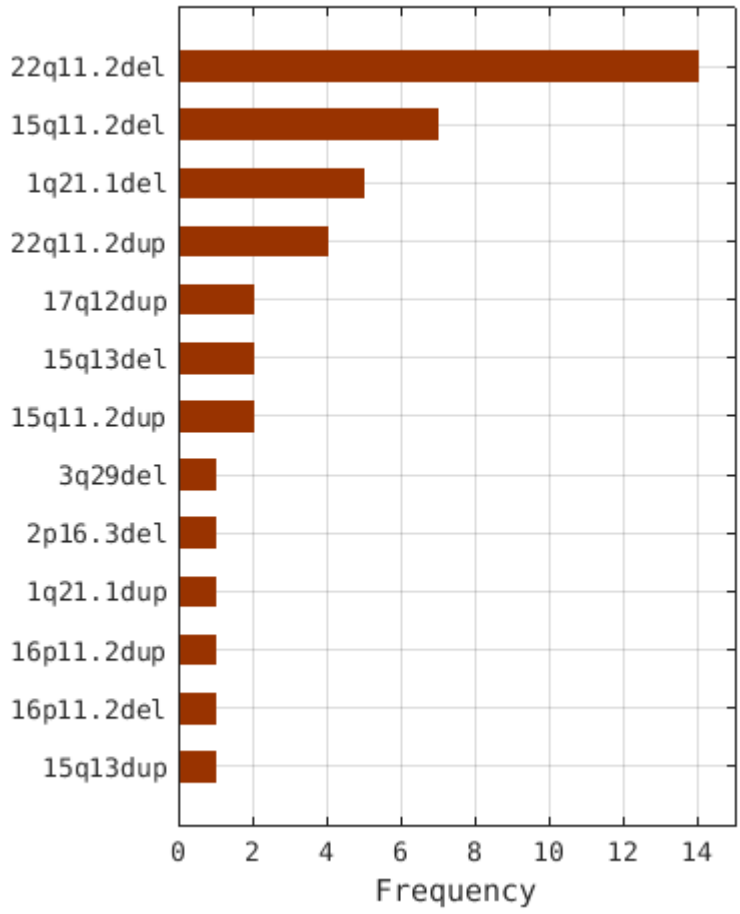


FIGURE 5.1: The number of participants with each genetic variant in the ND-CNV cohort ($N = 42$).

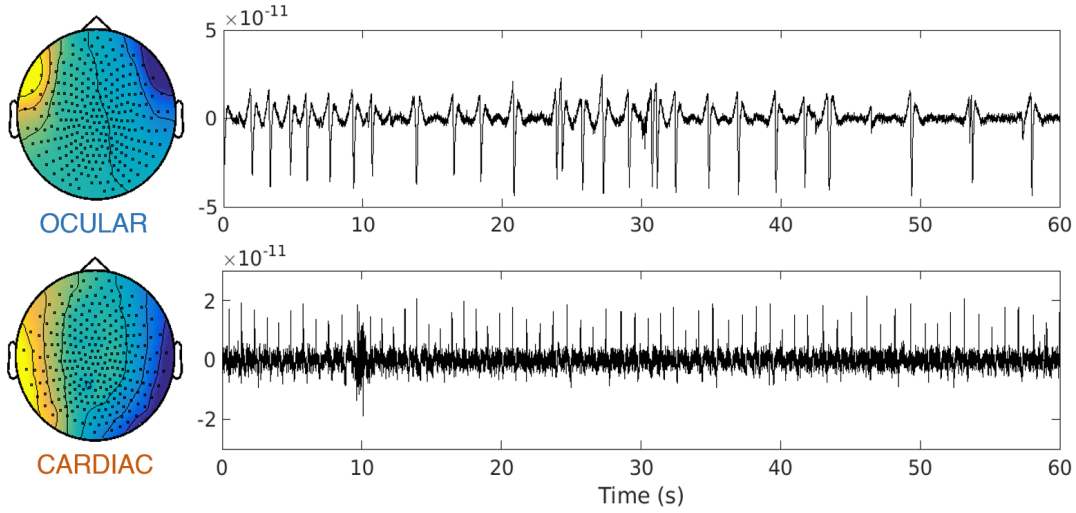


FIGURE 5.2: Examples of artefactual signal components that were removed during ICA cleaning, including ocular (above) and cardiac components (below). Both the spatial topography of the fields (left) and the component timecourses (right) were visually inspected to identify those that represented artefactual signals.

For the ICA-based cleaning method, the epochs containing muscle artefacts were first removed automatically using FieldTrip (Oostenveld et al., 2011). A 110-140Hz bandpass filter was first applied to the data, which were then split into two second epochs and transformed to $z$-scores using the Fisher transform. Segments containing $z$-scores above a participant-specific threshold were removed. Next, components of the signal from eye movement and cardiac artefacts were identified and removed from the data using ICA. Artefactual components were identified by visually inspecting the component timecourse and the spatial topography of the fields across the sensors. Examples of ocular and cardiac components are shown in Figure 5.2. Ocular components were associated with a frontal field pattern, with large fluctuations in the component timecourses that repeated at irregular intervals. Cardiac components were identified as having a broad field pattern, due to the field generator being further away from the sensors. The corresponding timecourses featured a rhythmic spiking pattern.

Connectivity analysis was then performed twice for each participant using data that had been cleaned using both methods. Functional connectivity was measured as in chapter 4 section 4.2.4 using both MRVE correlation and AEC. Valid connections were again determined as those with a mean rank > 0.8 (i.e. those that were among the 20% strongest connections on average across participants).

**Measuring connectivity differences associated with ND-CNVs**

For each AEC frequency band and MRVE scale frequency, it was determined whether there was a significant difference in connectivity strength between the ND-CNV and control cohorts at each edge by performing an unpaired $t$-test to compare the corresponding $z$-scores calculated for the participants in each group ($p<0.05$). To reduce the impact of noise, only those connections that were found to be valid in either cohort were included in the analysis.

To correct for multiple comparisons, a permutation omnibus test was used to obtain a critical $t$ value (Nichols and Holmes, 2001). For 10,000 permutations, the $z$ scores corresponding to each edge were randomly assigned to either participant group, and an unpaired $t$-test was performed at each edge as before. The maximum $t$ value across all edges was then found for each permutation. The threshold $t$ value was taken as the value at the upper 95% confidence interval on the distribution of these maximum $t$ values. Edges with an original $t$ value larger than this threshold were considered to exhibit a significant group difference in connectivity after correction for multiple tests.

**Using a machine learning classifier to determine ND-CNV status**

To assess the ability of each connectivity measure to detect alterations in connectivity due to the genetic conditions, it was investigated whether the connectivity profiles of the ND-CNV and control groups could be distinguished using a linear Support Vector Machine (SVM) classifier (Boser, Guyon, and Vapnik, 1992). If the connectivity of each participant can be described by $N$ features then these can be considered as a vector in $N$ dimensional space. An SVM classifier will find the optimal plane through this space, known as a hyperplane, that can separate the vectors from participants with ND-CNVs and those from control participants. This is done while maximising the classification margin - the distance between the hyperplane and the closest point to it. The SVM classifier was implemented using the MVPA for MEG MATLAB toolbox, which utilises the LibLinear toolbox (Fan et al., 2008).

The performance of the classifier can be quantified by calculating the percentage of participants that are classified correctly by the hyperplane - this is termed the

accuracy of the classifier. If a hyperplane can be found that can separate the majority of the connectivity vectors from each group, then the classifier is of high accuracy. If no consistent difference in connectivity between the two groups can be found then the classification may not improve upon random group assignment, which would give an expected accuracy of 50%. Two other metrics of classification performance are sensitivity and specificity. Sensitivity gives the fraction of ND-CNV carriers who are classified correctly (the true positive rate), whereas specificity gives the fraction of the control group that are correctly classified (the true negative rate).

A hyperplane may be found that can completely distinguish between the connectivity of two groups but it may be unable to correctly classify connectivity of new participants. The ability of the classifier to work on unseen data can be determined by performing cross validation. This involves dividing the data into two sets - one for training the classifier and one for testing. A hyperplane is produced based on the connectivity in the training set, and then its accuracy is determined based on its ability to classify the values in the testing set. This procedure is repeated a number of times, while permuting the training and testing sets, to obtain the average accuracy of the classifier. The method of cross validation chosen here was $k$-fold cross validation, with $k = 5$. This involved splitting the whole cohort randomly into five groups of approximately equal size. Each group of participants was subsequently held out to be used as testing data while a classifier was trained on the remaining data. This was performed over 100 iterations of group assignments, and the average performance of the classifier was taken across all iterations.

#### Network features from graph theory

Graph theory provides ways of quantifying the properties of brain networks based on functional connectivity matrices (Rubinov and Sporns, 2010). Calculating these can reduce the dimensionality of the data given to the SVM classifier as the connectivity that each AAL region exhibits with the rest of the brain can be reduced to a single value. This reduces the number of features used to perform the classification and can decrease the likelihood of the classifier 'overfitting' the data used to generate the hyperplane and being less able to classify new data.

A network is considered to be a set of regions, or 'nodes', connected by links called 'edges', where a path may be drawn between between each pair of nodes by following a set of connected edges. In the case of functional connectivity networks, the edges may be weighted according to the connectivity strength between each pair of nodes. The length of the path between each node pair is taken as the sum of the inverse of these weights, so a short path length indicates that a series of strong connections link the nodes. Six different metrics were used to quantify the properties of these networks, consistent with those used by Dima et al., 2019. These metrics were calculated using the graph and network algorithms in MATLAB R2019a and the Brain Connectivity Toolbox (Rubinov and Sporns, 2010).

**Degree.** The number of edges connected to a node. This indicates the importance of the node within the network.

**Betweenness centrality.** The fraction of all shortest paths that pass through a given node. This also indicates node importance.

**Eccentricity.** The maximum shortest path length that each node has with any other node, i.e. the distance from any given node to the furthest node from it.

**Global efficiency.** The inverse of the shortest path length between all pairs of nodes, averaged over all pairs. This is calculated to give one value for the network as a whole to give a measure of integration across the cortex.

**Local efficiency.** The global efficiency calculated on a node's neighbours gives a measure of segregation.

**Clustering coefficient.** The fraction of a node's neighbours that are also neighbours of each other, i.e. the fraction of neighbouring nodes that are connected in triangles. A network with high clustering coefficients will consist of subgroups of nodes that are highly interconnected, indicating segregation of cortical areas.

These metrics were used to assess the sensitivity of each connectivity measure to differences in network properties between the ND-CNV and control cohorts. First,

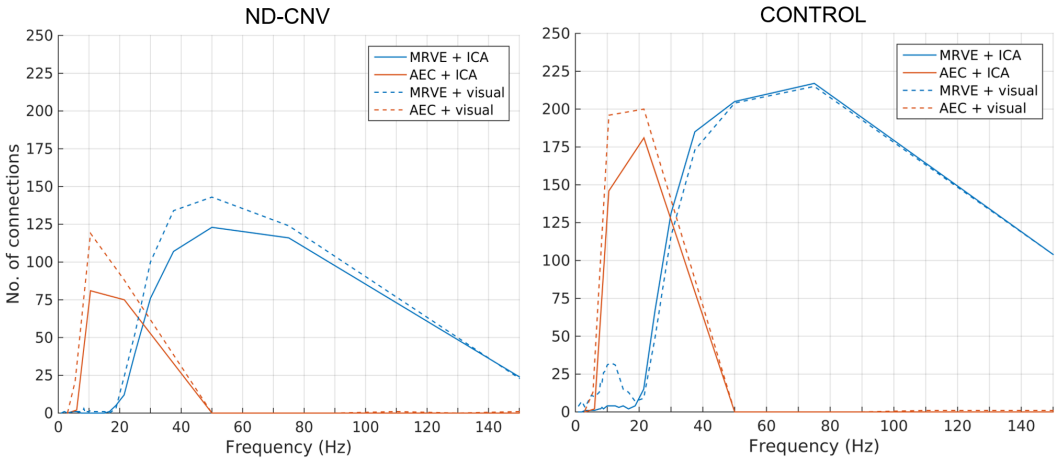


FIGURE 5.3: The number of valid connections found for the CNV carriers and the control cohort, using both MRVE correlation and AEC to measure functional connectivity of data that had been cleaned by visually identifying artefactual segments and data cleaned using the ICA-based method.

individual functional networks were obtained for each participant; for each MRVE scale frequency and AEC frequency band, a threshold was applied to each participant's individual connectivity profile to keep only the 20% most strongly weighted edges (rank > 0.8). The properties of these networks were then quantified using the six metrics outlined above. The calculated values for each metric were concatenated across all MRVE scale frequencies and separately across all AEC frequency bands. This gave six vectors describing the properties of networks produced using MRVE correlation for each participant, and six describing those obtained using AEC. The SVM algorithm then classified participants as ND-CNV carriers or controls based on these vectors. For both connectivity measures, classification was also performed using a combined vector that was produced for each participant by concatenating the vectors corresponding to the individual metrics.

## 5.3 Results

### 5.3.1 Group-level connectivity differences

Figure 5.3 shows the number of valid connections found in the ND-CNV and control cohorts. Fewer connections are detected as valid in ND-CNV carriers compared to controls, as measured using AEC and MRVE correlation. For MRVE correlation, in the control group most connections are detected using a scale frequency of

$f_s = 75Hz$, as was found in chapter 4. However, in the ND-CNV carrier group, the scale frequency showing the maximum number of connections is reduced to 50Hz. Using AEC to measure connectivity, the most connections for the control group are found within the beta frequency band, consistent again with results in chapter 4. For the ND-CNV carrier group the maximum number of connections were found in the alpha band.

Using the ICA-based method of data cleaning reduces the number of valid connections detected, using both connectivity measures, as compared to the visual method. Using AEC, the biggest difference in number of connections detected is found in the alpha band for both the ND-CNV and control groups. However, the effect of the cleaning method on the connections found using MRVE correlation is different between the two cohorts. In the control group, a peak in the number of connections is found at $f_S$ = 15Hz when data is cleaned visually. However, when data had been cleaned using ICA these connections were no longer observed, suggesting that they were perhaps spurious artefacts due to eye movements. In contrast, in the ND-CNV cohort there are very few valid connections detected at these lower scale frequencies using either cleaning method, but a reduction in the number of connections is found in the $f_S$ = 30-75Hz range when the ICA-based method is used. As the reduction in the number of valid connections suggests that the visual cleaning method did not remove all artefactual activity, unless specified, all further figures were produced using the data that had been cleaned using the ICA-based method.

Figure 5.4 shows the mean group difference in connectivity $z$-scores at each edge where the difference was found to be significant in an unpaired t-test ($p<0.05$). Measuring connectivity using AEC reveals group differences in three frequency bands: 3-8, 8-13 and 13-30Hz. Using MRVE correlation, group differences were found across all included scale frequencies in the 1-150Hz range. Using alpha and beta band AEC and MRVE at scales frequencies, $f_S \gtrsim$ 18Hz, most connections that exhibit group differences in strength are found between temporal, parietal and occipital nodes. Most are found to show weaker connectivity in the ND-CNV group than in the control group (shown as blue lines in Figure 5.4). However, there is some hyperconnectivity with the right temporal lobe observed in the ND-CNV cohort (shown as red lines in

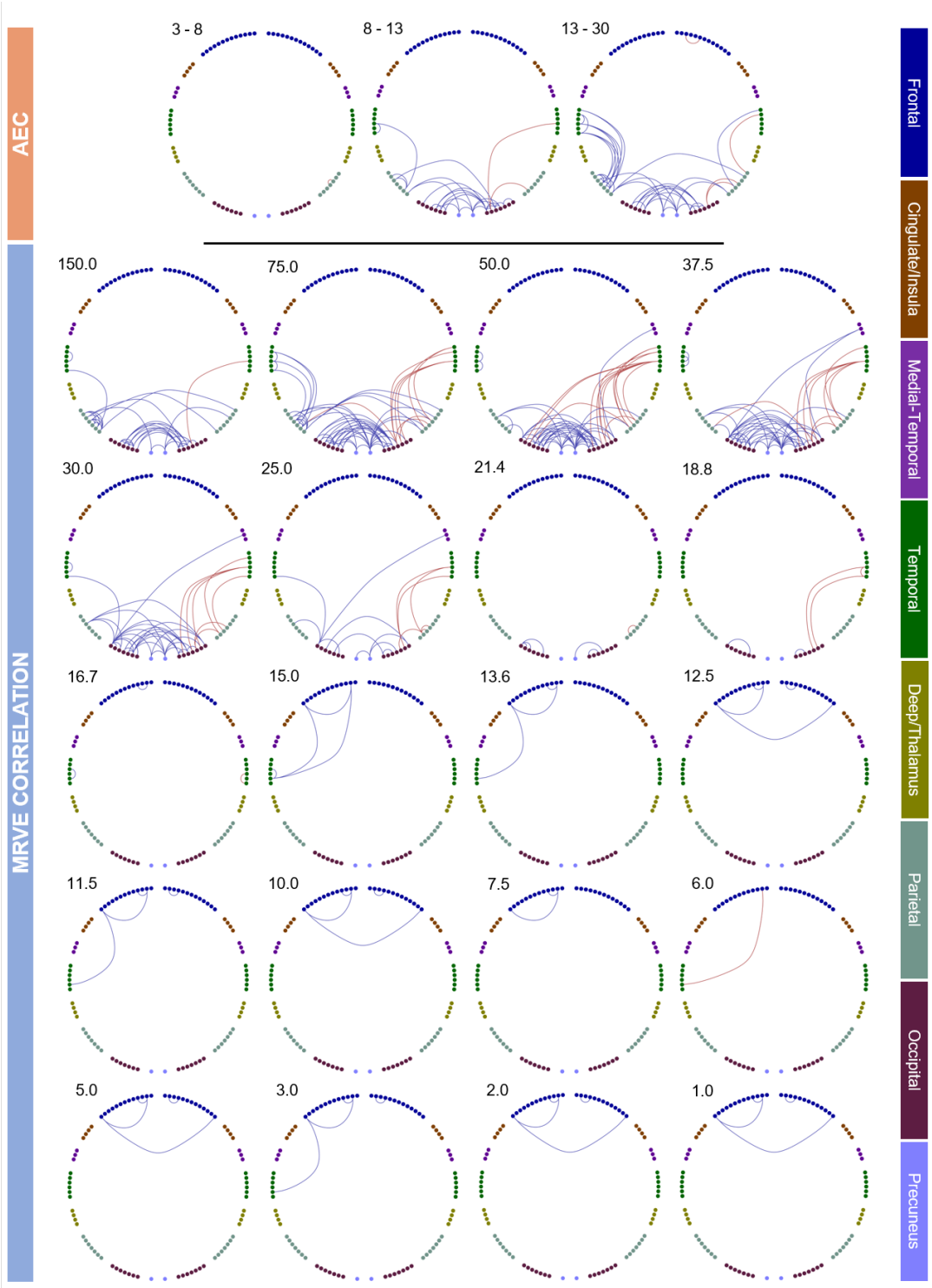


FIGURE 5.4: Connections where z-scores were found to be significantly different between the ND-CNV and control cohorts using a t-test ($p<0.05$). Connectivity was calculated using data that had been cleaned of eye movement artefacts using ICA. Connectivity differences were found using AEC correlation for three frequency bands (above). Significant differences were found across all scale frequencies when using MRVE correlation (below). Each point represents an AAL region and each line represents a connection. Red lines indicate stronger connectivity in the ND-CNV cohort than controls and blue lines indicate weaker connectivity in the ND-CNV group. The AEC frequency band or MRVE scale frequency is given in Hz in the top left corner of each plot. The key on the right indicates the brain region each AAL node is within.

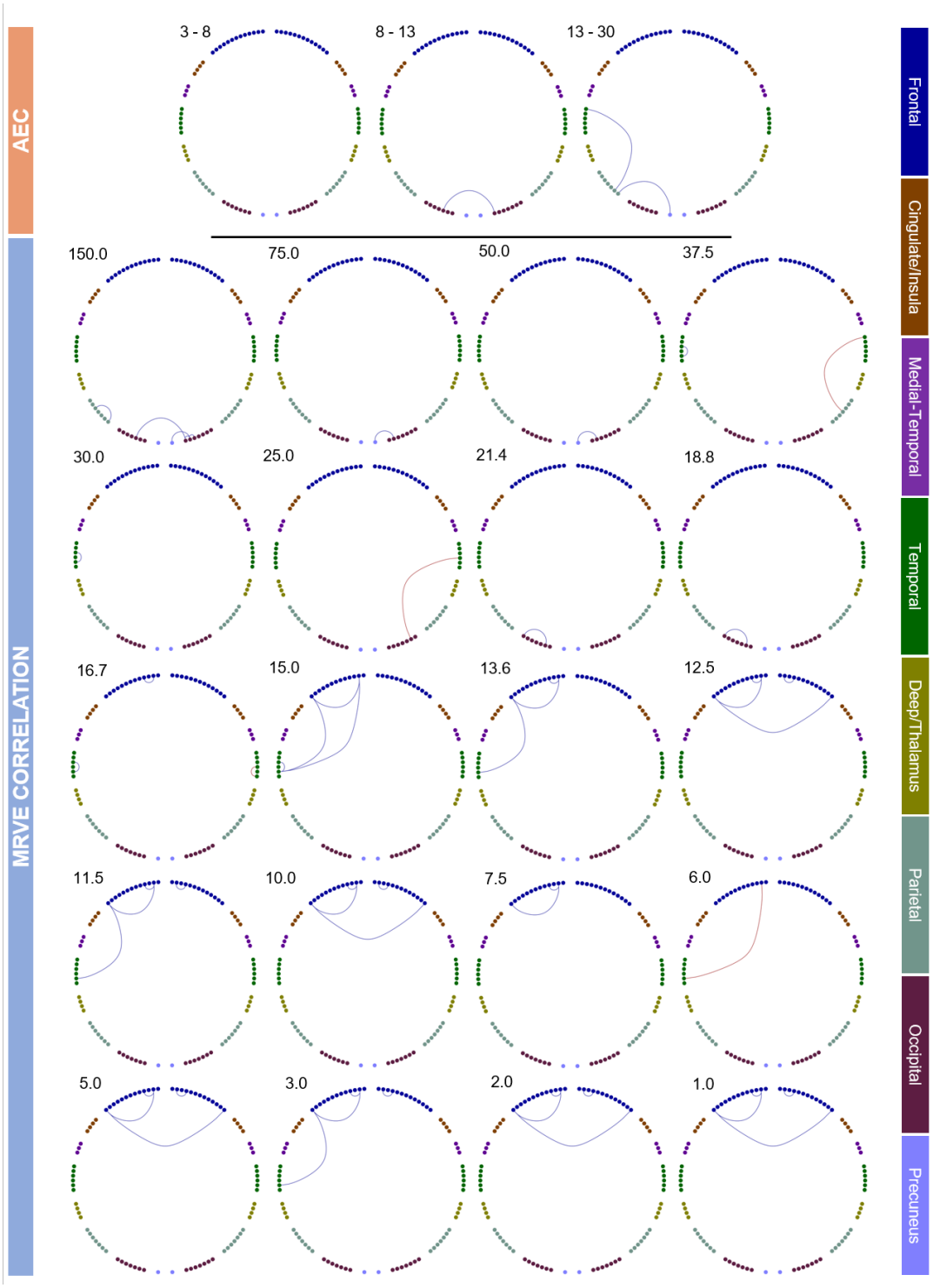


FIGURE 5.5: Connections where z-scores were found to be significantly different between the ND-CNV and control cohorts using a t-test ($p<0.05$), corrected for multiple comparisons. Connectivity was calculated using data that had been cleaned of eye movement artefacts using ICA.

Figure 5.4). Using MRVE correlation with $f_S \lesssim 15$Hz, some alterations in connectivity are found between frontal and left temporal nodes, although this is seen at few edges for each scale frequency.

Figure 5.5 shows the edges with significantly different connectivity between cohorts after correction for multiple comparisons. Across AEC frequency bands and MRVE scale frequencies, only a few connections were found to survive this more conservative thresholding.

Figure 5.6A shows the number of edges that show altered connectivity strength when not correcting for multiple comparisons. Measuring connectivity using MRVE correlation at $f_S$ = 75Hz gave the maximum number of 63 edges that exhibited altered connectivity strength. Using AEC, the maximum number was found in the beta band where 42 edges showed altered connectivity strength. The connectivity differences at this scale frequency and frequency band can be seen in Figure 5.6B plotted on a template brain.

The right panel of Figure 5.6A indicates the number of connections that were found to be stronger in the ND-CNV cohort and which were found to be weaker. It can be seen that MRVE correlation at high scale frequencies ($37 < f_S < 75$Hz) could be used to detect more edges that exhibit hypoconnectivity as well as more that show increased strength in the ND-CNV participants, as compared to the most sensitive AEC frequency band (the beta band).

It was also found that the ICA-based data cleaning procedure increases the number of edges found to be weaker, in ND-CNV carriers compared to controls, when assessed using MRVE correlation at scale frequencies $20 < f_S < 75$Hz. In contrast, the data cleaning method used made less of a difference to the sensitivity of AEC. Similar numbers of edges with altered connectivity were found using both cleaning methods across all frequency bands except the alpha band; in the 8-13Hz band, more hypoconnectivity was detected when the visual cleaning method was used.

Figure 5.6C shows the maximum absolute $t$-statistics obtained at each edge when connectivity was compared between participant groups across all AEC frequency bands and across all MRVE scale frequencies. The points represent all edges that were found to be valid using either connectivity measure at any frequency. It can be seen that there are some connectivity differences that are only detected by either

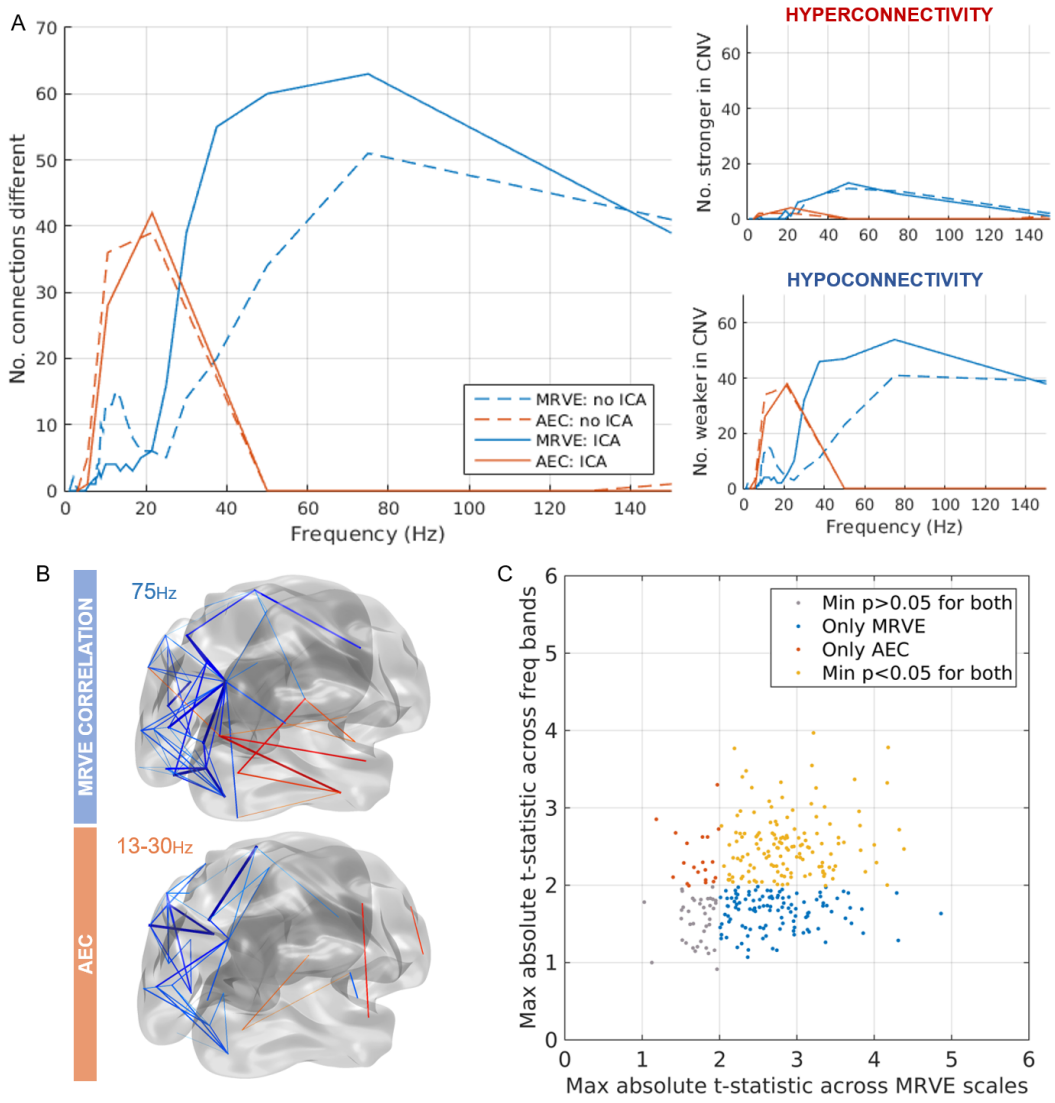


FIGURE 5.6: A) The main plot gives the number of edges that were found to exhibit altered connectivity in the ND-CNV cohort as measured using MRVE correlation and AEC. The plots to the right indicate how many of these exhibited increased connectivity in the ND-CNV group and how many showed reduced connectivity strength. B) The edges with significantly different connectivity between participant groups plotted on a template brain for the MRVE scale frequency and AEC frequency band that gave the largest number of altered edges. Blue lines indicate reduced connectivity in the ND-CNV cohort, whereas red indicates hyperconnectivity. C) The maximum absolute $t$ value obtained for each valid connection across all frequency bands vs. all scale frequencies, where the colour indicates whether a significant difference in connectivity strength ($p<0.05$) is detected by both MRVE correlation and AEC, detected by neither, or detected by only one of the methods.

MRVE correlation or AEC, which suggests, as in Chapter 4, that the two connectivity measures can provide complementary information. It is also apparent that there are more connections that were only found to exhibit altered strength using MRVE correlation than there are connections that were only found to be altered in strength when connectivity was measured using AEC.

### 5.3.2 Machine learning classifier performance

The ability of the SVM classifier to distinguish the network properties of the participants in each group is displayed in Figure 5.7. Figure 5.7A shows the classification results obtained using the graph theory metrics concatenated across all frequencies. The maximum accuracy for both connectivity measures was achieved when data had been cleaned using the ICA-based method and when the classifier was provided with the pooled features vector which combined all six metrics. For MRVE correlation the highest classification accuracy achieved was $80.7 \pm 0.6\%$; for AEC the maximum accuracy was $72.6 \pm 0.6\%$.

Considering the individual metrics, networks produced using MRVE correlation were most accurately classified when node properties were quantified by the local efficiency and the clustering coefficient, which both measure cortical segregation. When using AEC, the most informative metric was betweenness centrality, a measure of node importance. Classifiers based on MRVE correlation networks outperformed those using AEC networks when provided with all metrics except betweenness centrality.

Classification was also performed using combined information from both connectivity measures, the results of which are shown in Figure 5.7C. This gave a higher maximum classification accuracy of $83.0 \pm 0.5\%$, which was again observed when data had been cleaned using the ICA-based method and when the classifier was provided with the pooled features.

Due to the larger of number of MRVE scale frequencies included in this analysis, compared to the number of AEC frequency bands, the SVM classifier was provided with a larger number of features when classification was performed using metrics calculated using MRVE correlation networks. Therefore, classification was also performed using a single MRVE scale frequency ($f_S = 75$Hz) and a single AEC frequency

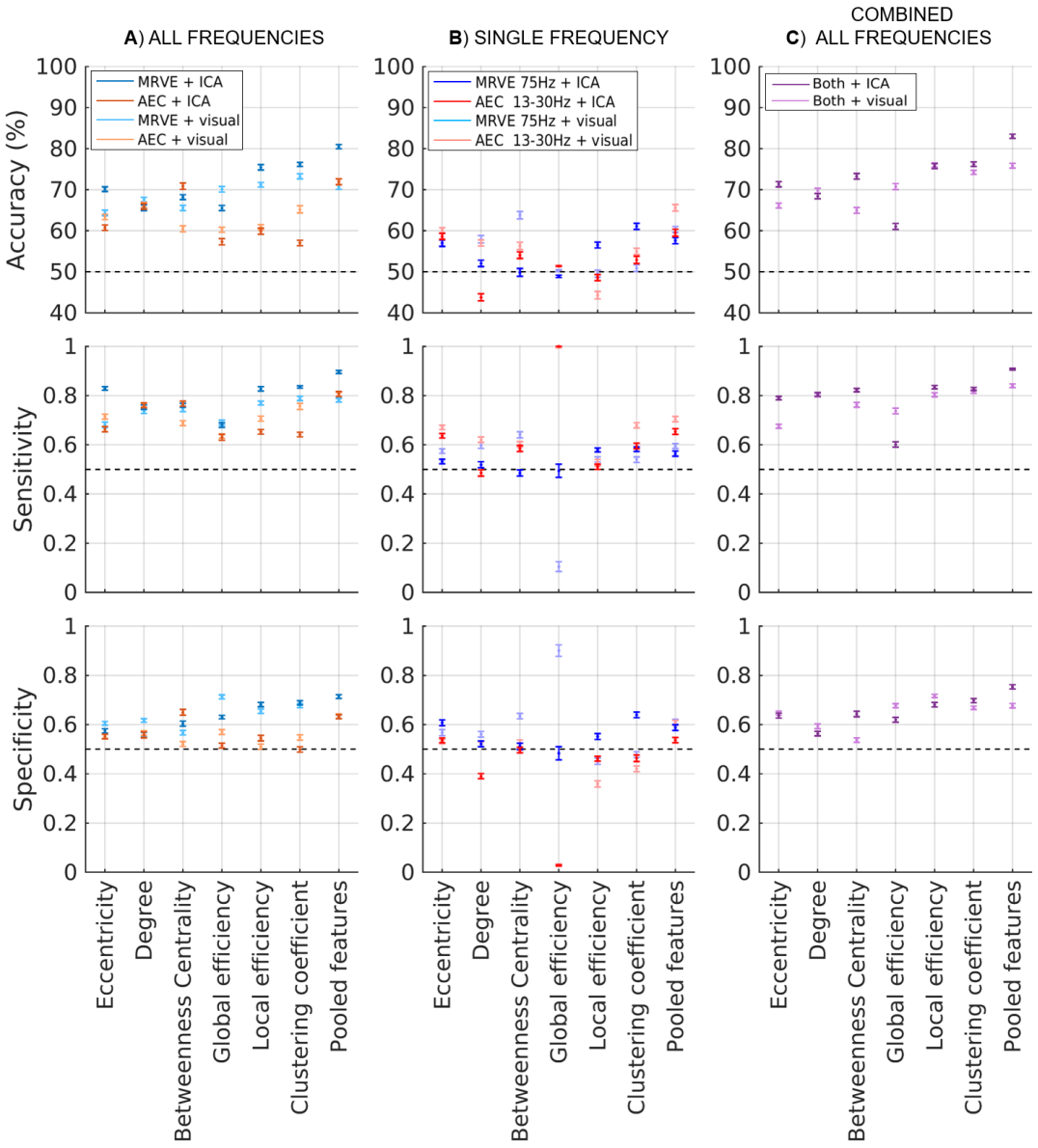


FIGURE 5.7: The cross-validated performance of the SVM classification, between ND-CNV and control groups, based on graph-theory network measures derived from individual connectivity profiles. Results are shown for classification performed using six different metrics that quantified node importance, network integration and segregation, as well as the results obtained when the combination of all metrics was used (pooled features). Average values are plotted over 100 iterations of 5-fold cross validation and error bars represent the 95% confidence intervals. A) shows the results obtained when the classifier was provided with metrics concatenated across frequencies whereas B) shows the performance achieved using a single MRVE scale frequency ($f_S$ = 75Hz) and the beta AEC frequency band. C) shows the results obtained when using combined information from MRVE correlation and AEC.

band (13-30Hz), the results of which are shown in Figure 5.7B. These frequencies were selected as those that indicated the highest sensitivity to the group level connectivity differences for each connectivity measure, as they were shown to detect the most edges exhibiting altered strength in Figure 5.6A. The maximum accuracy of $65.6 \pm 0.8\%$ was achieved using beta band AEC when data had been cleaned using the visual method and when the classifier was provided with the pooled features. For four of the individual metrics, a higher accuracy was obtained for 75Hz MRVE correlation than for beta band AEC, although the data cleaning method that gave the highest accuracy varied between metrics. When classifying MRVE correlation network metrics, the highest accuracy was achieved when data had been cleaned using the visual method and when the classifier was provided with the betweenness centrality metric, which gave an accuracy of $63.8 \pm 0.9\%$.

It has been found previously that the network properties of participants with 22q11.2 deletion syndrome could be distinguished from controls with higher accuracy than the general ND-CNV cohort (Dima et al., 2019). Therefore, classification was also performed while including only participants with this genetic variant and their matched controls. The results of the classification using this limited cohort are shown in Figure 5.8. Figure 5.8A shows the classification performance using network properties concatenated across frequencies for each connectivity measure, whereas Figure 5.8B shows the classifier performance obtained using the 75Hz MRVE correlation and beta band AEC network properties. For the combined and single frequency analysis, an increase in classification accuracy was seen across several network properties for each connectivity measure. However, compared to the classification using the whole ND-CNV cohort, it can be seen that the classifier performance was less stable for the 22q11.2del group. This can be seen in the larger uncertainty in the accuracy, as shown by the errorbars, and also in the larger difference between the corresponding sensitivity and specificity of each classifier. For example, in the single frequency analysis shown in the right panel, the highest accuracy of $76 \pm 1\%$ was obtained using the pooled features of AEC beta band networks generated from data cleaned using the visual method. However, the corresponding specificity is low, which indicates that members of the control cohort were frequently incorrectly classified by this classifier. The largest improvements in classification

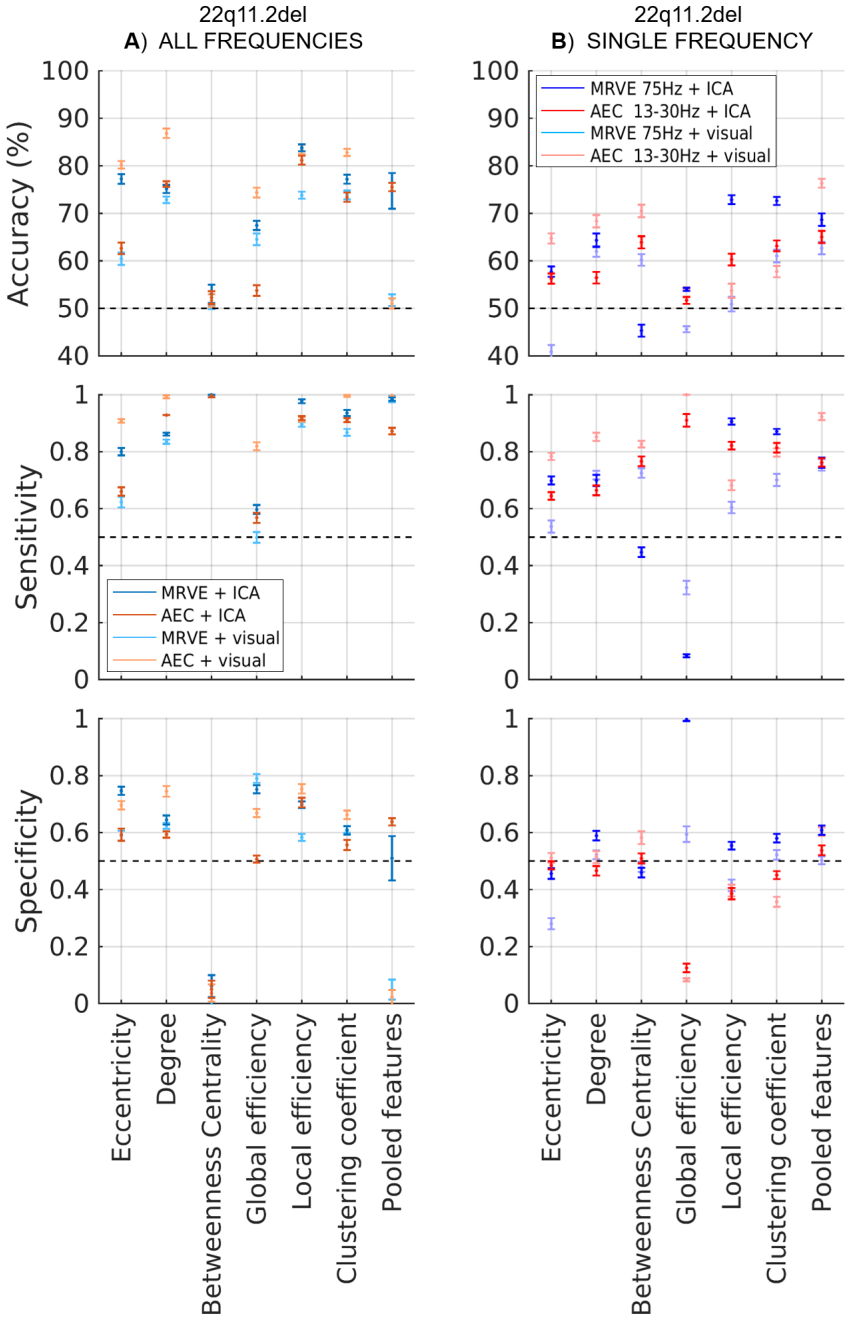


FIGURE 5.8: The performance of the SVM classification of the ND-CNV and control groups when including only participants with the most prevalent ND-CNV (22q11.2 deletion) and their matched controls. A) shows the results obtained when the classifier was provided with metrics concatenated across frequencies whereas B) shows the performance achieved using a single MRVE scale frequency ($f_S$ = 75Hz) and the beta AEC frequency band.

performance, where an increase in accuracy was accompanied by increased sensitivity and specificity, were found when classification was performed using the local efficiency and clustering coefficient of networks measured using 75Hz MRVE correlation (ICA based cleaning method). For these network properties, considering this genetic variant in isolation led to an increase in classification accuracy, which could suggest that network segregation is particularly affected in this group.

For classification performed using both the single and combined frequency information, the classifier performance was dependent on the method used to clean the data. In Figure 5.7A, a clear improvement in classifier performance can be observed for networks calculated using MRVE correlation when data is cleaned using the ICA based method. This can also be seen in Figure 5.7C in the results from the classification using combined information from both connectivity measures. However, when using AEC, when using a single frequency or when considering the limited 22q11.2del cohort, the choice of cleaning method had a less consistent effect on classifier performance. In these cases, the difference in accuracy obtained using the two cleaning methods varied in size and direction between the different metrics.

## 5.4 Discussion

### 5.4.1 Functional connectivity alterations associated with ND-CNVs

MRVE correlation was able to detect alterations in resting state functional connectivity that were robust across participants with a range of ND-CNVs. This indicates that abnormal functional connectivity is a common symptom across these genetic variants, consistent with results found by Dima et al., 2019.

Both MRVE correlation and AEC predominantly detected reduced connectivity in the ND-CNV cohort. However, MRVE correlation at scale frequencies $f_S \geqslant 25$Hz was able to also detect regions exhibiting increased connectivity in the right temporal lobe, indicating a non-straightforward effect of the genetic conditions on the resulting neuronal activity. The hyperconnectivity remained even after the conservative correction for multiple comparisons was applied, suggesting that this connectivity measure can provide complementary information to that provided by AEC.

The majority of research into connectivity alterations due to ND-CNVs has found them to cause reduced neural synchronisation (Padula et al., 2015; Bertero et al., 2018; Dima et al., 2019). However, more complex, spatially varying alterations in functional connectivity have also been found in ND-CNV carriers (Schreiner et al., 2014; Dubourg et al., 2019; Debbané et al., 2012). Similarly, while schizophrenia is more commonly associated with dysconnectivity (Friston et al., 2016), increases in resting state connectivity strength have been observed in schizophrenia patients between certain brain regions (Woodward, Rogers, and Heckers, 2011; Lottman et al., 2019). Abnormalities in connectivity have also been found in patients with ASD and ADHD that vary between brain regions and frequency bands (O'Reilly, Lewis, and Elsabbagh, 2017; Hull et al., 2017; De La Fuente et al., 2013). This suggests that complex alterations in connectivity due to the presence of ND-CNVs could be linked to an increase in risk of developing neurodevelopmental disorders.

Most edges showing altered connectivity strength were found between occipital, parietal and temporal regions when using MRVE correlation at high scale frequencies ($f_S \geqslant 18.8$Hz) and AEC in the alpha and beta bands. Similar patterns of functional connectivity alterations have been found previously in studies of schizophrenia (Brookes et al., 2016) and ASD (Lewis et al., 2014). However, in this analysis, a threshold was applied to the edges so that only those that were consistently strong within at least one group (mean rank > 0.8) were compared between groups. It can be seen in chapter 4, Figure 4.2, that the majority of connections that were detected as valid for these scale frequencies and AEC frequency bands were in these posterior regions during the resting state. Therefore, it is unclear from these results whether connectivity alterations located in these specific regions are linked to increased risk of disorder. To investigate whether other brain regions show similar alterations in MRVE correlation strength, alternative paradigms could be employed that are targeted to activate other functional networks.

There was also an apparent 'slowing' in the frequency distribution of connectivity observed in the ND-CNV cohort. For both connectivity measures, the frequency at which the peak number of valid connections is observed is lower in this cohort compared to the control group. There is little discussion in the literature regarding the frequency spectra of activity in the ND-CNV population, and from this analysis it

is difficult to deduce much about the nature of the frequency slowing. For example, it is unclear whether the results reflect a reduction of the strength and frequency of connections, or whether they reflect a reduction in strength of network connectivity that is larger at higher frequencies. However, this slowing could show parallels to atypical resting state oscillatory activity previously found in schizophrenia patients (Uhlhaas and Singer, 2010). Low frequency activity has been previously found to have higher amplitude in these patients (Boutros et al., 2009), whereas gamma band amplitude has been found to be reduced (Rutter et al., 2009). Similar alterations in oscillatory activity have also been found in patients with ADHD (Woltering et al., 2012). Further research into this topic could investigate whether a reduction in frequency of network activity in the ND-CNV cohort could be associated with disorder risk.

### 5.4.2 Machine learning classification based on graph theory metrics

The properties of MRVE correlation and AEC networks were then quantified using metrics derived from graph theory. These were successfully used by a machine learning classifier to distinguish participants with ND-CNVs from controls; metrics calculated from MRVE correlation networks gave 8.1% higher average classification accuracy than AEC when using the pooled metrics. The individual metrics that gave the highest accuracy were different for each connectivity measure. The metrics that gave the highest classification accuracy for AEC networks were measures of node importance. In contrast, cortical segregation metrics were the most informative when using MRVE correlation networks, especially in the 22q11.2 deletion cohort. This is in line with previous findings of increased segregation in structural networks in participants with 22q11.2 deletion syndrome (Ottet et al., 2013; Scariati et al., 2016). These results imply that the two measures are sensitive to different aspects of the connectivity abnormalities in ND-CNV carriers, and that MRVE correlation could add complementary sensitivity to alterations in the properties of functional networks.

Future work could investigate which nodes and frequencies of activity were most informative to the classifier, and to determine the direction of the differences between the cohorts, by examining the classification model weights. However, for this

analysis there was a limit on the interpretability of these weights, as more MRVE correlation scale frequencies have been included than AEC frequency bands and several of the MRVE correlation connectivity profiles showed high similarity at high scale frequencies. This means that the network property metrics corresponding to these frequencies may have been correlated across scale frequencies, so it is possible that the features provided to the classifier were multicollinear. This can introduce difficulties in identifying which scale frequencies were most informative for the classification and can cause $p$ values to be less reliable (Haufe et al., 2014). Future analysis of the model weights would require reducing the networks found using each connectivity measure to orthogonal components using some form of factor analysis, such as principal component analysis (PCA). However, while multicollinearity affects the ability to interpret the relative importance of individual scale frequencies or frequency bands within the classification model, it does not affect predictions made by a model (Kutner et al., 2005). Therefore, for the purposes of the current analysis, the stability of the classification accuracy should not be affected by multicollinearity, and the higher sensitivity afforded by MRVE correlation should not be regarded as spurious.

It was found by Dima et al., 2019 that several properties of the ND-CNV cohort networks were able to be distinguished from the control cohort significantly more accurately when classification was only performed on those with the 22q11.2 deletion variant and their matched controls. Given that data from the same participants were analysed during this chapter, it would be expected that a similar improvement in classification performance should have been observed. However, when classification was performed upon network properties that were combined across multiple frequency bands and time scales, low specificity was observed across several properties for both connectivity measures. This difference may be due to the number of features used for the classification in each study. Due to methodological differences, the number of features provided to the classifier during this analysis was higher when network properties were combined across frequencies compared to those generated by Dima et al., 2019. Generally, SVM classifiers maintain good performance when using a high number of features relative to the number of data points. However, this is dependent on using a finely tuned regularisation parameter (Cawley

and Talbot, 2007). The SVM regularisation parameter defines the extent to which the algorithm will allow incorrect classification of the training data when generating the hyperplane. When using a low regularisation parameter, the classifier will be less tolerant of mislabelled data, and will increase the complexity of the model to ensure that more data points are classified correctly. When the number of features is high, this can lead to overly complex classification models that overfit the training data and perform poorly when classifying unseen data (Cawley and Talbot, 2007). During this chapter, the regularisation parameter was kept constant regardless of the number of features used. A potential improvement to this analysis could, therefore, be to investigate the effects of varying the regularisation parameter on the performance of the classifier and to determine whether an optimal parameter value exists for obtaining the maximum sensitivity to group connectivity differences.

Another parameter which was held constant during this analysis was the rank threshold applied to extract the strongest connections for each participant. This determines which edges comprised the networks quantified using the graph theory metrics. It has been found previously that varying this threshold can have a large effect on the resulting network topography (Drakesmith et al., 2015). It is unknown how the somewhat arbitrary choice of rank threshold used here has influenced the metrics provided to the SVM classifier. This analysis could be improved by employing alternative thresholding algorithms (Bordier, Nicolini, and Bifone, 2017), or by investigating whether an optimal threshold exists for maximising classification accuracy.

### 5.4.3 Effects of the data cleaning method used at the pre-processing stage

The method utilised for cleaning the data during the pre-processing stage was found to affect results throughout this analysis. It was found that the peak in number of connections observed using MRVE correlation at $f_S$ = 15Hz, which was also observed in chapter 4, was only detected in the control group when the visual cleaning method was used. This suggests, as hypothesised, that these connections were spurious due to eye movement related artefacts. Somewhat surprisingly, very little connectivity was observed in the ND-CNV cohort at low scale frequencies using either cleaning method. Instead, applying the ICA-based method reduced the number

of connections seen at higher scale frequencies, which points to a difference in the MEG signals generated by eye movements in those with genetic conditions. While no studies to date have investigated atypical eye movement in ND-CNV carriers, dysfunctional eye movement has been observed in schizophrenia patients (Calkins, Iacono, and Ones, 2008) and in ASD (Kovarski et al., 2019). In a previous study of Parkinson's disease, impaired resting state functional connectivity was found to be associated with levels of eye movement dysfunction (Gorges et al., 2016), suggesting that there may be a link between the connectivity alterations observed here and the different properties of the signals generated by eye movements in the ND-CNV carriers. MRVE correlation could therefore be a valuable measure for further investigation of atypical eye movements in this population.

## 5.5 Conclusion

MRVE correlation was able to detect alterations in resting state functional connectivity associated with a range of ND-CNVs, showing higher sensitivity to group differences compared to AEC and providing complementary information to that given by the oscillatory based measure. This implies that there is value in using MRVE correlation in addition to the more established method when performing connectivity analysis in patient groups. The cleaning method applied to the data was also found to affect the connectivity measurements obtained using either method. The highest sensitivity to group differences was found, for both methods, when connectivity was calculated using data that had been cleaned using the ICA-based method. This suggests that data should be thoroughly cleaned of eye movement artefacts before connectivity analysis is performed to maximise the likelihood of detecting functional network alterations.

# Chapter 6

# MEEG: simultaneous MEG and EEG for observing the deep brain

In recent years, it has been established that activity within deep brain structures, such as the hippocampus, can be detected using MEG. However, the spatial resolution that can be obtained at this depth is limited due to the lower signal to noise ratio. In this chapter, it was investigated whether simultaneous MEG and EEG (MEEG) could improve upon the performance of MEG alone for source localisation within the medial temporal lobe (MTL). Source power across the brain was measured during a spatial memory task (the 'hometown walk') and contrasted with a control task involving mental arithmetic and resting state activity. Across the brain, it was found that the strongest differences in source power were found using MEG alone, indicating that MEEG did not provide any benefit for source localisation. Peaks in task-induced oscillatory power were also detected within the MTL, only when using MEG alone. These peaks were detected in a range of frequency bands, where the frequencies depended on the control task used for the contrast. Power decreases in the 1-4Hz and 4-8Hz bands were detected during the hometown walk task, when compared to the mental arithmetic control condition. When contrasting activity during the hometown walk task with resting baseline activity, it was instead found that power decreases in the MTL were found in the 8-13Hz and 13-30Hz frequency bands. No peaks in task-induced oscillatory power remained after correction for multiple comparisons when using EEG or MEEG. These findings suggest that MEG is capable of detecting oscillatory activity within the MTL, and that combining MEG and EEG requires careful methodological optimisation in order to reduce detrimental effects of EEG and, thus, improve upon the performance of MEG alone.

## 6.1 Introduction

MEG and EEG are direct measures of the magnetic fields and electric potentials generated by neuronal activity, and have excellent temporal resolution allowing the investigation of brain activity on the millisecond timescale. However, both techniques suffer from limited spatial resolution due to the ill-posed inverse problem that must be solved to localise current sources. MEG can obtain significantly better spatial resolution than EEG, as the electric potential measurements at the scalp are distorted due to the low and inhomogeneous conductivity of the skull, whereas magnetic fields are relatively unaffected by the electromagnetic properties of the head (Baillet, 2017). However, MEG is insensitive to radial sources. EEG, on the other hand, is most sensitive to radial sources, but least sensitive to those parallel to the scalp. EEG also has greater sensitivity to deeper sources as the MEG signal strength drops off more quickly with distance from a current source. Therefore, MEG and EEG have the potential to provide complementary information about brain function, due to their different relative sensitivities. It has been found using both simulations and experimentally that simultaneous measurement of MEG and EEG can lead to improved source localisation accuracy, compared to either modality alone (Dale and Sereno, 1993; Fuchs et al., 1998; Baillet et al., 1999; Ko and Jun, 2010; Babiloni et al., 2001; Liu, Dale, and Belliveau, 2002; Sharon et al., 2007; Henson, Mouchlianitis, and Friston, 2009; Hong et al., 2013; Aydin et al., 2015; Chowdhury et al., 2015).

Many studies utilising combined MEG and EEG (MEEG) have considered only neocortical sources. However, one study found that MEEG analysis gave improved localisation of face processing activity within the fusiform gyrus, compared to MEG and EEG alone (Henson, Mouchlianitis, and Friston, 2009), suggesting that MEEG could be beneficial for investigating function within deeper brain structures. The medial temporal lobe (MTL) is a sub-cortical brain region which plays a central role in spatial navigation and memory. Measuring activity in this brain region is vital for determining the location of seizure onset in mesial temporal lobe epilepsy (MTLE). The current gold standard for measurement of deep brain activity is intracranial EEG (iEEG) due to its excellent spatial and temporal resolution. However, as this method is highly invasive, it is predominantly used only in epilepsy patients for pre-surgical

planning, which prevents the characterisation of activity in healthy controls or patients with no clear hypothesis or indication to place electrodes. iEEG measurements are also limited to activity that occurs in close proximity to the implanted electrodes, so cannot be used to gain a picture of activity across large brain regions. fMRI is a non-invasive functional neuroimaging alternative with excellent spatial resolution, which doesn't show reduced sensitivity for deeper sources. It has been used to reliably show MTL activation during memory tasks (Towgood et al., 2015). However, this modality lacks the temporal resolution to characterise the oscillatory dynamics underpinning this activation.

In recent years, it has been established that signals from the MTL, particularly the hippocampus, are visible to MEG and EEG sensors. While EEG is currently too limited by poor spatial resolution to localise sources at this depth, MEG has shown to be able to detect hippocampal activity in simulation (Quraan et al., 2011; Attal and Schwartz, 2013; Meyer et al., 2017b) and empirical studies (Cornwell et al., 2008; Backus et al., 2016; Pu et al., 2017; Pizzo et al., 2019) (see Pu et al., 2018 for a review). However, the amplitude of signals generated at this depth is much lower at the sensors. The reduced SNR means that there is a higher level of source leakage in these regions, so source estimations are dispersed. This makes hippocampal activity hard to dissociate when activation occurs simultaneously elsewhere in the brain (Quraan et al., 2011; Stephen et al., 2005). MEEG therefore may have the potential for allowing the non-invasive investigation of deep brain activity at high temporal resolution, while improving on the spatial resolution of MEG alone.

To engage structures within the MTL, an experimental paradigm was chosen for this study that required spatial memory. In fMRI studies, the 'hometown walk' (Roland and Friberg, 1985) has been shown to produce reliable bilateral activation of the MTL in healthy controls, with the strongest activation in the parahippocampal gyrus (Towgood et al., 2015; Maguire, Frackowiak, and Frith, 1997; Jokeit, Okujava, and Woermann, 2001; Ino et al., 2002; Beisteiner et al., 2008; Ávila et al., 2006; Strandberg et al., 2011). This task is based on the retrieval of long term spatial memory where participants mentally navigated a route familiar to them. Studies of MTLE patients have also successfully used this task to lateralise the location of seizure onset (Beisteiner et al., 2008; Towgood et al., 2015; Schacher et al., 2006; Toller et

al., 2015). However, to date, there have been no studies of the electrophysiological activity underlying the BOLD response during the hometown walk. Considering studies that have utilised more direct measures of neuronal activity during other spatial memory paradigms, it could be hypothesised that increases in oscillatory activity may be observed in the theta frequency band during the hometown walk task. Theta band oscillations ($\sim 4-8$Hz) were first detected within the hippocampus in rats using intracranial electrodes. These were found first during voluntary movement (Vanderwolf, 1969), and have since been associated with spatial memory (Keefe and Recce, 1993). Theta band oscillations have also since been observed in humans during spatial memory tasks using iEEG (Kahana et al., 1999; Caplan et al., 2003; Ekstrom et al., 2005; Kaplan et al., 2012). Theta band increases have also been measured during a range of memory tasks with MEG. Using a virtual adaptation of the Morris water maze paradigm, Cornwell et al., 2008 found that theta power increased in the left hippocampus while finding a hidden platform from memory, when contrasted with a control task involving free movement. Theta power was also found to be positively correlated with task performance, a finding which was replicated by Pu et al., 2017. An increase in theta band power within the MTL was also found by Fuentemilla et al., 2014 during detailed episodic and general semantic memory retrieval. MTL theta power has also been found to correlate with decision making performance (Guitart-Masip et al., 2013), and to be involved in image recognition (Riggs et al., 2009). However, some studies have reported lower frequency, delta band oscillations ($\sim$1-4Hz) during spatial memory paradigms. It has been suggested that oscillatory activity in humans associated with spatial navigation occurs at lower frequencies (Jacobs, 2014). In one iEEG study by Ekstrom et al., 2005, delta band activity was observed in addition to or in place of theta band activity, depending on the specific paradigm used.

In this chapter, the oscillatory activity induced by the hometown walk task will be investigated using EEG, MEG and combined MEEG. It will then be determined whether MEEG can improve upon the recreation of current sources within the MTL during this task, compared with EEG and MEG individually.

## 6.2 Methods

### 6.2.1 Participants and data acquisition

28 healthy participants (22 female) performed the 'hometown walk' task while being scanned with simultaneous MEG and EEG. All participants had normal or corrected-to-normal vision, had no history of neurological or psychiatric disorders, including epilepsy, and gave written informed consent prior to participation. Each participant received £10 per hour for taking part. This study was approved by the Cardiff University School of Psychology ethics committee.

Participants were asked to remain relaxed and as still as possible during the scan. To minimise head movement, each participant was provided with a chin rest and their head was surrounded by foam padding within the MEG dewar. Head movement was measured by fiducial coils as in Chapter 2 section 3.2.1. Participants were excluded from analysis if they exceeded 5mm head movement during the scan. 19 participants (16 female) completed this task while remaining below the head movement threshold.

Simultaneous MEG and EEG data were collected with participants in a seated position. Participants wore an EasyCap EEG cap with 56 Ag-Cl electrodes. Abrasive conductive paste was used to bring each electrode into conductive contact with the scalp (impedence $< 5k\Omega$). MEG data were collected as in Chapter 2 section 3.2.1. All data were collected at 600Hz. An anatomical MRI was also obtained for each participant.

For each participant, a Polhemus digitiser was used to measure the shape of the head and the relative locations of the EEG electrodes and MEG fiducial coils. The EEG and MEG sensor locations could then be coregistered with their anatomical MRI.

### 6.2.2 The hometown walk

The 'hometown walk' task was based on the paradigm described by Roland and Friberg, 1985. Before entering the MEG scanner, each subject was asked to choose a walking route that was very familiar to them and to provide 11 evenly spaced landmarks along this route. During scanning, each participant was 'guided' along

this journey in 30 second sections; beginning at the first landmark, the landmarks were presented two at a time on a screen. Participants were instructed to mentally navigate the section of their route between the two displayed landmarks. Subjects were asked to imagine as much detail regarding what they might see, hear or smell along the route as possible, and to not concern themselves with necessarily reaching their next destination within the allotted time.

Each trial corresponding to one section of the journey was immediately followed by a control task, which served as a cognitively demanding baseline. During the control trials, participants were instructed to select a random two-digit number and silently count back in threes from that number. To avoid practice effects, participants were asked to select a different starting number for each trial. These control trials were followed by periods of resting, during which participants were given no specific task.

This sequence of trials repeated 10 times for each participant, in the order 'walk', 'count', 'rest'. Each trial lasted 30 seconds. A fixation point was also presented on screen, which participants were instructed to watch throughout the scan.

### 6.2.3 Pre-processing

Pre-processing of the EEG and MEG data was performed separately, but the same procedure was used for both modalities. First, a bandpass filter of 1-150Hz was applied, and the data was downsampled to 300Hz. Data was cleaned in a semi-automated ICA-based procedure as outlined in Chapter 5 section 5.2.2. Muscle artefacts were removed by removing signal epochs that contained high amplitude in the 110-140Hz frequency band. Channels exhibiting high levels of variance were also visually identified and removed, to minimise the effects of these high amplitude channels on the resulting ICA components. Components of the signal corresponding to eye movement and cardiac artefacts were then identified and removed from the data using ICA. Finally, the cleaned data was bandpass filtered into nine frequency bands: 1-4, 4-8, 8-13, 13-30, 40-60, 60-80, 80-100, 100-120 and 120-140Hz. While the literature indicates that low frequency activity (<8Hz) was most likely to occur during this task, oscillatory power during the hometown walk task was thus measured across the available frequency spectrum.

### 6.2.4 Source localisation

This section describes how the EEG and MEG data were analysed to create functional images that display task-related changes in oscillatory power. Functional images were created to contrast oscillatory activity between each pair of trial conditions: *walk* and *count*, *walk* and *rest*, and *count* and *rest*. For the rest of this section, the trial conditions to be compared will be referred to as the 'active' and 'baseline' trials.

#### Combining magnetic field and electric potential measurements

Before the EEG and MEG data could be analysed simultaneously, it had to be scaled by a channel dependent factor. Without such scaling, the EEG and MEG data would be of different dimensions and the source localisation would be skewed by the different orders of magnitude of the magnetic field and electric potential measurements. The scaling factor chosen for each EEG and MEG channel was the standard deviation of the baseline trial data recorded by that sensor. Each data point from channel, $i$ and time, $t$, is divided by the scaling factor corresponding to its channel. This is shown in equation 6.1 for an example magnetic field measurement, $B_{i,t}$, where the hat denotes scaled data.

$$\widehat{B}_{i,t} = \frac{B_{i,t}}{\sigma_i} \tag{6.1}$$

This method was proposed by Fuchs et al., 1998 to level all measurements to approximately the same order of magnitude and to weight channels based on their SNR. The resulting scaled data is also dimensionless. A combined MEEG dataset, $\mathbf{X}$, was then formed by appending the MEG data, $\mathbf{B}$, to the EEG data, $\mathbf{E}$, as in equation 6.2.

$$\mathbf{X} = \begin{bmatrix} \widehat{\mathbf{E}} \\ \widehat{\mathbf{B}} \end{bmatrix} \tag{6.2}$$

### Forward model

To produce the electric lead fields, individualised head models were produced using the boundary element method (BEM) using the OpenMEEG toolbox (Gramfort et al., 2010; Kybic et al., 2005), which was implemented in MATLAB via Fieldtrip (Oostenveld et al., 2011). Each head model consisted of three-layers, including the brain, skull and scalp, formed using 3000, 2000 and 1000 vertices and assigned conductivities of 0.43, 0.011 and 0.33, respectively (McCann, Pisano, and Beltrachini, 2019). The magnetic lead fields were produced in Fieldtrip by modelling the brain as a single-shell conductor with a boundary at the inner skull surface, extracted from each participant's coregistered MRI.

Voxel locations were placed on a $6\text{mm}^3$ grid in template space, as in previous chapters. This grid was then warped to fit within each participant's single-shell brain model. This allowed the comparison of activity at each voxel across participants.

### Beamforming

A scalar LCMV beamformer (Van Veen et al., 1997; Sekihara et al., 2004) was used to estimate source power at each voxel location in each frequency band, for each participant. This was performed for EEG and MEG separately, as well as for the combined MEEG dataset.

Regularised covariance matrices were calculated separately for the scaled MEG and EEG data. For the MEEG analysis, combined covariance matrices were formed from these single modality matrices as in Figure 6.1. 'Active' and 'baseline' covariance matrices were calculated using only active and baseline trial data, respectively.

Vector lead fields were then calculated for each voxel for dipoles orientated along the Cartesian $(x, y, z)$ unit vectors. These were calculated separately for EEG and MEG. As the fields produced by radial current sources are invisible to MEG, the MEG sensors only measure a two-dimensional projection of the fields generated by the brain. Therefore, the weakest component of the magnetic lead field was removed for each voxel to produce a two-dimensional lead field. For the MEEG analysis, the lead field values for each sensor were then scaled by the same factor as the data from

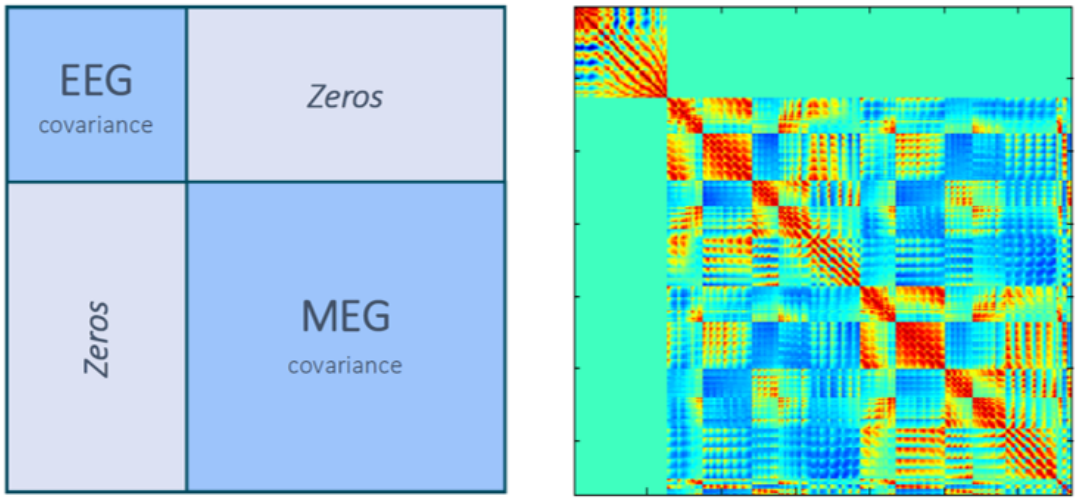


FIGURE 6.1: A schematic illustrating the formation of the combined MEEG covariance matrix (left) and an example of a real covariance matrix (right).

the corresponding channel, and the magnetic lead field matrix was appended to the electric lead field as in equation 6.3.

$$\mathbf{L} = \begin{bmatrix} \mathbf{L}_E \\ \mathbf{L}_B \end{bmatrix} \tag{6.3}$$

Scalar lead fields were then calculated for a single, optimal dipole orientation for each voxel. At each voxel, the beamformer weights were then calculated separately for the active and baseline conditions by using the corresponding covariance matrices in equation 1.5.

### Estimating task-related source power

For each participant, functional images were then produced to compare the current distributions in the brain during the active and baseline trial conditions. This was done by calculating the pseudo-T statistic, $\mathrm{T}$, at each voxel, $\mathbf{r}$, for each frequency band and modality. This was calculated as described by Vrba and Robinson, 2001, and is given by equation 6.4.

$$\mathrm{T}(\mathbf{r}) = \frac{\hat{Q}_a(\mathbf{r}) - \hat{Q}_b(\mathbf{r})}{\hat{v}_a(\mathbf{r}) + \hat{v}_b(\mathbf{r})} \tag{6.4}$$

$\hat{Q}_a(\mathbf{r})$ and $\hat{Q}_b(\mathbf{r})$ are the estimations of the current density at voxel location during the active and baseline conditions, respectively, and are given by equations 6.5.

$$\begin{aligned}\hat{Q}_a(\mathbf{r}) &= \mathbf{w}_a(\mathbf{r})^T \mathbf{C}_a \mathbf{w}_a(\mathbf{r}) \\ \hat{Q}_b(\mathbf{r}) &= \mathbf{w}_b(\mathbf{r})^T \mathbf{C}_b \mathbf{w}_b(\mathbf{r})\end{aligned} \tag{6.5}$$

$\hat{v}_a(\mathbf{r})$ and $\hat{v}_b(\mathbf{r})$ are estimates of the noise power, and are given by equations 6.6. As the baseline condition was used to estimate the noise power, the calculation of $\hat{v}_b(\mathbf{r})$ is equivalent to that of $\hat{Q}_b(\mathbf{r})$.

$$\begin{aligned}\hat{v}_a(\mathbf{r}) &= \mathbf{w}_a(\mathbf{r})^T \mathbf{C}_b \mathbf{w}_a(\mathbf{r}) \\ \hat{v}_b(\mathbf{r}) &= \mathbf{w}_b(\mathbf{r})^T \mathbf{C}_b \mathbf{w}_b(\mathbf{r})\end{aligned} \tag{6.6}$$

Therefore, the pseudo-T statistic gives an estimate of the task-related change in 'source to noise' power in any given voxel. By normalising by the noise power, this quantity also corrects for the depth bias inherent to beamformers, as it avoids the source power measurements being dominated by noise at depths where the signal to noise ratio is low. For each participant, by calculating $\mathrm{T}$ at each voxel, a map of task-related source power across the brain was produced for each frequency band.

## 6.3 Results

For each frequency band, the overall difference in source power between each pair of conditions, across participants, was found by performing a single sample $t$-test at each voxel to determine whether the mean pseudo-T statistic significantly differed from zero at that location. The peaks in these functional images were then analysed to determine whether differences in power had been observed within the hippocampus and parahippocampal gyrus.

### 6.3.1 Walk vs. count

Figure 6.2 shows the $t$-statistic obtained at each voxel when comparing the *walk* and *count* conditions, using a significance threshold of $\alpha = 0.05$. These were corrected for multiple comparisons using the false discovery rate (FDR). Significant differences in source power were found within five frequency bands: 1-4, 4-8, 8-13, 60-80 and 80-100Hz. Differences were detected using MEG alone across each of the five bands, whereas EEG only detected differences in the 4-8Hz band and differences were only

observed in the 8-13Hz and 60-80Hz bands with MEEG. For each frequency band, the spatial distribution of source power difference was generally consistent across modalities. The AAL atlas locations of the biggest changes in source power were also found to be largely consistent. However, the highest $t$ values were observed using MEG. These findings suggest that MEG alone gave greater sensitivity to task-related differences in source power than EEG or MEEG.

The spatial distribution of source power alterations was found to vary across frequency bands. Lower source power was observed in frontal regions during the *walk* trials compared to the *count* condition in the lower frequency bands (up to 13Hz). However, higher source power was detected during the *walk* condition within occipital regions. This occipital power increase was observed at low frequencies, within the 1-4Hz and 4-8Hz bands, as well as at higher frequencies, in the 60-80Hz and 80-100Hz bands.

It was then investigated whether task-related activity changes could be detected within the hippocampus and parahippocampal gyrus. This was determined by finding all peaks in the $t$-statistic image for each frequency band and modality that were in locations that showed a significant task-related source power difference (i.e. the regions shown in Figure 6.2). The closest distance was then found between the peak location and any voxel within the hippocampus or parahippocampal gyrus.

Figure 6.3 shows the peak locations that were found within one voxel (6mm) of the hippocampal regions. Using MEG, a minimum was detected in the 1-4Hz frequency band within the right parahippocampal gyrus. Two minima were detected that were adjacent to the hippocampal regions, in the MEG only functional images, in the 4-8Hz and 8-13Hz frequency bands. The theta band minimum was localised within the white matter adjacent to the right hippocampus. The alpha band minimum was located on the edge of the lingual gyrus. A region of decreased power within the 4-8Hz band can be seen that overlaps with the left hippocampus. However, there was no peak within the hippocampal regions so it is possible that this decrease occurred elsewhere in the brain and is only observed here due to source leakage. No peaks were detected within the hippocampus across any frequency band for EEG or MEEG after correction for multiple comparisons. However, a minimum was observed in the 1-4Hz band within the left hippocampus, using MEEG, that was

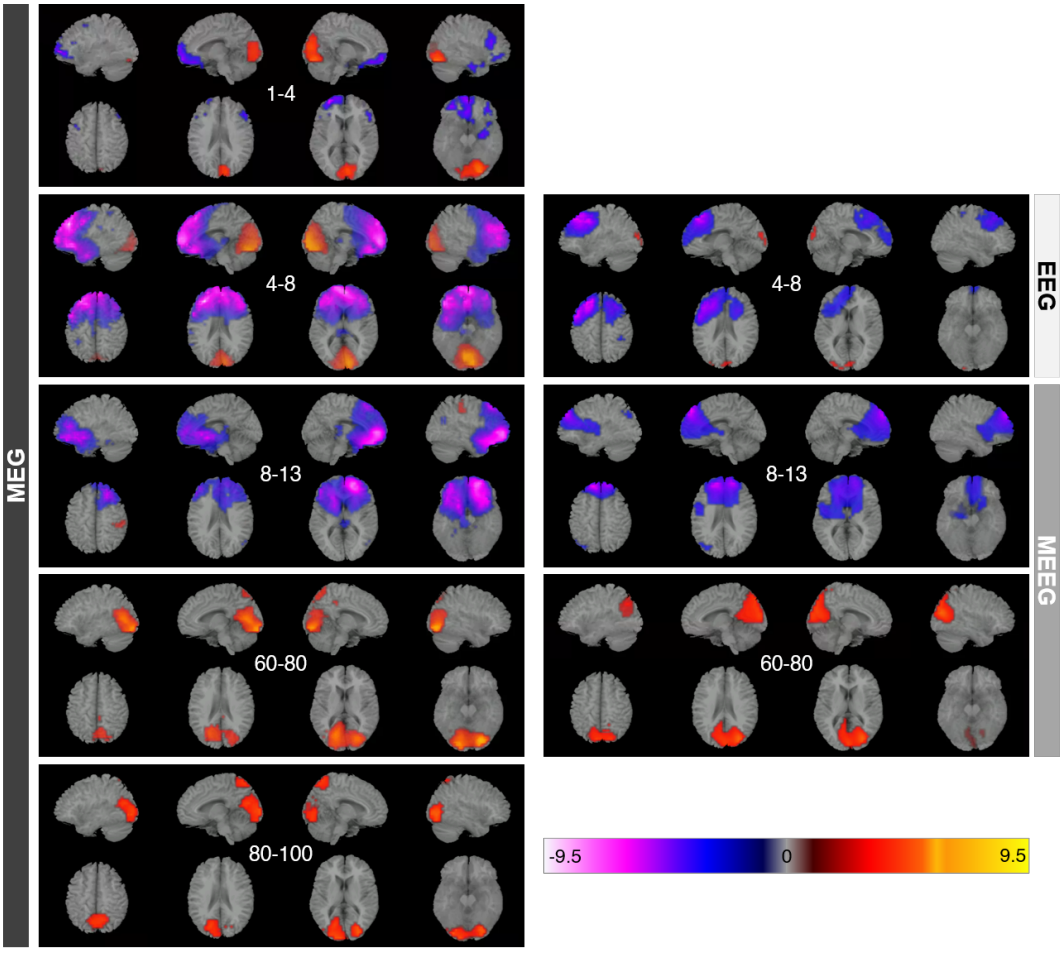


| Frequency (Hz) | MEG | EEG | MEEG |
|---|---|---|---|
| 1-4 | Superior frontal gyrus (L) | - | - |
| 4-8 | Middle frontal gyrus (L) | Middle frontal gyrus (L) | - |
| 8-13 | Superior frontal gyrus (R) | - | Superior frontal gyrus (L) |
| 60-80 | Fusiform gyrus (R) | - | - |
| 80-100 | Fusiform gyrus (R) | - | Middle occipital gyrus (R) |

FIGURE 6.2: *Walk vs. count*: The above colour plots show the voxel-wise $t$-statistic indicating the difference in source power between the *walk* and *count* conditions across participants ($p<0.05$, FDR corrected). $t$ values are displayed on a template brain as indicated by the colour bar. Warmer colours indicate that higher source power was observed during the *walk* condition whereas cooler colours indicate that higher power was observed during the *count* trials. The corresponding frequency band is given in hertz in the centre of each plot, and the modality is indicated by the vertical bars. All five of these frequency bands showed significant task-related differences in source power using MEG, whereas differences were only found in the 4-8Hz band for EEG, and in the 8-13Hz and 60-80Hz bands when using MEEG. Below, the table gives the AAL atlas locations of the largest differences in source power across the brain for each frequency band and modality.

found to be significant at the $\alpha = 0.05$ level. Using MEG alone, maxima were also found within the left parahippocampal gyrus across three gamma frequency bands (40-100Hz) before correction for multiple comparisons.

### 6.3.2 Walk vs. rest

Figure 6.4 shows the *t*-statistic images contrasting source power during the *walk* and *rest* conditions (p<0.05, FDR corrected). Differences in source power were found within seven frequency bands. Differences were detected using MEG alone across each of the seven bands (all except 100-120Hz and 120-140Hz). Using EEG only, differences were detected in the 4-8Hz, 8-13Hz and 13-30Hz bands. Using MEEG, source power changes were detected only in the 8-13Hz and 13-30Hz bands.

Similarly to the comparison of the *walk* and *count* conditions, occipital increases in source power can be observed at low frequencies (1-8Hz) and at higher frequencies (40-100Hz) using MEG. In the 60-80Hz and 80-100Hz bands the increase is seen across a wider volume than in Figure 6.2, including some parietal regions. However, increases in this region were not detected using EEG or MEEG. In fact, even while frontal and temporal decreases in 4-8Hz source power were detected using EEG, similarly to the decreases seen in the MEG functional image, no occipital increase is observed.

Widespread decreases in power during the *walk* condition can also be seen within the 8-13Hz and 13-30Hz bands across all modalities. However, there are inconsistencies between modalities as to where the largest decreases are observed. In the 8-13Hz band, the decreases observed using MEG are more inferior compared to those observed using MEEG. Decreases are found more within the temporal and left frontal lobes using MEG, whereas the main decreases observed with MEEG are within the right frontal and left parietal lobes. In the 13-30Hz band, decreases are observed across most of the brain using MEG and EEG. In contrast, the decreases are more focal using MEEG, and are more concentrated around the peaks observed in the medial superior frontal lobe and the left parietal lobe.

Figure 6.5 shows the peak locations that were found within one voxel of the hippocampus when comparing activity during the *walk* and *rest* conditions. In contrast to the *walk* vs. *count* analysis, the only peaks within the hippocampal regions were

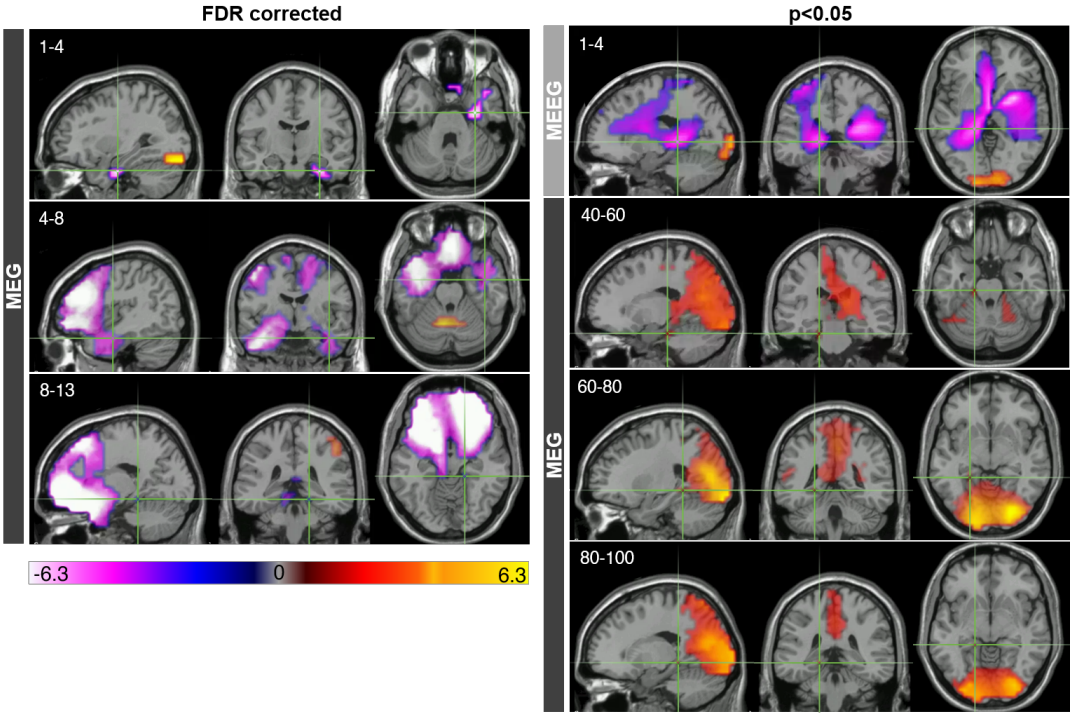


| Frequency (Hz) | MEG | EEG | MEEG |
|---|---|---|---|
| 1-4 | **Parahippocampal gyrus (R)** | - | Hippocampus (L) |
| 4-8 | *nearest* **Hippocampus (R)** | - | - |
| 8-13 | **Lingual gyrus (R)** | - | - |
| 40-60 | Parahippocampal gyrus (L) | - | - |
| 60-80 | Parahippocampal gyrus (L) | - | - |
| 80-100 | Parahippocampal gyrus (L) | - | - |

FIGURE 6.3: The left three plots show the significant peaks in the *walk* vs. *count* functional images that were located within or adjacent to the hippocampus or parahippocampal gyrus (p<0.05, FDR corrected). Peaks were only found in these regions using MEG. The right four plots show peaks within the hippocampus or parahippocampal gyrus that were found to be significant at the $\alpha = 0.05$ level but did not remain after correction for multiple comparisons. The corresponding frequency band is given in hertz in the top left of each plot and the corresponding modality is given by the vertical bars. The table gives the AAL atlas regions where each peak is located. Where a peak is located within white matter, the nearest AAL region is given.

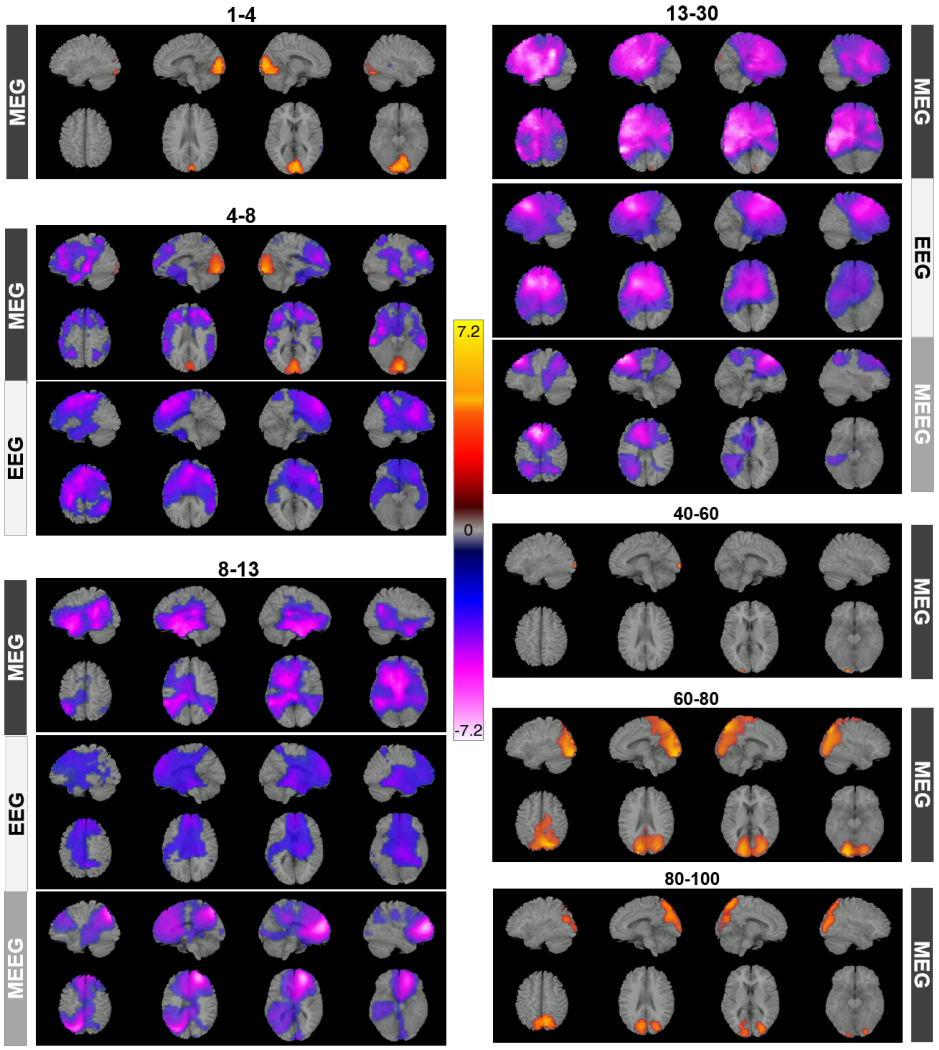


| Frequency (Hz) | MEG | EEG | MEEG |
|---|---|---|---|
| 1-4 | Calcarine sulcus (R) | - | - |
| 4-8 | *nearest* Calcarine sulcus (L) | Precentral gyrus (L) | - |
| 8-13 | Olfactory bulb (L) | Precuneus (R) | *nearest* Superior frontal gyrus (L) |
| 13-30 | Supramarginal gyrus (L) | Supplementary motor area (R) | Medial superior frontal gyrus (L) |
| 40-60 | Calcarine sulcus (L) | - | - |
| 60-80 | Superior occipital gyrus (L) | - | - |
| 80-100 | Superior parietal lobule (R) | - | - |

FIGURE 6.4: *Walk vs. rest*: The above colour plots show the voxel-wise *t*-statistic indicating the difference in source power between *walk* and *rest* conditions ($p<0.05$, FDR corrected). *t* values are displayed on a template brain as indicated by the colour bar. Warmer colours indicate that higher source power was observed during the *walk* condition whereas cooler colours indicate that higher power was observed during the *rest* trials. The plots are grouped by frequency band which is indicated above each group, and the modality is given by the vertical bars. Below, the table gives the AAL atlas locations of the largest differences in source power across the brain for each frequency band and modality. Where this was localised to a region not labelled by the AAL atlas, the nearest AAL region is given.

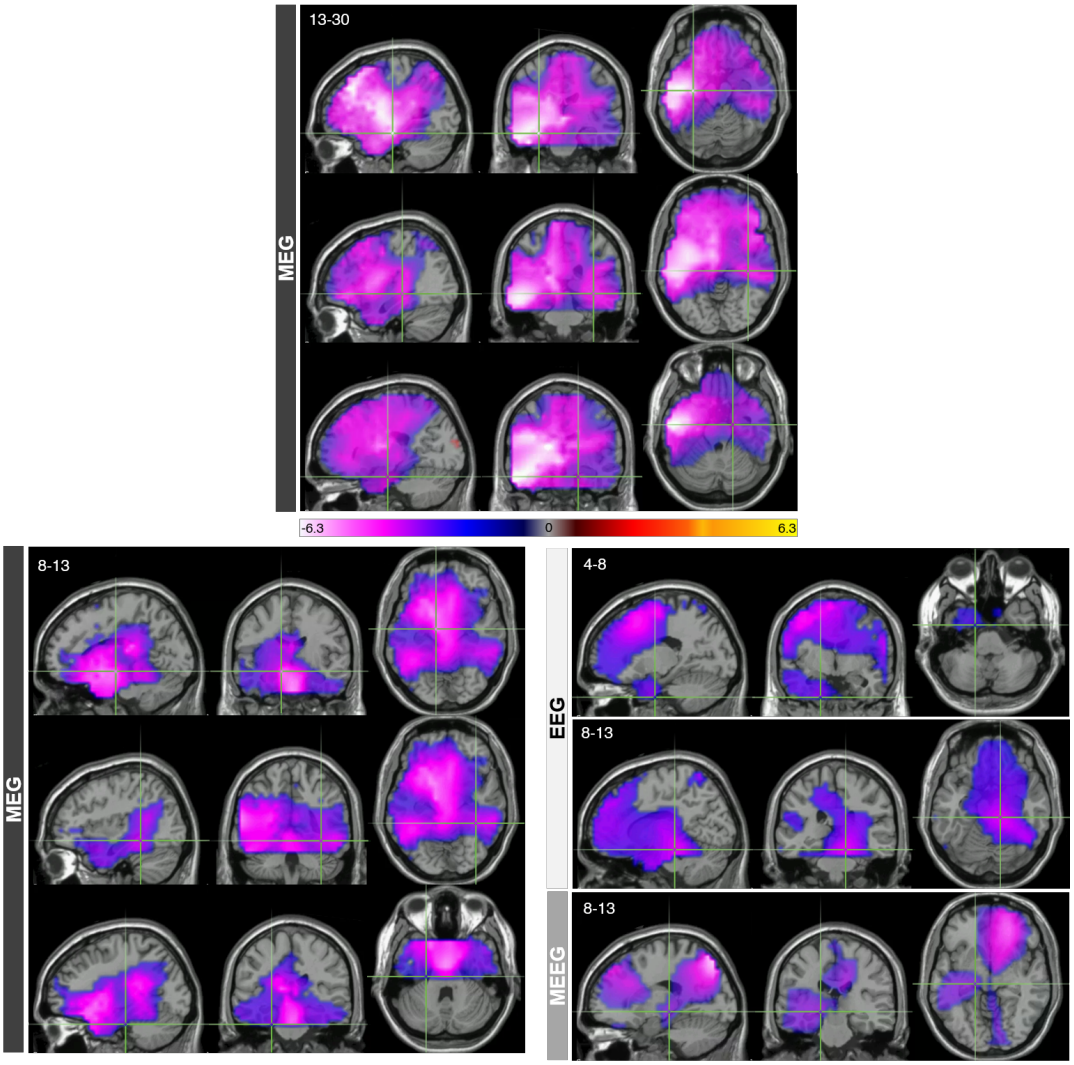


| Frequency (Hz) | MEG | EEG | MEEG |
|---|---|---|---|
| 4-8 | - | *nearest* **Parahippocampal gyrus (L)** | - |
| 8-13 | *nearest* **Hippocampus (L)**<br>**Fusiform gyrus (R)**<br>*nearest* **Parahippocampal gyrus (L)** | *nearest* **Parahippocampal gyrus (R)** | *nearest* **Hippocampus (L)** |
| 13-30 | **Hippocampus (L)**<br>**Hippocampus (R)**<br>**Parahippocampal gyrus (R)** | - | - |

FIGURE 6.5: The top three plots show the significant peaks in the *walk* vs. *rest* functional images that were located within the hippocampus or parahippocampal gyrus. Peaks were only found in these regions using MEG in the 13-30Hz frequency band. The bottom six plots show significant peaks that were located adjacent to the hippocampus or parahippocampal gyrus. The corresponding frequency band is given in hertz in the top left of each plot and the corresponding modality is given by the vertical bars. The table gives the AAL atlas regions where each peak is located. Where this was localised to a region not labelled by the AAL atlas, the nearest AAL region is given. All peaks displayed were found to be significant after FDR correction for multiple comparisons.

found in the 13-30Hz band using MEG. Minima were observed bilaterally, in both hippocampi. A minimum was also found within the right parahippocampal gyrus. However, significant peaks were detected that were adjacent to the hippocampal regions using all modalities, across a range of frequency bands. Adjacent minima were detected in the 8-13Hz frequency band across all modalities. Using MEG and MEEG, minima were found adjacent to the left hippocampus. Alpha band minima were also detected on the border of the right fusiform gyrus and in the white matter adjacent to the left parahippocampal gyrus, using MEG. Using EEG, minima were detected in the 4-8Hz and 8-13Hz bands in the white matter adjacent to the left and right parahippocampal gyri respectively.

### 6.3.3 Count vs. rest

Figure 6.6 shows the *t*-statistic images contrasting source power during the *count* and *rest* conditions ($p<0.05$, FDR corrected). Source power differences between these conditions were only observed within three frequency bands: 4-8, 8-13 and 13-30Hz. Significant differences were detected across each of these bands using MEG, whereas changes were only detected in the 13-30Hz band using EEG, and no significant differences were detected using MEEG. In the 4-8Hz and 8-13Hz bands, a frontal increase in source power is observed using MEG during the *count* task compared to during resting. A decrease in power is also observed in the 8-13Hz band, using MEG, which is strongest within the superior temporal gyrus and is lateralised to the left hemisphere. In the 13-30Hz band, widespread decreases are observed across frontal and temporal regions, using MEG and EEG. These are strongest for both modalities within the motor cortex.

Figure 6.7 shows the peak locations that were found within one voxel of the hippocampus or parahippocampal gyrus, when comparing activity during the *count* and *rest* conditions. After correction for multiple comparisons, peaks are only found in the 13-30Hz frequency band using MEG. One minimum was detected in the left hippocampus. However, the other two peaks are local maxima that still show a relative decrease in power during *count* trials in this frequency band, but are located in voxels that are surrounded by regions that show a stronger decrease. Peaks were

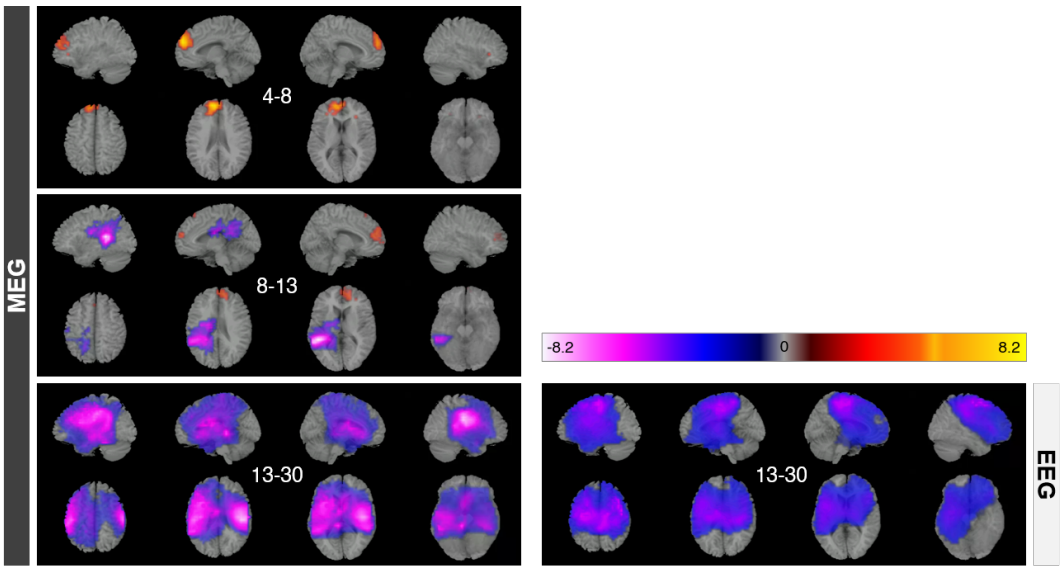


| Frequency (Hz) | MEG | EEG | MEEG |
|---|---|---|---|
| 4-8 | Superior frontal gyrus (L) | - | - |
| 8-13 | Superior temporal gyrus (L) | - | - |
| 13-30 | *nearest* Rolandic operculum (R) | Precentral gyrus (R) | - |

FIGURE 6.6: *Count vs. rest*: The above colour plots show the voxel-wise *t*-statistic indicating the difference in source power between *count* and *rest* conditions, across participants ($p<0.05$, FDR corrected). *t* values are displayed on a template brain as indicated by the colour bar. Warmer colours indicate that higher source power was observed during the *count* condition whereas cooler colours indicate that higher power was observed during the *rest* trials. The corresponding frequency band is given in hertz in the centre of each plot, and the modality is indicated by the vertical bars. Below, the table gives the AAL atlas locations of the largest differences in source power across the brain for each frequency band and modality. Where this was localised to a region not labelled by the AAL atlas, the nearest AAL region is given.

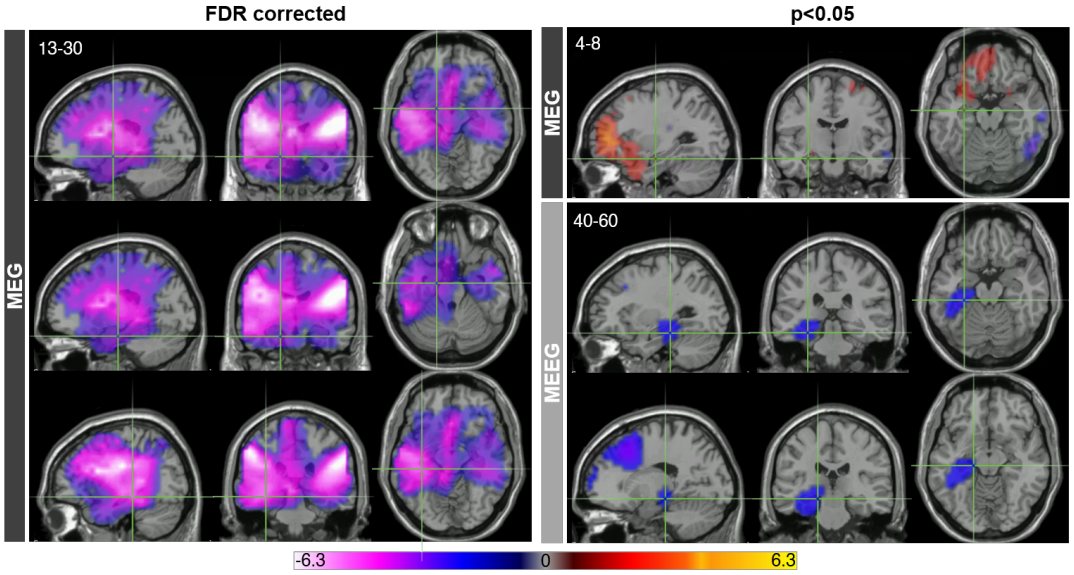


| Frequency (Hz) | MEG | EEG | MEEG |
|---|---|---|---|
| 4-8 | Hippocampus (L) | - | - |
| 13-30 | **Hippocampus (L)**<br>**Parahippocampal gyrus (L)**<br>**Hippocampus (L)** | - | - |
| 40-60 | - | - | Parahippocampal gyrus (L)<br>Hippocampus (L) |

FIGURE 6.7: The left three plots show the significant peaks in the *count* vs. *rest* functional images that were located within the hippocampus or parahippocampal gyrus (p<0.05, FDR corrected). Peaks were only found in these regions using MEG in the 13-30Hz frequency band. The right three plots show peaks within the hippocampus or parahippocampal gyrus that were found to be significant at the $\alpha = 0.05$ level but did not remain after correction for multiple comparisons. The corresponding frequency band is given in hertz in the top left of each plot and the corresponding modality is given by the vertical bars. The table gives the AAL atlas regions where each peak is located. Where a peak is located within white matter, the nearest region is given.

detected in two other frequency bands within the hippocampal regions before correction for multiple comparisons. These included a weak increase in 4-8Hz power within the left hippocampus, observed using MEG, and two minima in 40-60Hz power observed using MEEG, which were also lateralised to the left MTL.

## 6.4 Discussion

### 6.4.1 Source analysis

Alterations in brain activity were detected across a range of frequency bands during the hometown walk task, using EEG, MEG and MEEG. This included source power

changes within the MTL that were observed in different frequency bands depending on the control task used for contrast.

When comparing source power during the *walk* and *count* conditions, using MEG, a peak in the 1-4Hz functional images was localised within the right parahippocampal gyrus. This peak was stronger and was more focally localised to the MTL than the peak observed adjacent to the hippocampus in the 4-8Hz band. This is consistent with the hypothesis that oscillations associated with spatial memory occur at delta band frequencies within the MTL (Jacobs, 2014). However, the weaker activity observed in the theta band perhaps suggests that the activity alterations occur across a range of frequencies that crosses the boundary between these bands. Future work could therefore investigate the frequencies of activity changes with finer resolution to define appropriate frequency bands for use in human memory research.

One surprising result of this study was that these peaks indicate a decrease in low frequency activity within the MTL during the *walk* condition, compared to the *count* trials. These results are not necessarily contradictory to those from fMRI hometown walk studies. An increase in parahippocampal BOLD response is usually observed in the *walk* condition compared to the *count* condition. It is also well established that the BOLD response negatively correlates with low frequency oscillatory amplitude (Mukamel et al., 2005; Zumer et al., 2010). It could therefore be possible that this increase in BOLD activation is associated with a decrease in 1-8Hz oscillatory amplitude during the spatial memory task.

However, from previous electrophysiological studies of memory, including those that implemented spatial memory and autobiographical memory retrieval paradigms, it was expected that an increase in delta and/or theta band power would be observed during the imagined navigation (Cornwell et al., 2008; Fuentemilla et al., 2014; Ekstrom et al., 2005). One potential explanation is that the choice of control task was unusual compared to those used in other electrophysiological studies of spatial memory. For example, the studies of Cornwell et al., 2008 and Ekstrom et al., 2005 investigated activity associated with finding a specific location from memory, and used control tasks involving free movement around a space. In contrast, the control task implemented here was one of mental arithmetic. Studies of mental arithmetic have shown that relatively simple problems may be solved by retrieval of answers

from long term memory, and that the functional activity associated with solving problems in this manner is an increase in left mid-line frontal theta band power (Smedt, Grabner, and Studer, 2009; Gärtner, Grimm, and Bajbouj, 2015). Theta band increases can be observed in these regions in Figure 6.6. Therefore the differences in observed activity alterations, compared to previous studies, may be due to comparing activity during the spatial memory task to that during an arithmetic memory task, which both require the retrieval of long term memories, rather than to a free movement task that does not require memory. This hypothesis is supported by one recent MEG study which found bilateral decreases in 1-8Hz power within the hippocampus during imagination of a scene compared to a counting control task (Tierney et al., 2021).

An alternative explanation for this unexpected result could be that an increase in oscillatory activity occurred within the MTL but was not detected. In healthy participants, activation is usually observed bilaterally and symmetrically within the MTL using fMRI. However, beamformers are known to suppress sources of correlated activity (Van Veen et al., 1997), so any correlated activity between the MTL structures of each hemisphere may not be visible in the resulting functional images. Also, it was found by Quraan et al., 2011 in a simulation study that hippocampal activity could be obscured by simultaneous activation of the visual cortex, due to source leakage. Using MEG, increases in 1-4Hz and 4-8Hz power were observed within the occipital lobe in the *walk* condition compared to both control conditions. Future work could compare the frequency spectra of orthogonalised virtual sensor timecourses within the MTL and occipital lobe, to investigate whether there was activity within the MTL that was obscured by this occipital increase.

In contrast to the *walk* vs *count* functional images, where MTL activity differences were predominantly observed in the delta and theta bands, the *walk* vs. *rest* contrast images exhibited the most peaks within the MTL in the alpha and beta bands. These were also found bilaterally. Areas of the medial temporal lobe, including the hippocampus, are thought to be part of the default mode network (Andrews-Hanna, Smallwood, and Spreng, 2014). It is therefore likely that these regions exhibited higher levels of functional connectivity with other areas of the brain during the resting sections of the task (Vincent et al., 2006). This difference in connectivity could

explain the higher alpha and beta band power observed within the MTL, and within other brain regions, during the *rest* condition as it was found in chapter 4 that amplitude in these frequency bands correlated with the resting state connectivity strength exhibited by a region.

### 6.4.2 MEEG

The pattern of activity differences observed within each frequency band was generally consistent across modalities. However, it was not found that MEEG improved upon the performance of MEG alone for the localisation of activity within the MTL and was, in fact, worse.

The strongest source power changes were observed using MEG alone, both within the MTL and for more superficial sources. Stronger decreases in oscillatory power were detected in frontal regions using MEG than MEEG or EEG. The inclusion of EEG also resulted in source reconstructions without the posterior source power increases, seen using MEG alone, during the *walk* task. However, other studies have reported that combined MEG and EEG analysis improves source analysis for these superficial sources. This suggests that the worse performance found here may have been due to methodological choices that were specific to this study.

There were technical difficulties involved in the simultaneous acquisition of MEG and EEG. Passive EEG electrodes were used to minimise the artefacts produced in the MEG data. However, even with this precaution, the presence of conductive material on the head due to the electrodes, wiring and conductive paste introduced artefacts in both the MEG and EEG recordings. The majority of noise was produced in the occipital channels at harmonics of the mains frequency, potentially due to the higher density of wiring in this region. High levels of noise in these channels meant that more occipital channels were excluded from analysis, which could have contributed to the lack of sensitivity to occipital sources in the EEG and MEEG source images. Future studies employing simultaneous MEG and EEG recordings could aim to reduce the noise produced by the EEG system by applying the least possible amount of conductive paste and by distributing the wiring across the scalp, rather than create areas with higher densities of wiring. A notch filter could also be used

to remove the noise from the data at each of the harmonic frequencies at the pre-processing stage. However, this may then affect the measurement of activity within the overlapping gamma frequency bands. Another step to reducing artefacts would be to reduce participant motion. This will be discussed further in section 6.4.3.

There were also methodological choices at the analysis stage that could have contributed to the worse performance of the MEEG beamformer. As the inclusion of EEG seems to have been detrimental to the SNR of the functional images, this suggests that the EEG measurements were too heavily weighted in the MEEG beamformer. For this study, the EEG and MEG data were scaled on a channel-wise basis by dividing by the standard deviation of all measurements from each channel (Fuchs et al., 1998). This SNR-based weighting method has been used in other studies that have shown that MEEG gives an improvement in source localisation performance (Aydin et al., 2015; Chowdhury et al., 2015; Fuchs et al., 1998). However, there are other weighting methods that may have been more suitable for use in this study. For example, Ko and Jun, 2010 presented a method for determining parameters for weighting the EEG and MEG measurements, which are optimised to obtain the maximum localisation accuracy of simulated activity. This method selects a single parameter corresponding to each modality which is used to scale data across all channels. This would therefore allow the preferential weighting of MEG measurements to maximise the beamformer performance. Alternatively, Piastra et al., 2020 propose that MEG and EEG measurements could be weighted on a voxel-wise basis depending on how sensitive each modality is to activity in that location, which can be determined by maps of their relative SNR within each voxel (Piastra et al., 2020). This method may reduce the detrimental effects of EEG by reducing the weighting of this modality in areas where MEG can provide more information about activity, such as tangential sources or locations further from an EEG electrode.

Another way to improve the quality of the EEG and MEEG source analysis could be to use a more realistic forward model for the calculation of the electric lead fields. EEG signals are more affected by the inhomogeneous conductivity of the head, and therefore the use of a realistic head model is more important for EEG than MEG for accurate source localisation (Vorwerk et al., 2014). For this study, the electric lead fields were calculated using a three-layer BEM head model which was created based

on individual structural MRIs. This method has been used in previous MEEG studies that have shown that combined analysis provides a benefit over the individual modalities. However, a realistic head model is more important for accurate localisation of deeper sources (Attal and Schwartz, 2013; Meyer et al., 2017b). More detailed and realistic forward models can be produced using FEM, which can segment the head into more compartments of more realistic shape. It has been shown in simulation studies (Vorwerk et al., 2014) and experimentally (Rice et al., 2013) that including the cerebrospinal fluid (CSF) has a significant impact on the accuracy of electric lead field models. A MEG simulation study has also shown that hippocampal activity can be more accurately localised when a segmented hippocampus is included in the head model (Meyer et al., 2017b). The use of a realistic forward model is even more important for accurate source localisation using EEG. Using a FEM head model featuring segmentations of structures within the MTL may therefore improve the beamformer performance for all modalities, and could be particularly beneficial for the performance of the EEG and MEEG beamformers.

Another factor that may have affected the relative performance of each modality is the choice of the beamformer regularisation parameter. During this study, the regularisation parameter was kept constant across modalities. However, it could be that different modalities require different levels of regularisation. Increasing the regularisation parameter can increase SNR (Brookes et al., 2008), so it is possible that increasing the parameter used for the EEG and MEEG source analysis may increase the detected source power within the MTL for these modalities. However, increasing the SNR in this way would lead to reduced spatial resolution. Future work could investigate whether an optimal regularisation parameter exists for each modality, and whether this varies between superficial and sub-cortical sources.

### 6.4.3 Study limitations

There were several limitations of this study which may have affected all modalities. One factor that has been shown to influence the ability to localise sub-cortical sources is the accuracy of the coregistration between sensor space and participants' MRIs. It was found by Meyer et al., 2017b that hippocampal activity could only be reliably localised with a coregistration error of less than 3mm. However, a head

movement threshold of 5mm was used here. This threshold was taken as a compromise to maintain cohort size. Even when asked to remain as still as possible, only 8 out of the 28 scanned participants had recorded head movement less than 3mm during the scan, compared to 19 who moved less than 5mm. This could potentially be due to participant fatigue after the long experimental set up required when recording EEG. The set up time was increased by as much as an hour as conductive paste needed to be applied at each electrode to bring it into conductive contact with the scalp, and the location of each electrode needed to be recorded during the head shape digitisation step. The transformation to template space and then subsequent group averaging that was performed during this study should have helped to counter any individual localisation errors, as coregistration errors are not likely to be consistent across participants. However, this would be an issue for potential future studies with the aim of measuring MTL activity in individual subjects, such as MTLE patients. Attempts could be made to limit head movement in future studies, which would both reduce coregistration errors and increase the available sample size for analysis, as fewer participants would be excluded due to excessive head movement. This could be done by using head casts (Meyer et al., 2017a), performing continuous head localisation and compensation (Stolk et al., 2013) or laying participants in a supine position. Alternatively, recording MEG with optically pumped magnetometers (OPMs) could be ideal for MTL source localisation. These can be mounted on the head, which removes the possibility of participants moving relative to the sensors. Also, as OPMs can be brought closer to the brain compared to traditional sensors, which require cryogenic cooling, they can also provide an increase in SNR. OPMs have been shown to increase reconstructed source power within the hippocampus when one sensor was placed in a participant's mouth (Tierney et al., 2021).

The scope of this analysis was limited to comparison of modalities empirically by considering SNR and determining whether peaks in task-related activity alterations occurred in expected locations. The spatial resolution and localisation accuracy of images produced using each modality has therefore not been assessed quantitatively. It is possible that while MEEG images had lower SNR, the localisation of task-related activity may have been more accurate compared to the performance of the individual modalities. An analysis of the full width at half maximum (FWHM)

of the peaks in the functional images produced using each modality could determine whether MEEG gives more focal images, indicating higher spatial resolution. Future work could also produce functional images based on simulated activity to determine how the accuracy of localisation differs between modalities.

It may also have been beneficial to use different source localisation algorithms, which may have been more suited to MTL source localisation. MEG beamformers have been shown to be able to detect hippocampal activity (Pu et al., 2018), and to be able to localise hippocampal activity more accurately than MNE source estimation (Meyer et al., 2017b). However, exact low resolution electromagnetic tomography (eLORETA) is a popular inverse solution algorithm used in EEG research as it is able to attain zero localisation error, even for deep sources (Pascual-marqui, 2007; Pascual-Marqui et al., 2011). It has also been found that eLORETA is less affected by cross-talk than beamforming, and so source estimations are less affected by source leakage (Tait et al., 2020). This may help with detecting sources within the MTL in the presence of concurrent occipital activity, as was detected here. eLORETA may therefore be an inverse solution that is well suited to the localisation of activity within the MTL. The relative ability of beamformers and eLORETA to localise MTL activity using MEEG could be tested in future work.

It may have also been interesting to include an alternative spatial memory paradigm. The hometown walk paradigm has a number of advantages. The reliability of bilateral MTL BOLD activation in healthy controls allows this task to be used for the lateralisation of seizure onset in MTLE (Towgood et al., 2015). This task is also easy to perform so is available for challenging patient groups. However, this task has no behavioural measures, which limits the potential for probing how oscillatory activity within the MTL correlates with performance, such as the accuracy of recall.

## 6.5 Conclusion

MEEG has been shown in previous studies to improve source localisation compared to MEG and EEG individually. However, the inclusion of EEG was shown here to be detrimental for the localisation of sub-cortical sources, as source power changes were only detected in the MTL when using MEG alone. It is possible that

MEEG source localisation may be improved by implementing different methodological choices to reduce the detrimental effects of EEG, such as altering the relative weightings of the EEG and MEG measurements, using a more realistic head model to calculate the lead fields, and optimising the beamformer regularisation parameter. However, it has been shown here that MEG alone can localise sub-cortical activity. Without the simultaneous recording of EEG, it is possible that the performance of the MEG beamformer may have been improved, as the presence of EEG electrodes increases the distance between the brain and the MEG sensors and so decreases the MEG signal strength. Based on these results, it is clear that source analysis methods using the combination of MEG and EEG require careful optimisation to gain the complementary information afforded by EEG and improve upon MEG alone.

# Chapter 7

# Discussion

In this thesis, I have described studies that have contributed to the development of methods for the analysis of MEG and EEG data. In this chapter, I outline the main findings of the thesis and discuss possible avenues for future research which these findings have highlighted.

## 7.1 RVE

The majority of the work in this thesis was concerned with the moment-to-moment variability, or 'irregularity', of neuronal activity. The quantity chosen to investigate this was rank-vector entropy (RVE), as it gives dynamic irregularity timecourses which can take advantage of the excellent temporal resolution of MEG (Robinson et al., 2013). The first study described here, in chapter 2, sought to optimise the RVE measure for MEG research by investigating the effects of varying the tunable RVE parameters: the decay time constant, $\tau$, and the sliding window length, $W$. The parameters were found to be interdependent; the effect of varying each of the parameters was found to depend on the value of the other. For each value of $W$, the value of $\tau$ was found empirically that maximised the temporal resolution of the RVE timecourses of simulated pink noise. However, it was found that increasing the temporal resolution came at the cost of decreasing the SNR of the entropy timecourses. The parameter set was also identified that maximised the temporal correlation between the RVE and low frequency oscillatory amplitude of resting state MEG virtual sensor timecourses.

In chapters 2 and 3, a consistent relationship was found between RVE and oscillatory amplitude across the brain, during the resting state and during a movie watching task. It was found that RVE exhibited negative temporal correlation with

low frequency amplitude envelopes, which was strongest for amplitude in the alpha and beta bands, and positive correlation was observed with gamma band amplitude. This relationship was consistent with the findings of Brookes et al., 2015.

An original finding presented in chapter 3 was that the RVE of MEG virtual sensor timecourses could explain the BOLD response. Positive temporal correlation was found in areas that were active during the movie task. This provides evidence that more irregular activity, indicated by higher RVE values, represents an increase in local processing. One surprising finding was the negative correlation between RVE and the BOLD signal in the regions comprising the default mode network (DMN). This suggests that there may be atypical neurovascular coupling in these regions. It was hypothesised in the discussion of chapter 3 that this negative correlation could be due to the suppression of connectivity within the DMN during the task. I.e. a decrease in the BOLD response within the DMN could be associated with a decrease in network connectivity between these regions and, thus, an increase in local neuronal entropy. The results presented in chapter 4 support the inverse relationship between functional connectivity and RVE, as higher resting state connectivity strength was found to be associated with more regular activity at high scale frequencies (and RVE is equivalent to MRVE at the highest scale frequency). Future work could investigate whether the negative correlation observed here was driven by DMN connectivity by investigating how this relationship is modulated by connectivity strength. Variation in connectivity strength could be assessed using an alternative paradigm where connectivity is compared between trial conditions, or by utilising a dynamic connectivity measure to obtain a timecourse of connectivity strength at nodes within the DMN. This method could be extended to examine other networks to examine whether the DMN truly shows atypical neurovascular coupling or if the results can be explained by connectivity alterations.

It may also be interesting to investigate the relationship between BOLD fMRI and neuronal irregularity further by correlating the BOLD signal with MRVE at a range of scale frequencies. The relationship between MRVE and oscillatory amplitude, as presented in Figure 4.8, varied widely across scale frequencies. It is therefore possible that MRVE at different scale frequencies could exhibit a stronger, or altered, relationship with the BOLD response.

## 7.2 MRVE correlation

RVE measures entropy at a single time scale which is defined by the bandwidth of the data (Robinson et al., 2013). However, brain activity contains structure across a range of time scales (Costa, Goldberger, and Peng, 2005). In chapter 4, MRVE was introduced to measure time resolved neuronal irregularity at a range of time scales. MRVE correlation was shown to be capable of detecting robust resting state functional connectivity from MEG recordings. MRVE correlation at 75Hz was found to show high similarity to amplitude envelope correlation (AEC) networks in the alpha and beta bands. MRVE correlation at this scale frequency was found to give the same level of inter-subject consistency as the beta band, which was the frequency band that gave the most robust AEC networks.

In chapter 5, it was found that MRVE correlation was more sensitive than AEC to resting state connectivity alterations in a cohort at genetic risk of neurodevelopmental disorders (ND-CNV carriers). Reduced connectivity was found using AEC and MRVE correlation but MRVE correlation also detected some temporal-occipital hyperconnectivity in the right hemisphere. When network properties were quantified by graph theory metrics, MRVE correlation was also found to be more sensitive to differences between the healthy and ND-CNV cohorts when classified using a machine learning algorithm.

The results of chapters 4 and 5 suggest that MRVE correlation can provide complementary information about functional connectivity beyond that which is available from AEC. In both chapters it was found that MRVE correlation could detect robust functional connections that weren't visible using AEC. In chapter 5, the machine learning analysis also showed that MRVE correlation was more sensitive to differences in cortical segregation between cohorts, whereas AEC was most sensitive to differences in node importance. The results presented in this thesis therefore suggest that MRVE correlation can provide valuable additional information about functional connectivity when used alongside measures based on oscillatory synchronisation.

A limitation of MRVE correlation is that the underlying mechanisms driving the variation in the MRVE of MEG signals are unknown. It is therefore unclear what drives the correlation between MRVE timecourses. The inability to interpret the

nature of activity underlying MRVE correlation networks has meant that some interesting results presented in this thesis are currently unexplained. For example, it is unknown why the alpha and beta band AEC networks show such high similarity to MRVE correlation networks at high scale frequencies (50 and 75Hz), but low similarity to MRVE correlation networks at scale frequencies within the 8-30Hz range. Future research could investigate the MRVE of simulated network activity to determine what parameters influence the irregularity of activity at a particular scale frequency. This could allow MRVE correlation to be used to gain more insight into the mechanisms underlying network connectivity.

Another limitation of MRVE correlation is that it assumes that resting state connectivity is stationary over the duration of the MEG recording. In recent years, dynamic functional connectivity measures have been used to detect the transient activation of different resting state networks on the millisecond timescale (Baker et al., 2014; Vidaurre et al., 2016; O'Neill et al., 2017). It may be interesting to determine whether MRVE correlation could be extended to provide complementary information about dynamic functional connectivity. This would also allow MRVE correlation to be used in a wider variety of experimental paradigms, including those where network connectivity is thought to change rapidly over time.

## 7.3 Effects of eye movements on resting state MEG functional connectivity measurements

It was found in chapter 4 that the variance in the EOG could explain some frontal connectivity measured using MRVE correlation at low scale frequencies. Therefore, the subsequent chapters included ICA at the data pre-processing stage to remove eye movement artefacts from the MEG and EEG recordings. In chapter 5, this data cleaning method was found to alter the functional connections detected using MRVE correlation and AEC. Reduced connectivity was measured using both methods, although the effect of the cleaning method used was found to vary between different frequencies and between the two cohorts. In healthy controls, ICA cleaning reduced the number of occipital and parietal AEC connections detected in the alpha and beta frequency bands. When using MRVE correlation, ICA cleaning reduced the frontal

connectivity measured at low scale frequencies (<20Hz). While some frontal connectivity was measured at these scale frequencies in chapter 4, this was not seen in the healthy cohort after ICA cleaning in chapter 5, which suggests that these connections were spurious due to eye movement artefacts. In the ND-CNV cohort, AEC networks were affected in the same way as for the control cohort. However, when measuring connectivity using MRVE correlation, a reduction in connectivity was instead found at high scale frequencies (>20Hz). The differences in the effects of ICA between cohorts may indicate differences in the properties of resting state eye movements and the related MRVE correlation networks in ND-CNV carriers, which may be interesting to investigate further in future research.

However, it was found that using the ICA cleaning method resulted in higher sensitivity to network property differences between the cohorts in the graph theory analysis. Therefore, removing eye movement artefacts from MEG data is recommended to maximise the possibility of detecting resting state functional connectivity alterations in patient cohorts.

## 7.4 MEEG

A limitation of MEG research is reduced sensitivity to activity within deeper brain regions due to the rapid drop off of magnetic field strength with distance from the source. EEG has higher sensitivity to radial and deep sources and has previously been shown to provide complementary information to MEG (Dale and Sereno, 1993; Sharon et al., 2007; Henson, Mouchlianitis, and Friston, 2009). While EEG lacks the spatial resolution to localise activity within deep brain structures, such as the MTL (Lam et al., 2018), it is thought that the inclusion of MEG can rule out incorrect solutions that would be given by EEG alone, and thus improve the localisation accuracy of deep sources (Dale and Sereno, 1993). Therefore, in chapter 6 MEG and EEG were combined (MEEG) to look at the medial temporal lobe (MTL), a sub-cortical brain region that has a vital role in memory and spatial navigation. However, in contrast with previous research, MEEG was not found to improve upon the performance of MEG alone. Instead, task related activity was only detected in the MTL using MEG alone. While the MEEG beamformer did not perform as expected, this result does

support the findings of recent studies that have found that MEG alone is capable of detecting activity within these deeper brain regions (Pu et al., 2018).

Many previous studies have found that MEEG can improve localisation accuracy, including one study that saw an increase in localisation performance even in deeper brain regions (Henson, Mouchlianitis, and Friston, 2009). This suggests that optimisation of the combined analysis procedure could lead to improved performance of the MEEG beamformer. For example, different studies have implemented different methods of giving relative weighting to the MEG and EEG data (Baillet et al., 1999; Ko and Jun, 2010). The use of a more realistic head model for calculating the electric lead fields may also improve source reconstructions when using EEG and MEEG. It may also be beneficial to investigate the effects of varying the level of beamformer regularisation, to determine whether there is an optimal regularisation parameter for each modality. Future research could focus on these methodological improvements to work towards optimising the MEEG beamformer for deep brain source localisation.

Upon the improvement of the MEEG beamformer, it could then be interesting to see whether MEEG would increase sensitivity to resting state functional connectivity in deeper regions. For example, the hippocampus is thought to be part of the default mode network (Andrews-Hanna, Smallwood, and Spreng, 2014). However, connectivity with the MTL was not detected using AEC or MRVE correlation with MEG alone in chapters 4 and 5. An increased sensitivity to functional connectivity in deeper brain structures could greatly benefit the study of patient groups where such regions are affected. Future work could investigate deep-brain functional connectivity during the hometown walk paradigm by using an improved MEEG beamformer to generate virtual sensor timecourses. These could then be used to calculate the AEC and MRVE correlation networks.

The use of optically pumped magnetometers (OPMs) may be beneficial for studying the deep brain with MEEG. The simultaneous recording of MEG with OPMs and EEG has been previously demonstrated (Boto et al., 2019). It has also been shown that OPMs alone can detect activity in the hippocampus (Tierney et al., 2021). As OPMs can be mounted on the scalp, the use of this sensor type would remove the possibility of coregistration errors due to head movement relative to the sensors.

OPMs may therefore increase the localisation accuracy of MEG and MEEG functional images within the deep brain. However, current OPM MEG systems alone do not have sufficient numbers of sensors to perform functional connectivity analysis between 90 locations in the brain. The inclusion of EEG would increase the rank of the combined dataset, and so could allow the functional connectivity measures described in this thesis to be applied to current OPM MEG data.

## 7.5 Conclusions

During this thesis, measures of time resolved neuronal irregularity have shown to be useful as a complement to measures of oscillatory activity in the analysis of MEG data. It was shown that RVE could provide insight into neurovascular coupling, and that the regions comprising the default mode network may exhibit an atypical relationship between the BOLD response and the underlying neuronal activity.

An important development put forward in this thesis was the extension to multiscale RVE, which could measure dynamic neuronal entropy over a range of temporal scales. MRVE correlation was shown to provide insight into functional connectivity across temporal scales in health and disease and gave complementary information to that given by measures based on oscillatory synchronisation.

The discovery that functional connectivity measurements depend to some extent on the data cleaning method used has important implications for all MEG and EEG analysis. It is suggested that ICA cleaning should be used to remove eye movement artefacts if the aim is to increase sensitivity to resting state connectivity alterations in patient groups. However, these results also suggest caution as the ICA cleaning procedure also suppressed some non-spurious network connectivity.

In the final chapter, MEEG was not shown to improve source localisation in the deep brain over MEG alone. However, the many methodological differences present in the literature suggest that there are many avenues for methodological improvement that could improve the combined beamformer performance.

# Bibliography


Achermann, P and A A Borbely (1997). "Low-frequency (<1Hz) oscillations in the human sleep electroencephalogram". In: Neuroscience 81.1, pp. 213–222.

Andreou, Christina et al. (2015). "Increased Resting-State Gamma-Band Connectivity in First-Episode Schizophrenia". In: Schizophrenia Bulletin 41.4, pp. 930–939. DOI: 10.1093/schbul/sbu121.

Andrews-Hanna, Jessica R, Jonathan Smallwood, and Nathan R Spreng (2014). "The default network and self-generated thought: component processes, dynamic control, and clinical relevance". In: Annals of the New York Academy of Sciences 1316.1, pp. 29–52. ISSN: 1749-6632. DOI: 10.1111/nyas.12360.The. arXiv: NIHMS150003.

Andrews-hanna, Jessica R et al. (2007). "Disruption of Large-Scale Brain Systems in Advanced Aging". In: Neuron 56.5, pp. 924–935. DOI: 10.1016/j.neuron.2007.10.038.Disruption.

Attal, Yohan and Denis Schwartz (2013). "Assessment of Subcortical Source Localization Using Deep Brain Activity Imaging Model with Minimum Norm Operators: A MEG Study". In: PLoS ONE. ISSN: 19326203. DOI: 10.1371/journal.pone.0059856.

Ávila, César et al. (2006). "Memory lateralization with 2 functional MR imaging tasks in patients with lesions in the temporal lobe". In: American Journal of Neuroradiology 27, pp. 498–503. ISSN: 01956108.

Aydin, Ümit et al. (2015). "Combined EEG/MEG can outperform single modality EEG or MEG source reconstruction in presurgical epilepsy diagnosis". In: PLoS ONE. ISSN: 19326203. DOI: 10.1371/journal.pone.0118753.

Babiloni, Fabio et al. (2001). "Linear Inverse Source Estimate of Combined EEG and MEG Data Related to Voluntary Movements". In: Human Brain Mapping 14, pp. 197–209.

Backus, Alexander R et al. (2016). "Hippocampal-Prefrontal Theta Oscillations Support Memory Integration". In: Current Biology 26, pp. 450–457. DOI: 10.1016/j.cub.2015.12.048.

Baillet, Sylvain (2017). "Magnetoencephalography for brain electrophysiology and imaging". In: Nature Neuroscience. ISSN: 1097-6256. DOI: 10.1038/nn.4504.

Baillet, Sylvain et al. (1999). "Combined MEG and EEG Source Imaging by Minimization of Mutual Information". In: IEEE transactions on bioedical engineering 46.5, pp. 522–534.

Baker, Adam P et al. (2014). "Fast transient networks in spontaneous human brain activity". In: eLife 3, pp. 1–18. ISSN: 2050084X. DOI: 10.7554/eLife.01867.

Barratt, Eleanor L et al. (2018). "Mapping the topological organisation of beta oscillations in motor cortex using MEG". In: NeuroImage 181, pp. 831–844. ISSN: 1053-8119. DOI: 10.1016/j.neuroimage.2018.06.041. URL: https://doi.org/10.1016/j.neuroimage.2018.06.041.

Bartoli, Eleonora et al. (2019). "Functionally Distinct Gamma Range Activity Revealed by Stimulus Tuning in Human Visual Cortex". In: Current Biology 29, pp. 3345–3358. DOI: 10.1016/j.cub.2019.08.004.

Beisteiner, Roland et al. (2008). "Does clinical memory fMRI provide a comprehensive map of medial temporal lobe structures?" In: Experimental Neurology 213, pp. 154–162. DOI: 10.1016/j.expneurol.2008.05.019.

Berger, Hans (1929). "Uber das Elektrenkephalogramm des Menschen." In: Archiv für Psychiatrie 87, pp. 527–568.

Berman, Jeffrey I et al. (2016). "Relationship between M100 Auditory Evoked Response and Auditory Radiation Microstructure in 16p11.2 Deletion and Duplication Carriers". In: AJNR Am J Neuroradiol 37.6, pp. 1178–1184. DOI: 10.3174/ajnr.A4687.Relationship.

Bertero, Alice et al. (2018). "Autism-associated 16p11.2 microdeletion impairs prefrontal functional connectivity in mouse and human". In: Brain 141.7, pp. 2055–2065. ISSN: 14602156. DOI: 10.1093/brain/awy111.

Boon, Lennard I et al. (2017). "Changes in resting-state directed connectivity in cortico-subcortical networks correlate with cognitive function in Parkinson's disease". In: Clinical Neurophysiology 128, pp. 1319–1326. ISSN: 1388-2457. DOI: 10.1016/j.clinph.2017.04.024. URL: http://dx.doi.org/10.1016/j.clinph.2017.04.024.

Bordier, Cécile, Carlo Nicolini, and Angelo Bifone (2017). "Graph analysis and modularity of brain functional connectivity networks: Searching for the optimal threshold". In: Frontiers in Neuroscience 11, pp. 1–9. ISSN: 1662453X. DOI: 10.3389/fnins.2017.00441.

Boser, Bernhard E, Isabelle M Guyon, and Vladimir N Vapnik (1992). "Training algorithm for optimal margin classifiers". In: Proceedings of the Fifth Annual ACM Workshop on Computational Learning Theory, pp. 144–152. ISBN: 089791497X. DOI: 10.1145/130385.130401.

Bosl, William J, Tobias Loddenkemper, and Charles A Nelson (2017). "Nonlinear EEG biomarker profiles for autism and absence

epilepsy". In: Neuropsychiatric Electrophysiology 3.1, pp. 1–22. ISSN: 2055-4788. DOI: 10.1186/s40810-017-0023-x. URL: http://npepjournal.biomedcentral.com/articles/10.1186/s40810-017-0023-x.

Boto, Elena et al. (2018). "Moving magnetoencephalography towards real-world applications with a wearable system". In: Nature 555.7698, pp. 657–661. ISSN: 14764687. DOI: 10.1038/nature26147. arXiv: NIHMS150003. URL: http://dx.doi.org/10.1038/nature26147.

Boto, Elena et al. (2019). "Wearable neuroimaging: Combining and contrasting magnetoencephalography and electroencephalography". In: NeuroImage 201.August, p. 116099. ISSN: 10959572. DOI: 10.1016/j.neuroimage.2019.116099. URL: https://doi.org/10.1016/j.neuroimage.2019.116099.

Boutros, Nash N et al. (2009). "The Status of Spectral EEG Abnormality as a Diagnostic Test for Schizophrenia". In: Schizophrenia Research 99.1-3, pp. 225–237.

Brookes, Matthew J. et al. (2005). "GLM-beamformer method demonstrates stationary field, alpha ERD and gamma ERS co-localisation with fMRI BOLD response in visual cortex". In: NeuroImage 26, pp. 302–308. ISSN: 10538119. DOI: 10.1016/j.neuroimage.2005.01.050.

Brookes, Matthew J et al. (2008). "Optimising experimental design for MEG beamformer imaging". In: NeuroImage 39, pp. 1788–1802. DOI: 10.1016/j.neuroimage.2007.09.050.

Brookes, Matthew J et al. (2011a). "Investigating the electrophysiological basis of resting state networks using magnetoencephalography". In: PNAS 108.40, pp. 16783–16788. DOI: 10.1073/pnas.1112685108.

Brookes, Matthew J. et al. (2011b). "Measuring functional connectivity using MEG: Methodology and comparison with fcMRI". In: NeuroImage. ISSN: 10538119. DOI: 10.1016/j.neuroimage.2011.02.054.

Brookes, Matthew J et al. (2015). "Complexity Measures in Magnetoencephalography: Measuring "Disorder" in Schizophrenia". In: Plos One 10.4. DOI: 10.1371/journal.pone.0120991.

Brookes, Matthew J. et al. (2016). "A multi-layer network approach to MEG connectivity analysis". In: NeuroImage 132, pp. 425–438. ISSN: 10959572. DOI: 10.1016/j.neuroimage.2016.02.045.

Brookes, Matthew J et al. (2018). "Altered temporal stability in dynamic neural networks underlies connectivity changes in neurodevelopment". In: NeuroImage 174, pp. 563–575. ISSN: 1053-8119. DOI: 10.1016/j.neuroimage.2018.03.008. URL: https://doi.org/10.1016/j.neuroimage.2018.03.008.

Calkins, Monica E, William G Iacono, and Deniz S Ones (2008). "Eye Movement Dysfunction in First-Degree Relatives of Patients with Schizophrenia: A

Meta-analytic Evaluation of Candidate Endophenotypes". In: Brain Cogn. 68.3, pp. 436–461. DOI: 10.1016/j.bandc.2008.09.001.Eye.

Caplan, Jeremy B et al. (2003). "Human theta oscillations related to sensorimotor integration and spatial learning." In: The Journal of neuroscience 23.11, pp. 4726–4736. ISSN: 1529-2401. DOI: 23/11/4726[pii].

Catarino, Ana et al. (2011). "Atypical EEG complexity in autism spectrum conditions: A multiscale entropy analysis". In: Clinical Neurophysiology 122, pp. 2375–2383. ISSN: 13882457. DOI: 10.1016/j.clinph.2011.05.004. URL: http://dx.doi.org/10.1016/j.clinph.2011.05.004.

Cawley, Gavin C. and Nicola L.C. Talbot (2007). "Preventing over-fitting during model selection via bayesian regularisation of the hyper-parameters". In: Journal of Machine Learning Research 8, pp. 841–861. ISSN: 15324435.

Chawner, Samuel J.R.A. et al. (2019). "Genotype–phenotype associations in children with copy number variants associated with high neuropsychiatric risk in the UK (IMAGINE-ID): a case-control cohort study". In: The Lancet Psychiatry 6, pp. 493–505. ISSN: 22150374. DOI: 10.1016/S2215-0366(19)30123-3. URL: http://dx.doi.org/10.1016/S2215-0366(19)30123-3.

Cheyne, Douglas et al. (2007). "Event-related beamforming: A robust method for presurgical functional mapping using MEG". In: Clinical Neurophysiology 118.8, pp. 1691–1704. ISSN: 13882457. DOI: 10.1016/j.clinph.2007.05.064. URL: http://linkinghub.elsevier.com/retrieve/pii/S1388245707002076.

Chowdhury, Rasheda Arman et al. (2015). "MEG-EEG Information Fusion and Electromagnetic Source Imaging: From Theory to Clinical Application in Epilepsy". In: Brain Topography 28, pp. 785–812. ISSN: 15736792. DOI: 10.1007/s10548-015-0437-3.

Cohen, D (1972). "Magnetoencephalography: Detection of the Brain's Electrical Activity with a Superconducting Magnetometer". In: Science 175.4022, pp. 664–666.

Colclough, G. L. et al. (2015). "A symmetric multivariate leakage correction for MEG connectomes". In: NeuroImage 117, pp. 439–448. ISSN: 10959572. DOI: 10.1016/j.neuroimage.2015.03.071.

Colclough, G. L. et al. (2016). "How reliable are MEG resting-state connectivity metrics?" In: NeuroImage 138, pp. 284–293. ISSN: 10959572. DOI: 10.1016/j.neuroimage.2016.05.070. URL: http://dx.doi.org/10.1016/j.neuroimage.2016.05.070.

Conner, Christopher R et al. (2011). "Variability of the Relationship between Electrophysiology and BOLD-fMRI across Cortical Regions in Humans". In: The Journal of Neuroscience 31.36, pp. 12855–12865. DOI: 10.1523/JNEUROSCI.1457-11.2011.

Coquelet, N et al. (2017). "The electrophysiological connectome is maintained in healthy elders: a power envelope correlation MEG study". In: Scientific Reports 7.13984, pp. 1–10. DOI: 10.1038/s41598-017-13829-8.

Cornwell, Brian R et al. (2008). "Human Hippocampal and Parahippocampal Theta during Goal-Directed Spatial Navigation Predicts Performance on a Virtual Morris Water Maze". In: The Journal of Neuroscience 28.23, pp. 5983–5990. DOI: 10.1523/JNEUROSCI.5001-07.2008.

Costa, Madalena, Ary L Goldberger, and C K Peng (2005). "Multiscale entropy analysis of biological signals". In: Physical Review E - Statistical, Nonlinear, and Soft Matter Physics 71.2, pp. 1–18. ISSN: 15393755. DOI: 10.1103/PhysRevE.71.021906.

Courtiol, Julie et al. (2016). "The multiscale entropy: Guidelines for use and interpretation in brain signal analysis." In: Journal of neuroscience methods 273.January 2017, pp. 175–190. ISSN: 1872-678X. DOI: 10.1016/j.jneumeth.2016.09.004. URL: http://www.ncbi.nlm.nih.gov/pubmed/27639660.

Dale, Anders and Martin Sereno (1993). "Improved Localizadon of Cortical Activity by Combining EEG and MEG with MRI Cortical Surface Reconstruction: A Linear Approach". In: Journal of Cognitive Neuroscience 5.2, pp. 162–176. ISSN: 0898-929X. DOI: 10.1162/jocn.1993.5.2.162. URL: http://www.mitpressjournals.org/doi/10.1162/jocn.1993.5.2.162.

De La Fuente, Angelica et al. (2013). "A review of attention-deficit/hyperactivity disorder from the perspective of brain networks". In: Frontiers in Human Neuroscience 7, pp. 1–6. ISSN: 16625161. DOI: 10.3389/fnhum.2013.00192.

Debbané, Martin et al. (2012). "Resting-state networks in adolescents with 22q11.2 deletion syndrome: Associations with prodromal symptoms and executive functions". In: Schizophrenia Research 139, pp. 33–39. ISSN: 09209964. DOI: 10.1016/j.schres.2012.05.021. URL: http://dx.doi.org/10.1016/j.schres.2012.05.021.

Deco, Gustavo, Viktor K. Jirsa, and Anthony R. McIntosh (2011). "Emerging concepts for the dynamical organization of resting-state activity in the brain". In: Nature Reviews Neuroscience 12.1, pp. 43–56. ISSN: 1471003X. DOI: 10.1038/nrn2961. URL: http://dx.doi.org/10.1038/nrn2961.

Delorme, Arnaud and Scott Makeig (2004). "EEGLAB: an open source toolbox for analysis of single-trial EEG dynamics including independent component analysis". In: Journal of Neuroscience Methods 134.

Dima, Diana C et al. (2019). "Electrophysiological network alterations in adults with copy number variants associated with high neurodevelopmental risk". In: bioRxiv.

Dima, Diana C et al. (2020). "Electrophysiological network alterations in adults with copy number variants associated with high neurodevelopmental risk". In: Translational Psychiatry 10.324. ISSN: 2158-3188. DOI: 10.1038/s41398-020-00998-w. URL: http://dx.doi.org/10.1038/s41398-020-00998-w.

Donner, Tobias H and Markus Siegel (2011). "A framework for local cortical oscillation patterns". In: Trends in Cognitive Sciences 15.5, pp. 191–199. ISSN: 1364-6613. DOI: 10.1016/j.tics.2011.03.007. URL: http://dx.doi.org/10.1016/j.tics.2011.03.007.

Drakesmith, M et al. (2015). "Overcoming the effects of false positives and threshold bias in graph theoretical analyses of neuroimaging data". In: NeuroImage 118, pp. 313–333. ISSN: 10959572. DOI: 10.1016/j.neuroimage.2015.05.011. URL: http://dx.doi.org/10.1016/j.neuroimage.2015.05.011.

Drakesmith, Mark et al. (2019). "Genetic risk for schizophrenia and developmental delay is associated with shape and microstructure of midline white-matter structures". In: Translational Psychiatry 9.1. ISSN: 21583188. DOI: 10.1038/s41398-019-0440-7. URL: http://dx.doi.org/10.1038/s41398-019-0440-7.

Dubourg, Lydia et al. (2019). "Divergent default mode network connectivity during social perception in 22q11.2 deletion syndrome". In: Psychiatry Research - Neuroimaging 291.July, pp. 9–17. ISSN: 18727506. DOI: 10.1016/j.pscychresns.2019.07.004. URL: https://doi.org/10.1016/j.pscychresns.2019.07.004.

Ekstrom, Arne D. et al. (2005). "Human hippocampal theta activity during virtual navigation". In: Hippocampus 15, pp. 881–889. ISSN: 10509631. DOI: 10.1002/hipo.20109.

Engel, Andreas K and Pascal Fries (2010). "Beta-band oscillations — signalling the status quo?" In: Current Opinion in Neurobiology 20, pp. 156–165. DOI: 10.1016/j.conb.2010.02.015.

Engels, M M A et al. (2017). "Directional information flow in patients with Alzheimer's disease. A source-space resting-state MEG study". In: NeuroImage 15, pp. 673–681. DOI: 10.1016/j.nicl.2017.06.025.

Fabiani, Monica et al. (2014). "Neurovascular coupling in normal aging: A combined optical, ERP and fMRI study". In: NeuroImage 85.1. DOI: 10.1016/j.neuroimage.2013.04.113.Neurovascular.

Fan, Rong-en et al. (2008). "LIBLINEAR: A Library for Large Linear Classification". In: Journal of Machine Learning Research 9, pp. 1871–1874.

Fan, Siyan et al. (2018). "Altered functional connectivity in resting state networks in Tourette's disorder". In: Frontiers in Human Neuroscience 12, pp. 1–9. ISSN: 16625161. DOI: 10.3389/fnhum.2018.00363.

Fernández, Alberto et al. (2013). "Complexity and schizophrenia". In: Progress in Neuropsychopharmacology and Biological Psychiatry 45, pp. 267–276. ISSN: 0278-5846. DOI: 10.1016/j.pnpbp.2012.03.015. URL: http://dx.doi.org/10.1016/j.pnpbp.2012.03.015.

Fonov, V S et al. (2009). "Unbiased nonlinear average age-appropriate brain templates from birth to adulthood". In: NeuroImage 47, S102. ISSN: 1053-8119. DOI: 10.1016/S1053-8119(09)70884-5. URL: https://www.sciencedirect.com/science/article/pii/S1053811909708845?via%3Dihub.

Fransson, Peter et al. (2014). "Slow fluctuations in eye position and resting-state functional magnetic resonance imaging brain activity during visual fixation". In: Cognitive neuroscience 40, pp. 3828–3835. DOI: 10.1111/ejn.12745.

Fries, Pascal (2005). "A mechanism for cognitive dynamics: neuronal communication through neuronal coherence". In: Trends in Cognitive Sciences 9.10, pp. 474–480. DOI: 10.1016/j.tics.2005.08.011.

Friston, K J, G Tononi, and G M Edelman (1996). "Characterising the Complexity of Neuronal Interactions". In: Human brain mapping 314.1995, pp. 302–314.

Friston, Karl et al. (2016). "The dysconnection hypothesis (2016)". In: Schizophrenia Research 176, pp. 83–94. ISSN: 0920-9964. DOI: 10.1016/j.schres.2016.07.014. URL: http://dx.doi.org/10.1016/j.schres.2016.07.014.

Fuchs, Manfred et al. (1998). "Improving source reconstructions by combining bioelectric and biomagnetic data". In: Electroencephalography and Clinical Neurophysiology 107.2, pp. 93–111. ISSN: 00134694. DOI: 10.1016/S0013-4694(98)00046-7.

Fuentemilla, L et al. (2014). "Theta oscillations orchestrate medial temporal lobe and neocortex in remembering autobiographical memories". In: NeuroImage 85, pp. 730–737. ISSN: 1053-8119. DOI: 10.1016/j.neuroimage.2013.08.029. URL: http://dx.doi.org/10.1016/j.neuroimage.2013.08.029.

Garrett, Douglas D. et al. (2013). "Moment-to-moment brain signal variability: A next frontier in human brain mapping?" In: Neuroscience and Biobehavioral Reviews 37, pp. 610–624. ISSN: 01497634. DOI: 10.1016/j.neubiorev.2013.02.015. arXiv: NIHMS150003.

Gärtner, Matti, Simone Grimm, and Malek Bajbouj (2015). "Frontal midline theta oscillations during mental arithmetic: effects of stress". In: Frontiers in Behavioural Neuroscience 9, pp. 1–8. DOI: 10.3389/fnbeh.2015.00096.

Ghanbari, Yasser et al. (2015). "Joint Analysis of Band-Specific Functional Connectivity and Signal Complexity in Autism". In: J Autism Dev Disord. 45.2, pp. 444–460. DOI: 10.1007/s10803-013-1915-7.Joint.

Godfrey, Megan and Krish D Singh (2021). "Measuring robust functional connectivity from resting-state MEG using amplitude and entropy correlation across frequency bands and temporal scales". In: NeuroImage 226. DOI: 10.1016/j.neuroimage.2020.117551.

Golestani, Ali M et al. (2016). "The association between cerebrovascular reactivity and resting-state fMRI functional connectivity in healthy adults: The influence of basal carbon dioxide". In: NeuroImage 132, pp. 301–313. ISSN: 1053-8119. DOI: 10.1016/j.neuroimage.2016.02.051. URL: http://dx.doi.org/10.1016/j.neuroimage.2016.02.051.

Gorges, Martin et al. (2013). "Functional Connectivity Within the Default Mode Network Is Associated With Saccadic Accuracy in Parkinson's Disease: A Resting-State fMRI and Videooculographic Study". In: Brain connectivity 3.3, pp. 265–272. ISSN: 2158-0022.

Gorges, Martin et al. (2016). "The association between alterations of eye movement control and cerebral intrinsic functional connectivity in Parkinson's disease". In: Brain Imaging and Behavior 10, pp. 79–91. ISSN: 19317565. DOI: 10.1007/s11682-015-9367-7.

Gramfort, Alexandre et al. (2010). "OpenMEEG: opensource software for quasistatic bioelectromagnetics". In: BioMedical Engineering OnLine 9.45, pp. 1–20.

Grassberger, P. (1991). Information dynamics. Ed. by Harald Atmanspacher and Herbert Scheingraber, p. 15.

Guitart-Masip, Marc et al. (2013). "Synchronization of Medial Temporal Lobe and Prefrontal Rhythms in Human Decision Making". In: The Journal of Neuroscience 33.2, pp. 442–451. DOI: 10.1523/JNEUROSCI.2573-12.2013.

Hall, Emma L et al. (2014). "The relationship between MEG and fMRI". In: NeuroImage 102, pp. 80–91. ISSN: 10959572. DOI: 10.1016/j.neuroimage.2013.11.005.

Hall, Michael B H (2017). "Localising epileptiform activity and eloquent cortex using Magnetoencephalography". PhD thesis, pp. 122–148.

Hamandi, Khalid et al. (2016). "Non-invasive brain mapping in epilepsy : Applications from magnetoencephalography". In: Journal of Neuroscience Methods 260, pp. 283–291. ISSN: 0165-0270. DOI: 10.1016/j.jneumeth.2015.11.012. URL: http://dx.doi.org/10.1016/j.jneumeth.2015.11.012.

Haufe, Stefan et al. (2014). "On the interpretation of weight vectors of linear models in multivariate neuroimaging". In: NeuroImage 87, pp. 96–110. ISSN: 1053-8119. DOI: 10.1016/j.neuroimage.2013.10.067. URL: http://dx.doi.org/10.1016/j.neuroimage.2013.10.067.

Henson, Richard N, Elias Mouchlianitis, and Karl J Friston (2009). "MEG and EEG data fusion: Simultaneous localisation of face- evoked responses". In: NeuroImage 47.2, pp. 581–589. DOI: 10.1016/j.neuroimage.2009.04.063.MEG.

Heuvel, Martijn P van den and Hilleke E Hulshoff Pol (2010). "Exploring the brain network : A review on resting-state fMRI functional connectivity". In: European Neuropsychopharmacology 20, pp. 519–534. ISSN: 0924-977X. DOI: 10.1016/j.euroneuro.2010.03.008. URL: http://dx.doi.org/10.1016/j.euroneuro.2010.03.008.

Hillebrand, Arjan et al. (2012). "Frequency-dependent functional connectivity within resting-state networks: An atlas-based MEG beamformer solution". In: Neuroimage 59.4, pp. 3909–3921. DOI: 10.1016/j.neuroimage.2011.11.005.

Hipp, Joerg F et al. (2013). "Large-scale cortical correlation structure of spontaneous oscillatory activity". In: Nat Neurosci 15.6. DOI: 10.1038/nn.3101.Large-scale.

Hong, Jun Hee et al. (2013). "Localization of coherent sources by simultaneous MEG and EEG beamformer". In: Medical and Biological Engineering and Computing 51, pp. 1121–1135. DOI: 10.1007/s11517-013-1092-z.

Huang, M X, J C Mosher, and R M Leahy (1999). "A sensor-weighted overlapping-sphere head model and exhaustive head model comparison for MEG". In: Physics in medicine and biology 44, pp. 423–440.

Hull, Jocelyn V et al. (2017). "Resting-state functional connectivity in autism spectrum disorders: A review". In: Frontiers in Psychiatry 7, pp. 1–17. ISSN: 16640640. DOI: 10.3389/fpsyt.2016.00205.

Ino, Tadashi et al. (2002). "Mental navigation in humans is processed in the anterior bank of the parieto-occipital sulcus". In: Neuroscience letters 322, pp. 182–186.

Jacobs, Joshua (2014). "Hippocampal theta oscillations are slower in humans than in rodents: implications for models of spatial navigation and memory". In: Phil. Trans. R. Soc. B 369. DOI: 10.1098/rstb.2013.0304. URL: http://dx.doi.org/10.1098/rstb.2013.0304.

Jokeit, Hennric, Michael Okujava, and Friedrich G Woermann (2001). "Memory fMRI lateralizes temporal lobe epilepsy". In: Neurology Journal of the American Heart Association 57.10, pp. 1786–1793.

Jongh, Arent de et al. (2005). "Differences in MEG/EEG Epileptic Spike Yields Explained by Regional Differences in Signal-to-Noise Ratios". In: Journal of Clinical Neurophysiology 22.2, pp. 153–158. ISSN: 0736-0258. DOI: 10.1097/01.WNP.0000158947.68733.51. URL: http://content.wkhealth.com/linkback/openurl?sid=WKPTLP:landingpage&an=00004691-200504000-00010.

Kahana, Michael J et al. (1999). "Human theta oscillations exhibit task dependence during virtual maze navigation". In: Nature 399, pp. 781–784.

Kalcher, Klaudius et al. (2014). "The Spectral Diversity of Resting-State Fluctuations in the Human Brain". In: PLoS ONE 9.4. DOI: 10.1371/journal.pone.0093375.

Kaplan, Raphael et al. (2012). "Movement-Related Theta Rhythm in Humans: Coordinating Self-Directed Hippocampal Learning". In: PLoS Biology 10.2. DOI: 10.1371/journal.pbio.1001267.

Keefe, John O and Michael L Recce (1993). "Phase Relationship Between Hippocampal Place Units and the EEG Theta Rhythm". In: Hippocampus 3.3, pp. 317–330.

Kirov, George et al. (2014). "The penetrance of copy number variations for schizophrenia and developmental delay". In: Biological Psychiatry 75.5, pp. 378–385. DOI: 10.1016/j.biopsych.2013.07.022.The.

Ko, Seokha and Sung Chan Jun (2010). "Beamformer for simultaneous magnetoencephalography and electroencephalography analysis". In: Journal of Applied Physics 107, pp. 1–4. DOI: 10.1063/1.3360184.

Koelewijn, Loes et al. (2015). "Resting-state oscillatory dynamics in sensorimotor cortex in benign epilepsy with centro-temporal spikes and typical brain development". In: Human Brain Mapping. ISSN: 10970193. DOI: 10.1002/hbm.22888.

Koelewijn, Loes et al. (2019). "Oscillatory hyperactivity and hyperconnectivity in young APOE -epsilon4 carriers and hypoconnectivity in Alzheimer's disease". In: eLife 30.8.

Kovarski, Klara et al. (2019). "Faster Eye Movements in Children with Autism Spectrum Disorder". In: Autism research 12, pp. 212–224. DOI: 10.1002/aur.2054.

Kutner, Michael H et al. (2005). Applied Linear Statistical Models Fifth Edition, p. 283. ISBN: 0072386886.

Kybic, Jan et al. (2005). "A Common Formalism for the Integral Formulations of the Forward EEG Problem". In: IEEE transactions on medical imaging 24.1, pp. 12–28.

Lam, Alice D et al. (2018). "SCOPE-mTL: a non-invasive tool for identifying and lateralizing mesial temporal lobe seizures prior to scalp EEG ictal onset". In: Clinical Neurophysiology 128.9, pp. 1647–1655. DOI: 10.1016/j.clinph.2017.06.040.SCOPE-mTL.

Lee, Megan H, Christopher D Smyser, and Joshua S Shimony (2013). "Resting state fMRI: A review of methods and clinical applications". In: American Journal of Neuroradiology 34.10, pp. 1866–1872. DOI: 10.3174/ajnr.A3263.Resting.

Lewis, J. D. et al. (2014). "Network inefficiencies in autism spectrum disorder at 24 months". In: Translational Psychiatry 4, pp. 1–11. ISSN: 21583188. DOI: 10.1038/tp.2014.24.

Lippé, Sarah, Natasa Kovacevic, and Anthony Randal Mcintosh (2009). "Differential maturation of brain signal complexity in the human auditory and visual system".

In: Frontiers in human neuroscience 3.48, pp. 1–9. DOI: 10.3389/neuro.09.048.2009.

Little, Simon and Peter Brown (2014). "The functional role of beta oscillations in Parkinson's disease". In: Parkinsonism and Related Disorders 20.1, S44–S48. ISSN: 1353-8020. DOI: 10.1016/S1353-8020(13)70013-0. URL: http://dx.doi.org/10.1016/S1353-8020(13)70013-0.

Liu, Arthur K., Anders M. Dale, and John W. Belliveau (2002). "Monte Carlo simulation studies of EEG and MEG localization accuracy". In: Human Brain Mapping 16, pp. 47–62. ISSN: 10659471. DOI: 10.1002/hbm.10024.

Liuzzi, Lucrezia et al. (2017). "Optimising experimental design for MEG resting state functional connectivity measurement". In: NeuroImage 155, pp. 565–576. ISSN: 1053-8119. DOI: 10.1016/j.neuroimage.2016.11.064. URL: http://dx.doi.org/10.1016/j.neuroimage.2016.11.064.

Logothetis, Nikos K (2003). "The Underpinnings of the BOLD Functional Magnetic Resonance Imaging Signal". In: The Journal of Neuroscience 23.10, pp. 3963–3971.

Lottman, Kristin K. et al. (2019). "Examining resting-state functional connectivity in first-episode schizophrenia with 7T fMRI and MEG". In: NeuroImage: Clinical 24, pp. 1–10. ISSN: 22131582. DOI: 10.1016/j.nicl.2019.101959.

Lowenstein, Otto, Richard Feinberg, and Irene E Loewenfeld (1963). "Pupillary movements during acute and chronic fatigue: A new test for the objective evaluation of tiredness". In: Investigative Ophthalmology 2.2, pp. 138–157.

Maguire, Eleanor A, Richard S J Frackowiak, and Christopher D Frith (1997). "Recalling Routes around London: Activation of the Right Hippocampus in Taxi Drivers". In: The Journal of Neuroscience 17.18, pp. 7103–7110.

Mateos, D M et al. (2018). "Measures of entropy and complexity in altered states of consciousness". In: Cognitive Neurodynamics 12, pp. 73–84. ISSN: 1871-4099. DOI: 10.1007/s11571-017-9459-8.

McCann, Hannah, Giampaolo Pisano, and Leandro Beltrachini (2019). Variation in Reported Human Head Tissue Electrical Conductivity Values. Vol. 32. 5. Springer US, pp. 825–858. ISBN: 0123456789. DOI: 10.1007/s10548-019-00710-2. URL: https://doi.org/10.1007/s10548-019-00710-2.

McDonald-McGinn, Donna M. et al. (2016). "22Q11.2 Deletion Syndrome". In: Nat Rev Dis Primers 1.15071. DOI: 10.1016/B978-0-323-44548-1.00154-6.

Mcdonough, Ian M et al. (2014). "Network complexity as a measure of information processing across resting-state networks: evidence from the Human Connectome Project". In: Frontiers in human neuroscience 8.June, pp. 1–15. DOI: 10.3389/fnhum.2014.00409.

McIntosh, A. R. et al. (2014). "Spatiotemporal dependency of age-related changes in brain signal variability". In: Cerebral Cortex 24.7, pp. 1806–1817. ISSN: 14602199. DOI: 10.1093/cercor/bht030.

McIntosh, Anthony Randal, Natasa Kovacevic, and Roxane J Itier (2008). "Increased Brain Signal Variability Accompanies Lower Behavioral Variability in Development". In: PLoS Computational Biology 4.7. DOI: 10.1371/journal.pcbi.1000106.

Meyer, Sofie S et al. (2017a). "Flexible head-casts for high spatial precision MEG". In: Journal of Neuroscience Methods 276, pp. 38–45. ISSN: 0165-0270. DOI: 10.1016/j.jneumeth.2016.11.009. URL: http://dx.doi.org/10.1016/j.jneumeth.2016.11.009.

Meyer, Sofie S et al. (2017b). "Using generative models to make probabilistic statements about hippocampal engagement in MEG". In: NeuroImage 149, pp. 468–482. DOI: 10.1016/j.neuroimage.2017.01.029. URL: www.elsevier.com/locate/neuroimage.

Miller, Kai J, Kurt E Weaver, and Jeffrey G Ojemann (2009). "Direct electrophysiological measurement of human default network areas". In: PNAS 106.29, pp. 12174–12177.

Mišić, Bratislav et al. (2011). "Functional embedding predicts the variability of neural activity". In: Frontiers in Systems Neuroscience 5, pp. 1–6. DOI: 10.3389/fnsys.2011.00090.

Mizuno, Tomoyuki et al. (2010). "Assessment of EEG dynamical complexity in Alzheimer's disease using multiscale entropy". In: Clinical Neurophysiology 121.9, pp. 1438–1446. ISSN: 1388-2457. DOI: 10.1016/J.CLINPH.2010.03.025. URL: https://www.sciencedirect.com/science/article/pii/S1388245710003135.

Monge, Jesús et al. (2015). "MEG analysis of neural dynamics in attention-deficit/hyperactivity disorder with fuzzy entropy". In: Medical Engineering and Physics 37, pp. 416–423. ISSN: 18734030. DOI: 10.1016/j.medengphy.2015.02.006.

Moradi, F et al. (2003). "Consistent and precise localization of brain activity in human primary visual cortex by MEG and fMRI". In: NeuroImage 18, pp. 595–609. DOI: 10.1016/S1053-8119(02)00053-8.

Mukamel, Roy et al. (2005). "Coupling Between Neuronal Firing, Field Potentials, and fMRI in Human Auditory Cortex". In: Science 309, pp. 951–954.

Murakami, Shingo and Yoshio Okada (2006). "Contributions of principal neocortical neurons to magnetoencephalography and electroencephalography signals". In: J Physiol 575.3, pp. 925–936. DOI: 10.1113/jphysiol.2006.105379.

Muthukumaraswamy, Suresh D and Krish D Singh (2008). "Spatiotemporal frequency tuning of BOLD and gamma band MEG responses compared in primary visual cortex". In: NeuroImage 40, pp. 1552–1560. DOI: 10.1016/j.neuroimage.2008.01.052.

— (2009). "Functional Decoupling of BOLD and Gamma-Band Amplitudes in Human Primary Visual Cortex". In: Human Brain Mapping 30, pp. 2000–2007. DOI: 10.1002/hbm.20644.

Nichols, Thomas E and Andrew P Holmes (2001). "Nonparametric permutation tests for functional neuroimaging: A primer with examples". In: Human Brain Mapping 15, pp. 1–25. ISSN: 10659471. DOI: 10.1002/hbm.1058.

Ogawa, Seiji et al. (1992). "Intrinsic signal changes accompanying sensory stimulation: Functional brain mapping with magnetic resonance imaging". In: Proc Natl Acad Sci USA 89, pp. 5951–5955.

O'Neill, George C et al. (2017). "Dynamics of large-scale electrophysiological networks: A technical review". In: NeuroImage. ISSN: 1053-8119. DOI: 10.1016/j.neuroimage.2017.10.003. URL: https://ac.els-cdn.com/S1053811917308169/1-s2.0-S1053811917308169-main.pdf?_tid=de372048-a9df-11e7-a07b-00000aacb35f&acdnat=1507216643_2d6f89d8ce4626e01ea33529a6ad08ac.

Ong, Ju Lynn et al. (2015). "Co-activated yet disconnected — Neural correlates of eye closures when trying to stay awake". In: NeuroImage 118, pp. 553–562. ISSN: 1053-8119. DOI: 10.1016/j.neuroimage.2015.03.085. URL: http://dx.doi.org/10.1016/j.neuroimage.2015.03.085.

Oostenveld, Robert et al. (2011). "FieldTrip: Open source software for advanced analysis of MEG, EEG, and invasive electrophysiological data." In: Computational intelligence and neuroscience 2011, pp. 1–9. ISSN: 1687-5273. DOI: 10.1155/2011/156869. URL: http://www.ncbi.nlm.nih.gov/pubmed/21253357%0Ahttp://www.pubmedcentral.nih.gov/articlerender.fcgi?artid=PMC3021840.

O'Reilly, Christian, John D. Lewis, and Mayada Elsabbagh (2017). "Is functional brain connectivity atypical in autism? A systematic review of EEG and MEG studies". In: PLoS ONE, pp. 1–28. ISSN: 19326203. DOI: 10.1371/journal.pone.0175870.

Ossandon, Tomas et al. (2011). "Transient Suppression of Broadband Gamma Power in the Default-Mode Network Is Correlated with Task Complexity". In: The Journal of Neuroscience 31.41, pp. 14521–14530. DOI: 10.1523/JNEUROSCI.2483-11.2011.

Ottet, Marie-Christine et al. (2013). "Graph theory reveals dysconnected hubs in 22q11DS and altered nodal efficiency in patients with hallucinations".

In: Frontiers in Human Neuroscience 7, pp. 1–10. ISSN: 16625161. DOI: 10.3389/fnhum.2013.00402.

Padula, Maria Carmela et al. (2015). "Structural and functional connectivity in the default mode network in 22q11.2 deletion syndrome". In: Journal of Neurodevelopmental Disorders 7.23, pp. 1–13. ISSN: 18661956. DOI: 10.1186/s11689-015-9120-y. URL: http://dx.doi.org/10.1186/s11689-015-9120-y.

Pascual-marqui, Roberto D (2007). "Discrete, 3D distributed linear imaging methods of electric neuronal activity. Part 1: exact, zero error localization". In: arxiv, pp. 1–16. arXiv: arXiv:0710.3341.

Pascual-Marqui, Roberto D et al. (2011). "Assessing interactions in the brain with exact low-resolution electromagnetic tomography". In: Philosophical Transactions. Series A, Mathematical, Physical, and Engineering Sciences 369, pp. 3768–3784. DOI: 10.1098/rsta.2011.0081.

Pasquale, Francesco de et al. (2010). "Temporal dynamics of spontaneous MEG activity in brain networks". In: Proceedings of the National Academy of Sciences 107.13, pp. 6040–6045. ISSN: 0027-8424. DOI: 10.1073/pnas.0913863107.

Petroni, Agustin et al. (2018). "The Variability of Neural Responses to Naturalistic Videos Change with Age and Sex". In: eNeuro 5.1, pp. 1–13.

Pettersson, Kati et al. (2019). "Saccadic eye movements estimate prolonged time awake". In: Journal of Sleep Research 28, pp. 1–13. DOI: 10.1111/jsr.12755.

Pfurtscheller, G and F H Lopes (1999). "Event-related EEG / MEG synchronization and desynchronization : basic principles". In: Clinical Neurophysiology 110, pp. 1842–1857. ISSN: 1388-2457. DOI: 10.1016/S1388-2457(99)00141-8. arXiv: S1388-2457(99)00141-8. [10.1016].

Piastra, Maria Carla et al. (2020). "A comprehensive study on electroencephalography and magnetoencephalography sensitivity to cortical and subcortical sources". In: Human brain mapping. DOI: 10.1002/hbm.25272.

Pizzo, F et al. (2019). "Deep brain activities can be detected with magnetoencephalography". In: Nature Communications 10.971, pp. 1–13. ISSN: 2041-1723. DOI: 10 . 1038 / s41467 - 019 - 08665 - 5. URL: http://dx.doi.org/10.1038/s41467-019-08665-5.

Protzner, A B et al. (2010). "Hippocampal signal complexity in mesial temporal lobe epilepsy: A noisy brain is a healthy brain". In: Archives Italiennes de Biologie 148.3, pp. 289–297. ISSN: 00039829.

Pu, Yi et al. (2017). "The Functional Role of Human Right Hippocampal/Parahippocampal Theta Rhythm in Environmental Encoding During Virtual Spatial Navigation". In: Human brain mapping 38, pp. 1347–1361. DOI: 10.1002/hbm.23458.

Pu, Yi et al. (2018). "Non-invasive Investigation of Human Hippocampal Rhythms Using Magnetoencephalography: A Review". In: Frontiers in Neuroscience 12. DOI: 10.3389/fnins.2018.00273.

Quraan, Maher A et al. (2011). "Detection and Localization of Hippocampal Activity Using Beamformers with MEG: A Detailed Investigation Using Simulations and Empirical Data". In: Human brain mapping, pp. 812–827. DOI: 10.1002/hbm.21068.

Raichle, Marcus E et al. (2001). "A default mode of brain function". In: PNAS 98.2, pp. 676–682.

Redon, Richard et al. (2006). "Global variation in copy number in the human genome". In: Nature 444.7118, pp. 444–454. DOI: 10.1038/nature05329.Global.

Rice, Justin K et al. (2013). "Subject position affects EEG magnitudes". In: NeuroImage 64, pp. 476–484. ISSN: 1053-8119. DOI: 10.1016/j.neuroimage.2012.09.041. URL: http://dx.doi.org/10.1016/j.neuroimage.2012.09.041.

Riggs, Lily et al. (2009). "A complementary analytic approach to examining medial temporal lobe sources using magnetoencephalography". In: NeuroImage 45, pp. 627–642. ISSN: 1053-8119. DOI: 10.1016/j.neuroimage.2008.11.018. URL: http://dx.doi.org/10.1016/j.neuroimage.2008.11.018.

Robinson, Stephen E et al. (2013). "Spatiotemporal imaging of complexity". In: Frontiers in Computational Neuroscience 6, pp. 101–114. DOI: 10.3389/fncom.2012.00101.

Roland, P E and L Friberg (1985). "Localization of Cortical Areas Activated By Thinking". In: Journal of neurophysiology 53.5, pp. 1219–1243.

Routley, Bethany Charlotte, Khalid Hamandi, and Krish D Singh (2017). "Investigating resting-state functional connectivity in health and epilepsy using Magnetoencephalography". PhD thesis.

Rubinov, Mikail and Olaf Sporns (2010). "Complex network measures of brain connectivity: Uses and interpretations". In: NeuroImage 52, pp. 1059–1069. ISSN: 1053-8119. DOI: 10.1016/j.neuroimage.2009.10.003. URL: http://dx.doi.org/10.1016/j.neuroimage.2009.10.003.

Rutter, Lindsay et al. (2009). "Magnetoencephalographic gamma power reduction in patients with schizophrenia during resting condition". In: Human Brain Mapping 30, pp. 3254–3264. ISSN: 10659471. DOI: 10.1002/hbm.20746.

Scariati, Elisa et al. (2016). "Large-scale functional network reorganization in 22q11.2 deletion syndrome revealed by modularity analysis". In: Cortex 82, pp. 86–99. ISSN: 19738102. DOI: 10.1016/j.cortex.2016.06.004.

Schacher, M et al. (2006). "Amygdala fMRI lateralizes temporal lobe epilepsy". In: Neurology 66, pp. 81–87.

Schäfer, Carmen B et al. (2014). "Oscillations, Networks, and Their Development: MEG Connectivity Changes with Age". In: Human Brain Mapping 35, pp. 5249–5261. DOI: 10.1002/hbm.22547.

Schlee, Winfried et al. (2012). "Age-related changes in neural functional connectivity and its behavioral relevance". In: BMC Neuroscience 13.16, pp. 1–11. ISSN: 1471-2202. DOI: 10.1186/1471-2202-13-16. URL: http://www.biomedcentral.com/1471-2202/13/16.

Schnitzler, Alfons and Joachim Gross (2005). "Normal and pathological oscillatory communication in the brain". In: Nature Reviews Neuroscience 6, pp. 285–296.

Schreiner, Matthew J. et al. (2014). "Default mode network connectivity and reciprocal social behavior in 22q11.2 deletion syndrome". In: Social Cognitive and Affective Neuroscience 9, pp. 1261–1267. ISSN: 17495024. DOI: 10.1093/scan/nst114.

Sekihara, Kensuke et al. (2004). "Asymptotic SNR of Scalar and Vector Minimum-Variance Beamformers for Neuromagnetic Source Reconstruction". In: IEEE Transactions on Biomedical Engineering 51.10, pp. 1726–1734. DOI: 10.1109/TBME.2004.827926.Asymptotic.

Shannon, C E (1948). "A mathematical theory of communication". In: Bell System Technical Journal 27, pp. 379–423.

Sharon, Dahlia et al. (2007). "The advantage of combining MEG and EEG: Comparison to fMRI in focally stimulated visual cortex". In: NeuroImage 36.4, pp. 1225–1235. ISSN: 10538119. DOI: 10.1016/j.neuroimage.2007.03.066.

Shumbayawonda, Elizabeth et al. (2019). "Sex Diferences in the Complexity of Healthy Older Adults' Magnetoencephalograms". In: Entropy 21.798, pp. 1–12.

Silva, Ana I et al. (2019). "Reciprocal White Matter Changes Associated With Copy Number Variation at 15q11.2 BP1-BP2: A Diffusion Tensor Imaging Study". In: Biological Psychiatry 85, pp. 563–572. ISSN: 0006-3223. DOI: 10.1016/j.biopsych.2018.11.004. URL: https://doi.org/10.1016/j.biopsych.2018.11.004.

Singh, Krish D (2006). "Magnetoencephalography". In: Methods in Mind. Ed. by Carl Senior. MIT Press, pp. 291–326.

— (2012). "Which "neural activity" do you mean? fMRI, MEG, oscillations and neurotransmitters". In: NeuroImage 62, pp. 1121–1130. ISSN: 10538119. DOI: 10.1016/j.neuroimage.2012.01.028.

Singh, Krish D et al. (2002). "Task-Related Changes in Cortical Synchronization Are Spatially Coincident with the Hemodynamic Response". In: Neuroimage 16, pp. 103–114. DOI: 10.1006/nimg.2001.1050.

Smedt, Bert de, Roland H Grabner, and Bettina Studer (2009). "Oscillatory EEG correlates of arithmetic strategy use in addition and subtraction". In: Exp Brain Res 195, pp. 635–642. DOI: 10.1007/s00221-009-1839-9.

Smith, Stephen M et al. (2009). "Correspondence of the brain's functional architecture during activation and rest". In: PNAS 106.31, pp. 13040–13045.

Stam, C J et al. (2006). "Magnetoencephalographic evaluation of resting-state functional connectivity in Alzheimer's disease". In: NeuroImage 32, pp. 1335–1344. DOI: 10.1016/j.neuroimage.2006.05.033.

Sten, S et al. (2017). "Neural inhibition can explain negative BOLD responses : A mechanistic modelling and fMRI study". In: NeuroImage 158.July, pp. 219–231. DOI: 10.1016/j.neuroimage.2017.07.002.

Stephen, Julia M et al. (2005). "Differentiability of Simulated MEG Hippocampal, Medial Temporal and Neocortical Temporal Epileptic Spike Activity". In: Journal of Clinical Neurophysiology 22.6, pp. 388–401.

Stolk, Arjen et al. (2013). "Online and offline tools for head movement compensation in MEG". In: NeuroImage 68, pp. 39–48. ISSN: 1053-8119. DOI: 10.1016/j.neuroimage.2012.11.047. URL: http://dx.doi.org/10.1016/j.neuroimage.2012.11.047.

Strandberg, Maria et al. (2011). "fMRI memory assessment in healthy subjects: a new approach to view lateralization data at an individual level". In: Brain Imaging and Behavior 5, pp. 1–11. DOI: 10.1007/s11682-010-9106-z.

Swettenham, J B, S D Muthukumaraswamy, and K D Singh (2013). "BOLD responses in human primary visual cortex are insensitive to substantial changes in neural activity". In: Frontiers in human neuroscience 7. DOI: 10.3389/fnhum.2013.00076.

Tait, Luke et al. (2020). "Cortical source imaging of resting-state MEG with a high resolution atlas: An evaluation of methods". In: bioRxiv.

Takahashi, Tetsuya (2013). "Complexity of spontaneous brain activity in mental disorders". In: Progress in Neuro-Psychopharmacology and Biological Psychiatry 45, pp. 258–266. ISSN: 02785846. DOI: 10.1016/j.pnpbp.2012.05.001. URL: http://dx.doi.org/10.1016/j.pnpbp.2012.05.001.

Tewarie, Prejaas et al. (2019). "Relationships Between Neuronal Oscillatory Amplitude and Dynamic Functional Connectivity". In: Cerebral Cortex 29, pp. 2668–2681. DOI: 10.1093/cercor/bhy136.

Tierney, Tim M et al. (2021). "Mouth magnetoencephalography: A unique perspective on the human hippocampus". In: NeuroImage 225. ISSN: 1053-8119. DOI: 10.1016/j.neuroimage.2020.117443. URL: https://doi.org/10.1016/j.neuroimage.2020.117443.

Toller, Gianina et al. (2015). "Nonvisual spatial navigation fMRI lateralizes mesial temporal lobe epilepsy in a patient with congenital blindness". In: Neurocase 21.6, pp. 748–752. ISSN: 1355-4794. DOI: 10.1080/13554794.2014.986136. URL: http://dx.doi.org/10.1080/13554794.2014.986136.

Tononi, Giulio, Olaf Sporns, and Gerald M Edelman (1994). "A measure for brain complexity: Relating functional segregation and integration in the nervous system". In: Neurobiology 91, pp. 5033–5037.

Towgood, Karren et al. (2015). "Bringing Memory fMRI to the Clinic: Comparison of Seven Memory fMRI Protocols in Temporal Lobe Epilepsy". In: Human brain mapping 36, pp. 1595–1608. DOI: 10.1002/hbm.22726.

Tzourio-Mazoyer, N et al. (2002). "Automated Anatomical Labeling of Activations in SPM Using a Macroscopic Anatomical Parcellation of the MNI MRI Single-Subject Brain". In: NeuroImage 15, pp. 273–289. DOI: 10.1006/nimg.2001.0978.

Uhlhaas, Peter J and Wolf Singer (2010). "Abnormal neural oscillations and synchrony in schizophrenia". In: Nature Reviews Neuroscience 11, pp. 100–113. ISSN: 1471-003X. DOI: 10.1038/nrn2774. URL: http://dx.doi.org/10.1038/nrn2774.

Vakorin, V. A., S. Lippe, and A. R. McIntosh (2011). "Variability of Brain Signals Processed Locally Transforms into Higher Connectivity with Brain Development". In: Journal of Neuroscience 31.17, pp. 6405–6413. ISSN: 0270-6474. DOI: 10.1523/jneurosci.3153-10.2011.

Van Dellen, Edwin et al. (2014). "Epilepsy surgery outcome and functional network alterations in longitudinal MEG: A minimum spanning tree analysis". In: NeuroImage 86, pp. 354–363. ISSN: 10959572. DOI: 10.1016/j.neuroimage.2013.10.010.

Van Veen, Barry D et al. (1997). "Localization of Brain Electrical Activity via Linearly Constrained Minimum Variance Spatial Filtering". In: IEEE TRANSACTIONS ON BIOMEDICAL ENGINEERING 44.9.

Vanderwolf, C H (1969). "Hippocampal electrical activity and voluntary movement in the rat". In: Electroencephalography and Clinical Neurophysiology 26, pp. 407–418.

Vidaurre, Diego et al. (2016). "Spectrally resolved fast transient brain states in electrophysiological data". In: NeuroImage 126, pp. 81–95. ISSN: 1053-8119. DOI: 10.1016/j.neuroimage.2015.11.047. URL: http://dx.doi.org/10.1016/j.neuroimage.2015.11.047.

Vincent, Justin L et al. (2006). "Coherent Spontaneous Activity Identifies a Hippocampal-Parietal Memory Network". In: J Neurophysiol 96, pp. 3517–3531. DOI: 10.1152/jn.00048.2006.Report.

Vorwerk, Johannes et al. (2014). "A guideline for head volume conductor modeling in EEG and MEG". In: NeuroImage 100, pp. 590–607. ISSN: 1053-8119. DOI: 10.1016/j.neuroimage.2014.06.040. URL: http://dx.doi.org/10.1016/j.neuroimage.2014.06.040.

Vrba, J (2002). "Magnetoencephalography: the art of finding a needle in a haystack". In: Physica C 368, pp. 1–9.

Vrba, Jiri and Stephen E. Robinson (2001). "Signal Processing in Magnetoencephalography". In: Methods 25, pp. 249–271. ISSN: 1046-2023. DOI: 10.1006/METH.2001.1238. URL: https://www.sciencedirect.com/science/article/pii/S1046202301912381?via%3Dihub.

Wang, Danny J.J. et al. (2018). "Neurophysiological basis of multi-scale entropy of brain complexity and its relationship with functional connectivity". In: Frontiers in Neuroscience 12, pp. 1–14. ISSN: 1662453X. DOI: 10.3389/fnins.2018.00352.

Weis, Susanne, Sophie Hodgetts, and Markus Hausmann (2019). "Sex differences and menstrual cycle effects in cognitive and sensory resting state networks". In: Brain and cognition 131, pp. 66–73. DOI: 10.1016/j.bandc.2017.09.003.

Wens, Vincent et al. (2014). "Inter- and Intra-Subject Variability of Neuromagnetic Resting State Networks". In: Brain Topography 27, pp. 620–634. DOI: 10.1007/s10548-014-0364-8.

Woltering, Steven et al. (2012). "Resting state EEG oscillatory power differences in ADHD college students and their peers". In: Behavioral and Brain Functions 8.60, pp. 1–9. ISSN: 17449081. DOI: 10.1186/1744-9081-8-60. URL: BehavioralandBrainFunctions.

Woodward, Neil D, Baxter Rogers, and Stephan Heckers (2011). "Functional resting-state networks are differentially affected in schizophrenia". In: Schizophrenia Research 130, pp. 86–93. ISSN: 09209964. DOI: 10.1016/j.schres.2011.03.010. URL: http://dx.doi.org/10.1016/j.schres.2011.03.010.

Yuen, Nicole H, Nathaniel Osachoff, and J Jean Chen (2019). "Intrinsic Frequencies of the Resting-State fMRI Signal: The Frequency Dependence of Functional Connectivity and the Effect of Mode Mixing". In: Frontiers in Neuroscience 13, pp. 1–17. DOI: 10.3389/fnins.2019.00900.

Zijlmans, Maeike et al. (2013). "High-Frequency Oscillations as a New Biomarker in Epilepsy". In: Annals of Neurology 71.2, pp. 169–178. DOI: 10.1002/ana.22548.High-Frequency.

Zumer, Johanna M. et al. (2010). "Relating BOLD fMRI and neural oscillations through convolution and optimal linear weighting". In: NeuroImage 49, pp. 1479–1489. ISSN: 10538119. DOI: 10.1016/j.neuroimage.2009.09.020.